University of Alberta

Library Release Form

Name of Author: Guifang Huang

Title of Thesis: Galactose-Derivatized Superparamagnetic Nanoparticles as Potential Targeted Carriers for Hepatocyte Delivery

Degree: Master of Science

Year This Degree Granted: 2003

University of Alberta

Galactose-Derivatized Superparamagnetic Nanoparticles as Potential Targeted Carriers for Hepatocyte Delivery

By

Guifang Huang

A thesis submitted to the Faculty of Graduate Studies and Research in partial fulfillment of the requirements for the degree of Master of Science

In

Pharmaceutical Sciences

Faculty of Pharmacy and Pharmaceutical Sciences

Edmonton, Alberta

Spring 2003

University of Alberta

Faculty of Graduate Students and Research

The undersigned certify that they have read, and recommend to the Faculty of Graduate Studies and Research for acceptance, a thesis entitled "**Galactose-Derivatized Superparamagnetic Nanoparticles as Potential Targeted Carriers for Hepatocyte Delivery**" submitted by **GuiFang Huang** in partial fulfillment of the requirements for the degree of Master of Science in Pharmaceutical Sciences.

DEDICATED

TO MY

Lovely daughter: Emma Huang and parents: Rong Tan and Chuanshong Huang

ABSTRACT

This project addresses the development of superparamagnetic nanoparticles as targeted magnetic carriers. Specifically, galactose-derivatized superparamagnetic nanoparticles (Gal-beads) have been prepared, and their specific uptake by a human hepatocyte cell line (Hep G2) has been investigated.

The molecular target of this delivery system, the asialoglycoprotein receptors (ASGPRs), is specific to hepatocyte cells. The binding between ^{125}I-galactose-terminal glycoprotein (ASOR) and ASGPRs in the membrane of Hep G2 can be competitively inhibited by galactose. Binding studies have shown that the number of ASGPRs per cell ranges from around 95,000 to 140,000.

The Gal-beads were prepared by reacting amino-terminated superparamagnetic nanoparticles and lactose in the presence of the reducing agent sodium cyanoborohydride. The uptake of Gal-beads by Hep G2 was greater than the uptake by neutral underivatized superparamagnetic nanoparticles (neutral particles). Furthermore, this uptake of Gal-beads was challenged by the addition of galactose, and evaluated visually with a phase contrast microscope. In contrast, the negative control, 143B (human osteosarcoma) cell line, displayed no visible uptake of Gal-beads. The MTT cell survival assay showed that the toxic concentration of Gal-beads was 1.5 mg/mL. The results obtained in this study encourage further study of Gal-beads as potentially selective carriers for targeting the liver.

ACKNOWLEDGMENT

I wish to express my deepest gratitude to Dr. L. I. Wiebe, Dr. Z. H. Xu and Dr. J. Diakur for their supervision, great encouragement, patience and kind support throughout my graduate study program.

My sincere thanks also go to Dr S. McQuarrie for his critical comments and valuable suggestions in editing my dissertation.

I wish to thank Yunli Gu, Ge Li, Aihua Zhou, Jianjun Liu for their technical assistance during course of the study.

Finally, I would like to thank the Faculty of Pharmacy & Pharmaceutical Sciences and Department of Chemical & Materials Engineering for providing a comfortable research environment.

TABLE OF CONTENTS

LIST OF TABLES

LIST OF FIGURES

LIST OF PLATES

List of Abbreviations

Ab	antibody
Ag	antigen
APS	ammonium persulfate
ASGPR	asialoglycoprotein receptor
ASOR	asialorosomucoid (asialoglycoprotein)
ASOR-PL	asialoglycoprotein-polylysine
BBB	blood brain barrier
CAT	chloramphenicol acetyltransferase
CDRs	complementarity-determining regions.
CT	computerized tomography
CT	chloramine-T
CNBr	cyanogen bromide
DC	dendritic cells
DF	dextran-ferrite
EDTA	ethylenediaminetetracetic acid
EMEM	eagle's minimum essential medium
emu	electromagnetic units
FACS	fluorescence-activated cell sorter
FBS	fetal bovine serum
FS	ferri- and ferro-magnetic suspensions
FWHM	full width half maximum
g	gram(s)
Gal-beads	galactose-derivatized magnetic nanoparticles
GM	glioblastoma multiformae
HEPES	N-2-hydroxyethethylpiperazine-N'-2-ethanesulfonic acid
HL	human lectin
Hz	hertz

IFF	immunoferrofluid
K_D	equilibrium binding constant
KD	kilodalton
L	litre(s)
M	molar(s)
mAb	monoclonal antibody
MC	magnetic carrier
mCi	millicurie
MCT	magnetic carrier technology
MFH	magnetic fluid hyperthermia
mg	milligram(s)
MHL	murine hepatic lectin
MHz	millihertz
min	minute(s)
mL	milliliter(s)
mM	millimolar(s)
mm	millimeter(s)
MW	molecular weight
MRI	magnetic resonance imaging
MV	millivolt
n	number of subjects studied
nm	nanometer(s)
NMR	nuclear magnetic resonance
PAGE	polyacrylamide gel electrophoresis
PBS	phosphate buffered saline
PEI	polyethylenimine
PET	positron-emission-tomography
RF	radiofrequency
RHL	rat hepatic lectin
RME	receptor-mediated endocytosis

RT	room temperature
SAR	specific power absorption
sec	second(s)
SDS	sodium dodecyl sulfate
° C	degree celsius
%	percentage(s)
TEM	transmission electron micrograph
TNF	necrosis factor
μL	microliter(s)
μm	micrometer(s)

1. INTRODUCTION

1.1. Magnetic carriers

1.1.1. General review

Magnetic carriers incorporate magnetic particles as a base material for engineering carriers. The objective of magnetic carrier technology is to confer magnetic properties of the carriers to naturally nonmagnetic targets, and then the target can be treated by utilizing a magnetic field. Magnetic particles can either be larger than the targets so that the targets are attached to the particles, or the magnetic particles can be smaller than the targets so that the particles deposit on the targets (Xu *et al.* 1999).

MCT originated in the early 1940s, from studies on waste water treatment where the objective was to adsorb organic matter onto small particles of magnetite (Fe_3O_4) and subsequently to separate the loaded magnetite from the bulk process liquor (Urbain and Steman, 1941; Kolarik *et al.* 1977).

Other principal applications of MCT include: 1) enzyme immobilization (Tamaura *et al.* 1986; Matsunaga and Kimiya, 1987; Mihama *et al.* 1988; Dekker, 1989; Pieters, 1989; Longo Gonzalez, 1990; Robinson *et al.* 1973) and purification (Dunnill and Lilly, 1974) in bioprocesses with the use of enzymes as biocatalysts, 2) affinity separation of bio-molecules (Burns and Graves, 1987; Terranova and Burn, 1989), both in immunoassay (Pourfarzaneh *et al.* 1982) and genetic engineering for the recovery of defined DNA and transcription factors (Gabrielsen *et al.* 1989; Hultman *et al.* 1989), 3) cell sorting for separating specific cell types from a cell population (Antoine *et al.* 1978; Kronick *et al.* 1978; Margel *et al.* 1979; Molday *et al.* 1977; Lea *et al.* 1988), 4) drug delivery (Widder *et al.* 1978), 5) magnetic resonance imaging in diagnostics (Kim *et al.* 2001) and 6) cancer therapy such as hyperthermia treatment of tumors (Nikolai *et al.* 2001). In the case of enzyme immobilization, MCT may offer a means of reducing some constraints, such as enzyme instability, loss of the enzyme or damage to the biocatalyst. In drug delivery, on the other hand, drugs in a biodegradable magnetic carrier are designed to reach a

specific locality in the body. In MRI, magnetic carriers are used as contrast enhancers.

Although magnetic carriers have been prepared in some areas of biotechnology for more than 20 years, MCT did not immediately gain widespread acceptance because the preparation of magnetic carriers is labor-intensive. Only in the 1980s did some of the magnetic carrier systems that were feasible for general use become commercially available.

Commercial production of magnetic carriers started in 1976, and now various products are available. The various products with manufacturer are shown in Table 1.1.1 (Williams, 1992).

Table 1.1.1. Major commercial magnetic carriers and their characteristics.

Commercial Name	Size Range (μm)	Manufacturer	References
Biomag	0.15 – 1.5	Advanced Magnetics, Inc./Metachem Diagnostic	Adalsteinsson *et al.* (1979); Menz *et al.* (1986)
Dynabead (M450)	4.5	Dynal	Ugelstad *et al.* (1982, 1988)
Enzacryl (FEO-M)	40 – 70	Aldrich	Nye *et al.* (1976); Forrest (1977)
Estapor (M)	0.7	Rhone Poulenc	Charmot, (1989)
Magnogel	60 – 140	IBF/LKB Instruments	Guesdon and Avrameas (1977)

For example, StemSep^{TM} is a negative selection system in which the unwanted cells are immunomagnetically labelled and bound to a magnetic column (www.stemcell.com). The unlabelled (desired) cells are collected in the column eluent. The advantages of negative selection include one-step clean up, and the procedure is efficient, flexible, rapid and simple.

CliniMACS products (Milytenyi Biotec GmbH Bergisch Gladbach, Germany) are available for clinical use only under an approved Investigational Device Exemption (IDE) in USA. Most magnetic cell sorting technology is used worldwide in biomedical research areas like cancer, AIDS or autoimmune diseases and in novel biomedical approaches such as bone marrow transplantation or gene therapy. Miltenyi Biotec is keen to support sophisticated ideas in research and clinical applications in affinity separation of bio-molecules; cell sorting; cancer gene therapy and so on, using biodegradable nanoparticles.

Endorem, manufactured by Advanced Magnetics (USA), has a rather coarse size distribution of 120-180 nm, and is used extensively in MRI diagnosis (Chachuat and Bonnemain, 1995). This material is composed of nanosize superparamagnetic iron oxide-dextran particles.

Standardized liver MRI of radiologyinfonet (www.radinfonet.com) for diagnosis of hepatic hemangioma and heptocellular carcinoma. In this study dynamic post gadolinium breathhold imaging is performed through the entire liver with patient inside the magnet.

A major challenge in this field is to optimize the properties of magnetic carriers to meet the requirements for application in biomedicine.

1.1.2. Components and properties of magnetic materials

Components

Most magnetic carriers consist of following components: 1) magnetic materials, 2) coated polymers, and 3) surface effectors (able to recognize an accessible receptor of the target cell or bio-molecule). Magnetic carriers can carry drugs such as active therapeutics, radionuclides for radiotherapy, plasmid DNA for gene therapy, or other desired entities (Petit *et al.* 2000).

Magnetic materials

An electron possesses magnetic characteristics because of its spin, that causes it to behave as a magnetic dipole. Molecules and materials may be classified into two groups, namely, those with unpaired electrons and those with spin-paired electrons. Members of the first group are attracted to regions with strong magnetic fields. This attraction is quantified in terms of the volumetric magnetic susceptibility Xv, which is

positive in this case. Members of the second group demonstrate repulsion under the same conditions and have a negative *Xv*.

Examples of magnetically susceptible materials include diamagnetic, paramagnetic, ferromagnetic and ferrimagnetic materials. In diamagnetic materials, which include SiO_2, NaCl, graphite, alumina, and most organic compounds, small magnetic dipoles originate from within the atoms when orbiting electrons become unbalanced. Paramagnetic materials include $NiSO_4$, some transition metal complexes, NO, O_2, and organic free radicals. Ferrimagnetic materials include ceramics that are created by mixing iron oxide (Fe_2O_3) with carbonates and iron powders. These materials are readily available in large quantities. The only elemental metals that can be magnetized and thus produce a strong magnetic field are Fe, Ni, and Co. Each of these atoms has several unpaired electron spins. These materials are known as ferromagnetic metals. Like ferromagnets, ferrimagnets show high magnetic susceptibilities. Magnetite, FeO Fe_2O_3 (or Fe_3O_4), is the most widely used ferrimagnetic material that is magnetically susceptible. An oxidized form of magnetite, maghemite (r-Fe_2O_3), is also used. Magnetite is a black mineral form of iron oxide, crystallizing in the cubic system. It is one of the major iron ores. Magnetite is strongly magnetic and some of its varieties, known as lodestone, are natural magnets. They were used as compasses in the ancient world (Isaacs *et al.* 1991). Magnetite can be obtained from comminuted ores or synthesized from Fe^{2+}/Fe^{3+} solutions that are heated to about 70 °C, when magnetite is precipitated by increasing the pH. Alternatively, magnetite can be isolated from magnetotactic algae or bacteria (Matsunaga and Kamiya, 1987). In practice, synthetic magnetite (50-150 nm) is most commonly used, but it may form aggregates of 1000-2000 nm in diameter, thus necessitating ultrasonic treatment before using the material for the manufacture of magnetic carriers. Biomagnetite does not aggregate to the same degree. However, its isolation from magnetotactic cell cultures is still difficult to achieve on an adequate scale (Matsunage and Kamiya, 1987).

Several ferri- and ferro-magnetic suspensions (FS) of uncoated Fe_3O_4, Fe_2O_3 and reduced Fe have been prepared according to the procedure (Kuznetsov, 1997). Four sonicated water-based ferro-carbon suspensions were reported (Brusentsov *et al.*

2000). Iron nanoparticles were prepared by the condensation of metal vapor in high-pressure argon plasma (Mykhaylyk *et al.* 1997; 2001).

Coated polymers

During the past ten years, several functional magnetic carriers have been developed (Margel *et al.* 2000). In this case, polymers microencapsulate magnetic materials. An appropriate polymer is attached directly onto the particle surface, or is attached via a spacer, to provide the desired functional groups. This modified surface thus fulfils the requirements for highly specialized magnetic carrier applications.

Polyacrylamide was used in the production of Biomag products (Adalsteinsson *et al.* 1979; Menz *et al.* 1986); Polystyrene, in Dynabead (M450) (Ugelstad *et al.* 1982; 1988) and in Estapor (M) (Charmot, 1989); Poly-1, 3-diaminobenzene, in Enzacryl (FEO-M) (Nye *et al.* 1976; Forrest, 1977) and polyacrylamide-agarose, in Magnogel (Guesdon and Avrameas, 1977; Antoine *et al.* 1978).

Properties

Intrinsic magnetic properties of magnetic carriers are useful for their applications in magnetically assisted guidance, MRI contrast enhancement and magnetocytolysis. The following discussion focuses on the properties of magnetic materials, as they are very important in applications of magnetic materials.

Magnetic moment (T_{max}/H)

The magnetic moment is the ratio between the maximum torque (T_{max}) exerted on a magnet, current-carrying coil, or moving charge situated in a magnetic field and the strength of that field (H). It is a measure of the strength of the magnet or current-carrying coil. Torque is the product of a force and its perpendicular distance from a point about which it causes rotation or torsion. T_{max} occurs when the axis of the magnet is perpendicular to the field (Cullity, 1972).

Magnetic susceptibility (Xv)

Magnetic susceptibility is a dimensionless quantity describing the contribution made by a substance when subjected to a magnetic field to the total magnetic flux

density present. It is equal to μ_r-1, where μ_r is the relative permeability of the material. μ_r is given by μ/μ_0 where μ_0 is the permeability of the free space. μ (=*B/H)* is the ratio of the magnetic flux density, *B*, in a substance to the external field strength, *H*. A high magnetic susceptibility often corresponds to the magnetic application efficiency (Garcia *et al*. 1999).

Magnetism

The term magnetism encompasses a group of phenomena associated with magnetic field. Whenever an electric current flows, a magnetic field is produced. The orbital motion and the spin of atomic electrons are equivalent to tiny current loops, and individual atoms create magnetic fields around them, when their orbital electrons have a net magnetic moment. Different materials have different characteristics in an applied magnetic field. Based on their characteristics, materials are classified as diamagnetic, paramagnetic, ferromagnetic and ferrimagnetic. In diamagnetism, the magnetization is in the opposite direction to that of the applied field. Diamagnetic materials have a low negative susceptibility (Isaacs, 1991).

Paramagnetism

In paramagnetism, the atoms of a substance have net orbital or spin magnetic moments that are capable of being aligned in the direction of the applied magnetic field. They therefore have a positive (but small) magnetic susceptibility *(Xv).* Paramagnetism occurs in metals as a result of the magnetic moments associated with the spins of the conducting electrons. Paramagnetic materials remain magnetized only when the magnetic field is applied. Also, paramagnetic effects increase with temperature (Garcia *et al*. 1999).

Ferromagnetism

In ferromagnetic substances, within a certain temperature range, net atomic magnetic moments are induced, which line up in such a way that magnetization persists after the removal of the applied field. Ferromagnetic materials typically have a high positive value of magnetization. Below a certain temperature, called the Curie point (or Curie temperature), an increasing magnetic field applied to a ferromagnetic

substance will cause increasing magnetization to a high constant value, called the saturation magnetization. Irreversibility becomes apparent. In this phenomenon, decreasing the applied field to zero does not remove all of the magnetization from the material. Above the Curie point, ferromagnetic materials become paramagnetic (Isaacs, 1991).

Ferrimagnetism

Ferrimagnetism is a type of magnetism exhibited by ferrites. It is also a special form of antiferromagnetism. The number of magnetic moments in one direction is greater than those in the opposite direction. Antiferromagnetism occurs below a certain temperature, called the Neel temperature, when an ordered array of atomic magnetic moments spontaneously forms in which alternate moments have opposite directions. Like ferromagnets, ferrimagnets show high magnetic susceptibilities, relative permeability and irreversibility. Above the Neel temperature, the substance is paramagnetic (Banerjee and Moskowitz, 1985).

Size of magnetic carriers

The particle size determines the particle's physical behaviour. Size of a magnetic carrier includes the size of its core (magnetic materials) and the size of coated components. Relatively large, dense particles tend to settle and aggregate, whereas small, light particles form homogenous suspensions or colloids. Smaller size particles exhibit higher ratios of surface area to the mass, offering better mass transfer and a reduced tendency to gravitational settling and mechanical attrition. However, taken to the extreme, submicron-size particles become increasingly difficult to separate magnetically as the magnetic force decreases at a given magnetic field strength and gradient, thus requiring a high magnetic field/field gradient to achieve efficient separation. The amount of magnetic material in carriers, known as the magnetic loading, determines the overall susceptibility of magnetic matter in an external magnetic field and therefore affects the speed of recovery. Magnetic loadings range from 20~50 weight % of the carriers (Garcia *et al.* 1999).

Magnetic aggregation

Mechanical instability (i.e. sedimentation under gravity) and magnetic flocculation, are phenomena through which magnetic particle aggregation can limit the application of given particle carrier system. The separation efficiency of biological species via magnetic carriers decreases markedly with aggregation, because the available surface area is greatly reduced. The values of the electrokinetics (zeta-potentials) of magnetic carriers are a measure of magnetic aggregation. If zeta-potential values of magnetic carriers are more than 30 mV, the carriers do not easily aggregate (Xu, 1999).

1.1.3. Classification of carriers

Figure 1.1.3 shows the basic types of magnetic carriers. Carrier 1 is simply a magnetic material that does not host a polymer. Such particles can be used directly and are suitable for the non-specific, reversible adsorption of cells or other organic materials. They are suitable for use in large-scale waste treatment applications (Kolarik *et al.* 1977).

Carrier 2 is comprised of a magnetic material coated with a polymer. A few coating methods are commonly used. These methods include formation of magnetic cores in porous media (Ugelstad *et al.* 1987), direct silanization (Chagnon *et al.* 1987; Xu *et al.* 1997) and silica coating following by silanization of magnetic particles (Xu *et al.* 1999). Polymer adsorption is generally not difficult to accomplish with polyamines such as albumin (Sato *et al.* 1986) or polyvinylamine (Patton *et al.* 1985). The polymerization of synthetic monomers requires prior derivatization of magnetite with vinyl trimethoxysilane (Tsunoda, 1985), a technique commonly used in magnetic toners (Canon, 1981). Finally, Fe^{2+}: Fe^{3+}: polymer co-precipitation under conditions similar to those used in the production of synthetic magnetite is popular, and has proven successful for chitosan (Yen *et al*, 1980). These techniques produce submicron carriers that are particularly useful for enzyme immobilization applications.

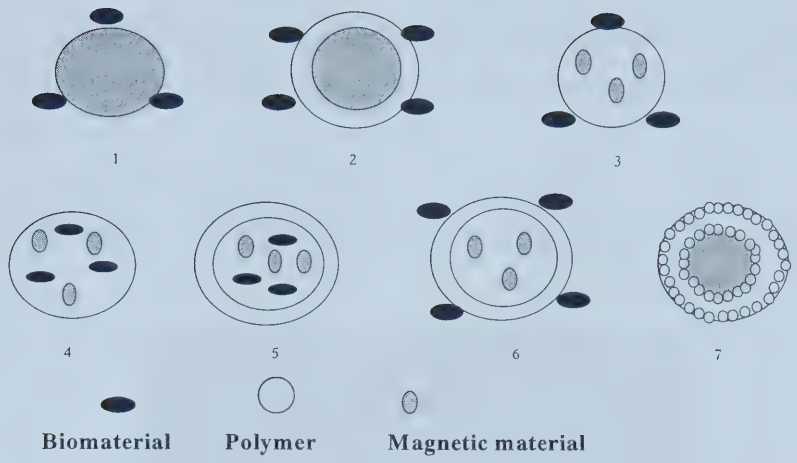

Figure 1.1.3. Classification of types of magnetic carriers.

Carriers 3, 4 and 5 are produced by embedding synthetic magnetite in dense (3), porous (4) or hollow structures (5). Carriers 3 and 4 are made via an emulsion polymerization route, to enable inclusion of magnetic materials within the polymer. In the preparation of carrier 3, short monomers are used and if possible, cross-linked to result in a very rigid and non-porous structure. This type of carrier is particularly suitable for the separation of cells and bio-molecules (Lea *et al.* 1988; Menz *et al.* 1986). In carrier 4 sufficiently large monomers and mild polymerization conditions are used to ensure that the resultant carrier is porous. Such carriers are suited for enzyme immobilization (Adalsteinsson *et al.* 1979) and in drug delivery (Widder *et al.* 1978). Carrier 5 is basically a microcapsule that can be made using a phase separation technique, interfacial polymerization or liquid drying method. Magnetic microcapsules have been manufactured for drug delivery (Ishii *et al.* 1984).

Carrier 6 uses Carrier 3 as a magnetic core. In this case, use of a low-cost polystyrene carrier is particularly convenient (Ugelstad *et al.* 1982). Porous coating is adsorbed onto core particles, thus alleviating the problems associated with the

rigidity of porous carriers (carrier 4). Applications in drug delivery with this type of carrier have been reported (Saslawski *et al.* 1988).

Carrier 7 is a magnetoliposome that can be used for cell sorting (Margolis *et al.* 1983) and drug delivery (Kiwada *et al.* 1986; Eley *et al.* 1986). The formation and structural characteristics of this type of carriers have been studied by De Cuyper and Joniau (1988).

The transmission electron micrograph (TEM) (Plate 1.1.3) shows polymer-coated Fe_3O_4 nanoparticles. The dark spots are the cores of the Fe_3O_4 nanoparticles.

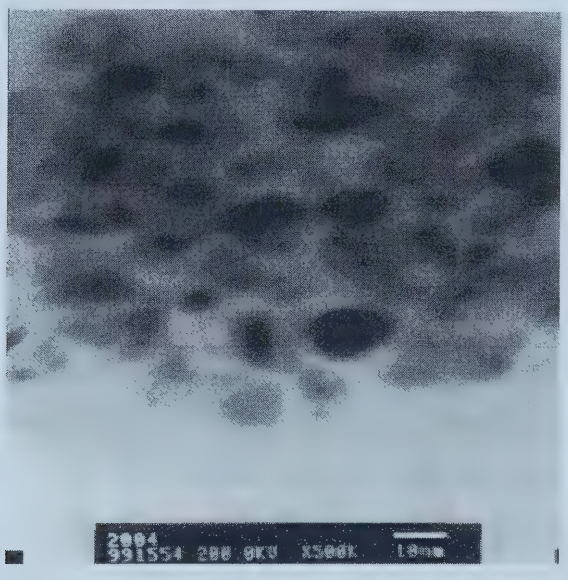

Plate 1.1.3. Transmission electron micrograph (TEM) of Fe_3O_4 nanoparticles coated with polyoxyethylene (10) oleyl ether (Kim *et al.* 2001).

1.1.4. Toxicity and safety

The potential therapeutic *in vivo* applications of magnetic particles with ligands include cancer therapy, blood purification, nuclear magnetic resonance (NMR) imaging and hyperthermia treatment of tumors. Particles need to be biocompatible and non-toxic. Iron oxide particles seem to be generally well tolerated, and magnetite-based MRI contrast agents have already been approved for human use (Hafeli *et al.* 1999). The intrathecal injection of these carriers into rats produced no obvious side effects over a twelve-month period. It may be interesting to compare

therapeutically feasible concentrations of a particular magnetic carrier to the physiological iron levels in humans. In general, adults contain 3 to 5 g of iron in the form of hemoglobin in their erythrocytes and as ferritin and hemosiderin in the storage compartments (Assembly of Life Science (U.S), 1979). Normally, only about 4 mg of the total iron is in the form of transferrin, the only accessible iron compound in the blood. Acute iron toxicity leading to death through acidosis in human occurs when more than 200-250 mg of iron per kilogram of body weight is reached (Crotty *et al.* 1971). Such concentrations, however, would never be attempted for *in vivo* therapy. It was estimated that magnetically-targeted local therapy would require only a few milligrams, and that systemic therapy should never exceed a few hundred milligrams of the magnetic material.

Considering the possible desorption of biological constituents from the magnetic carriers, the toxicity of all intermediates used in the preparation of magnetic carriers has to be investigated through *in vivo* tests. Morphological effects in spleen, liver and pancreas of mice have been observed after intraperitoneal administration of water-based magnetic carriers containing magnetite nanoparticles (Lacava *et al.* 1999). In experimental oncology, seventeen different ferromagnetic fluids and suspensions were prepared and evaluated by Nikolai *et al* (2001) for application in site-specific radiofrequency (RF)-induced hyperthermia. Survival of ascitic sarcoma MX11 cells mixed with ferrofluids and subjected to RF was much lower than that with RF without ferrofluid or ferrofluid alone. In this case no long-term toxicity or acute death of MX11 cells was detected when the cells were exposed to dextran-ferrite (DF) ferrofluids (up to 80 mg of DF/mL) alone at 37 °C, or to the RF field without a ferrofluid.

Mykhaylyk *et al* (2001) found that magnetic field manipulations significantly affect iron homeostasis. It had been found that application of a magnetic field of 0.075 Tesla with gradient 0.018 Tesla /cm to the brain for only 10 min resulted in an increase in transferrin iron concentration in the blood. This effect was statistically significant; therefore, transient abnormalities in the serum iron levels, which are routinely observed as a result of nanodispersed iron oxide injection (Weissleder, 1994), can be at least partially attributed to magnetic field effects. The accumulation

of endothelial lipid peroxidation products under steady magnetic fields may lead to the activation of heme oxygenase (Juckett *et al.* 1998) that catabolizes heme and produces chelatable iron, carbon oxide and biliverdin (Takeda *et al.* 1995). Hypothetically, the observed increase in transferrin iron concentration in the blood following the application of steady magnetic fields could arise from the activation of heme oxygenase and the corresponding increase in production of chelatable iron that is bound by transferrin.

Taking into account that certain diseases are associated with abnormal iron metabolism, in particular, with excess iron in tissues (Lauffer, 1992), development of iron-based treatments should be carried out in such a way as to avoid iron overload in patients.

Toxicity studies have revealed the maximum tolerable thermal dose to normal brain in dogs is 44 °C for 30 min. Known side effects of magnetic hyperthermia treatment of tumors in animal experiments include cerebral necrosis, edema, focal hemorrhage and infarction. A breakdown of the blood brain barrier is observed at temperatures of 42.5 -43 °C for 60 min. Toxicity was more frequent in the magnetic hyperthermia treatment of tumors with mild neurological changes and seizures (lasting $\leq$ 5 min), which were most probably caused by the overheating of normal brain tissue. No problems with edema and intracranial pressure or infarction or thrombosis were reported in the studies by Sneed *et al.* (1998). Clinical studies performed so far have shown that interstitial brain hyperthermia is feasible and that toxicity is acceptable under careful control of heating and limitation of the target volume (Jordan, 2001).

1.1.5. Biomedical applications

Cell sorting

Cell labelling with magnetic substances has become an increasingly common method for *in vitro* cell separation. Immunomagnetic cell sorting using MCT is attractive. Antibodies (Ab) bound to magnetic carriers can label the cell surface antigen (Ag). Examples are shown in Table 1.1.5 (Williams, 1992).

Table 1.1.5. Summary of cell sorting applications using MCT

Cell Type	Antibody	Ligand	Particle	Reference
Human red blood cells	Rabbit anti -human Ig	Anti-rabbit Ig	Polyglutaraldehyde	Margel *et al.* (1979)
Human red blood cells	Rabbit anti -human Ig	Pro A	Dextran	Molday and Mackenzie, (1982)
S.cereveside		Con A	Magnetite	Horisberger, (1976)
Legionella	Anti-legionella Ig	Pro A	Dextran	Kronick and Gilpin, (1986)
Langerhans Cells	Mouse anti -CD1 mAb	Anti-mouse Ig	Dynabead-450	Nilsson *et al.* (1987)
B-cells	Mouse anti -CD1 mAb	Anti-mouse Ig	Dynabead-450	Lea *et al.* (1988)
T-cells		Anti-CD8 Ig	Dynabead-450	Gaudernack *et al.* (1986)
Lymphoma	AB3mAb	Anti-mouse Ig	Dynabead-450	Danielsen *et al.* (1986)
Leukaemia	mAb-biotin	Avidin	CO_2B	Reading *et al.* (1987)
CD34+	*TAC		Rosette Sep™	www.stemcell.com
CD34+	CD34 antibody		CliniMACS	www.miltenyibiotec.com

*TAC: patented bispecific tetrameric antibody complexes. Con A: Concanavalin A. Pro A: Protein A.

StemSep™ is an example of negative systems. The principle of a negative cell separation is shown in Figure 1.1.5.

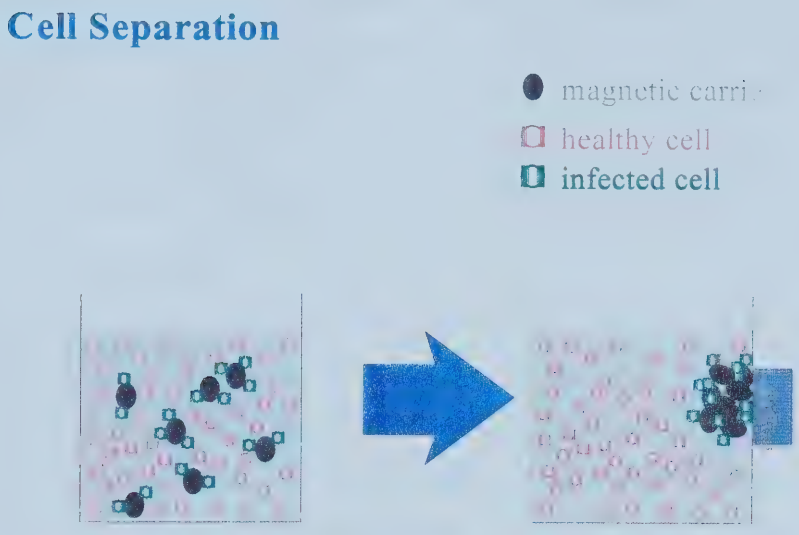

Figure 1.1.5. The principle of cell separation using magnetic nanoparticles

In a negative system the unwanted cells are magnetically labelled. The selective attachment of unwanted cells to the magnetic carriers is accomplished through molecular recognition, which confers magnetic properties to the unwanted cells only. By exposing the biological system in a magnetic column to an external magnetic field, the desired cells (unlabelled) are removed by the column eluent and there is no need to remove them from a separation matrix. It is not necessary to remove magnetic particles from the cells, since the desired cells have not been labelled. Adherent, damaged, and dead cells are removed together with unwanted cells labelled by magnetic carriers. In this type of system, the desired cells have not been labelled with antibody or other agents which may affect cell function and limit options for further analysis.

In positive systems, the wanted cells are magnetically labelled. After isolation of the cells is complete, several methods are available to dissociate the cell-magnetic particle complex for cell recovery. For instance, a polyclonal antibody mixture can be attracted to the monoclonal antibody. Such a mixture will compete with the cell receptor-binding site. Another possibility involves the addition of an enzymatic reagent to degrade the monoclonal antibody, which releases the cells. Both types of protocols are commercially available in the form of prepared isolation kits, and both offer cell recovery in the range of 85 % to 99 %. CliniMACS can be used to purify antigen (Ag) presenting cells: dendritic cells (DC) using a positive system.

Drug delivery

Magnetic carriers can be used as drug delivery vehicles. In this case the functional groups of biocompatible carriers are designed to bind to many therapeutic drugs. These systems should be designed to be biocompatible. Such magnetic carrier-bound drugs can be enriched in a desired body compartment using an external magnetic field or by the targeting of carrier itself.

The drug delivery by magnetic carriers involves two steps. The first step is the delivery of the bound drugs to the desired compartment in an organism, and the second is the release of the drugs from the carrier. Thus, only when this carrier system is delivered to the region of interest and the drug is released, can the drug begin to take effect. The development of magnetoliposomes for such a purpose is particularly promising (Eley *et al.* 1986; Kiwada *et al.* 1986).

Malignant gliomas are the most commonly encountered primary brain tumors in adults. Taking into account the limited permeability of the blood brain barrier, and high cytotoxicity of anticancer drugs, early detection and targeted drug delivery for brain tumors are of great importance. Significant results have already been achieved in the development of optimized magnetic carriers for brain tumor targeting. A series of magnetic microspheres has been tested for their ability to achieve localized drug delivery to brain tumors. Among them are chitosan microspheres with oxantrazole, filled with superparamagnetic iron oxide, Biomag-4125 with covalently linked methotrexate, and aminodextran microspheres filled with superparamagnetic iron oxide. It has been reported that smaller sized uncharged magnetic carriers are

concentrated in brain tumor at significantly higher levels than all microspheres previously studied (Pulfer *et al.* 1999).

Ferrofluids coated with starch polymers can be used as biocompatible magnetic drug delivery carriers. A study confirmed the enrichment of these magnetic carriers in tumor tissue using histological investigations and conventional imaging techniques, i.e. MRI (Alexiou *et al.* 2001).

In the past, various carriers (e.g. albumin and starch microspheres, poly-(alkyl-cyanoacrylate)-nanoparticles, magnetic emulsions, liposomes and magnetic granulas) were used for drug targeting (Gupta and Hung, 1994). In therapeutic experiments, animals such as mice and rats received drug-bound magnetic carriers by intravenous, intraarterial, intracavitary and intraspinal routes. The results from the subcutaneous mouse lymphoma model are promising and show that the locally concentrated magnetic microspheres incorporating a β^--emitting radioisotope are able to eradicate more than half of the tumors (Lübbe *et al.* 1999; Häfeli *et al.* 1996). One of the first applications in cancer patients was undertaken using intravenous injection. Drug targeting with a ferrofluid (1 % of the blood volume) that was bound to epirubicin (dose by itself not sufficient to have an anti-tumor effect) caused complete remissions of human colon as well as renal cancer (Lübbe *et al.* 1996).

Magnetic resonance imaging (MRI)

An atomic nucleus with unpaired electrons gives rise to electric moments and the intrinsic spin and rotational motion of the electrons give rise to magnetic moments. The absorption of electromagnetic radiation at a precise frequency by a nucleus with a nonzero magnetic moment in an external magnetic field occurs, in which case it behaves as a small magnet. In medicine, MRI has been developed to provide images of tissues by magnetic resonance techniques. Magnetic carriers have been used as contrast agents in MRI for localization and diagnosis of brain and cardiac infarcts as well as liver tumors where the particles tend to accumulate at higher levels due to the differences in tissue composition and/or endocytotic uptake processes (Weissleder *et al.* 1987).

Most MR contrast agents used routinely are nonselective and strongly dependent on their particle size as they are more or less intravascular in the initial

experiments. The aim of the present investigation is to design target specific tracers that can be used for detecting morphological and physiological microcirculatory changes of tissues *in vivo* using MR imaging.

It was suggested that the magnetic carriers conjugated to various monoclonal antibodies (Remsen *et al.* 1996), peptides or proteins (Schaffer *et al.* 1993) could achieve target-directed MRI. It was further demonstrated that receptor gene expression and regulation could be visualized *in vivo* by MRI technique (Bogdanov and Weissleder, 1998). Thus, the development of functionalized nanoparticles is expected to provide a break-through in the use of MRI techniques to visualize specific biochemical markers of mental and neurodegenerative diseases. To date, only the clinical descriptive diagnoses are available in these applications. Similarly, various pathological states such as stroke, trauma or brain tumors could be identified with the help of magnetic particle-targeted MRI technique.

A variety of superparamagnetic iron oxides have been developed for different MRI applications (Bulte *et al.* 1997). In brain research, nanodispersed iron oxides have been used for mapping blood brain barrier (BBB) disruption (Bulte *et al.* 1997), as carriers of diagnostic and therapeutic agents across the BBB (Rainov *et al.* 1995), and to improve tumor detection (Zimmer *et al.* 1995).

The use of nonionic surfactant (polyoxyethylene (10) oleyl ether) coated superparamagnetic Fe_3O_4 nanoparticles with narrow size distribution has shown feasibility for *in vivo* MRI of rat brains. Surfactant coating of Fe_3O_4 nanoparticles prolongs their stability (prevents aggregation) in buffered aqueous solutions and allows further chemical functionalization, e.g. by attaching proteins or antibodies to their surface (Kim *et al.* 2001). The intensity difference of energy radiation between fluid in rat brain and injected superparamagnetic Fe_3O_4 nanoparticles was shown by *in vivo* MRI.

Mykhaylyk *et al.* (2001) have tested a set of nanodispersed iron preparations synthesized as MRI contrast agents with special emphasis on the diagnosis and treatment of glial brain tumors. After temporary hyperosmotic disruption of the BBB, they found that intra-carotid injection of nanodispersed iron particles penetrated into the brain tissues of rats having glial brain tumors. These nanoparticles accumulated

predominantly in the brain tumor tissue and perifocal zone at concentrations high enough to cause a significant MRI contrast effect but not in the brain from the reference group. Tumor cells in animals and humans show a much higher uptake of transferrin iron and express very high levels of transferrin receptors compared with normal surrounding tissues. The same is true for various brain tumors, especially glioblastomas (Recht *et al.* 1990). This observation offers opportunity for glial brain tumor targeting using transferrin protein as a vector molecule covalently coupled to the surface of magnetic carrier. The approach has been successfully used for *in vivo* detection of rat mammary carcinoma (Kresse *et al.* 1998).

Cancer therapy

Because of higher sensitivity of tumor tissues to heat, several techniques were developed to increase the local temperature to 42-46 °C in the tumor. Cancer therapeutic effects can also be further increased by combining heating with chemotherapy and radiation, since malignant cells are more sensitive to these treatments at higher temperatures (Brusentsov, 1989; Sneed and Stea, 1996). With currently available external heating systems, it is difficult to selectively heat deep-seated tumors. Magnetic induction heating is one of the proposed methods of overcoming this problem. For this reason magnetic fluid hyperthermia (MFH) has attracted much attention. This method involves the introduction of magnetic particles into the tissues. Irradiation is carried out with an alternating electromagnetic field at RF of 10^4 to 10^7 Hz, and typically, about 1 MHz (Brusentsov, 1989; Chan *et al.* 1993, 1997; Jordan *et al.* 1999). The particles dissipate the energy of the radiowaves into heat by several physical mechanisms (Jordan *et al.* 1997).

MFH has selective activity in cancer cells (Jordan *et al.* 2001). Endocytosis of modified aminosilane magnetite nanoparticles in primary glioblastoma cells, but not in normal glial cells *in vitro,* has been reported previously (Jordan *et al.* 1999). In this report, Jordan *et al* reported a 10-fold higher uptake of nanoparticles by glioblastoma cells than by normal cells. Furthermore, new aminosilane type nanoparticles have been manufactured at the Institute of New Materials (Saarbruecken, Germany). These particles are taken up by prostate carcinoma cells

but not by normal prostate cells, endothelial cells or fibroblasts *in vitro*. The malignant cell exhibits a clearly visible pigmentation in phase-contrast light micrographs due to large nanoparticle uptake in contrast to the adjacent fibroblast.

MX11 cells were exposed to 43–45 °C temperatures either by RF-induced ferrimagnetic hyperthermia or by conventional water bath heating at 44 °C. Typically exposure-dependent cytotoxicities between cytotoxic effects of the two heating methods exhibit no significant differences. Dextran-ferrite (DF) produced by Nikolai *et al* (2001) exhibits sufficiently high specific power absorption (SAR) values that are comparable to other literature data. This technique has been used to estimate that only about 2 mg of Fe in the DF per gram of body tissue for a heating rate of 5 °C/min (Jordan *et al*. 1997).

Before each MFH therapy, CT and MRI are used to verify the appropriate load distribution of the magnetic particles. Positron-emission-tomography (PET) is also used routinely at the clinic to identify metabolically activity. In this case, residual tumor tissues are localized and treated by subsequent magnetic particle applications.

In addition to biocompatibility of magnetic nanoparticles stabilized as a magnetic fluid, MFH also requires an alternating electromagnetic field applicator system (Jordan *et al*. 2001). Besides RF, microwave and ultrasound applicators, self-regulating thermobeads (Brezovich and Meredith, 1989; Tucker *et al*. 1995), which are heated by an externally applied alternating electromagnetic field have also been used. In this case, the migration of the seeds is a limiting factor, which causes a decrease of the SAR because of thermal under dosage (Brezovich *et al*. 1990). Dextran magnetite complex generates heat when placed in an external alternating electromagnetic field (Mitsumori *et al*. 1996). The MFH selectively heats up tissues by coupling alternating electromagnetic fields to targeted magnetic fluids as such that boundary of different conductive tissues do not interfere with power absorption. Therefore MFH is a completely new approach for deep-tissue hyperthermia applications (Wust *et al*. 1996). The technical and medical requirements of such an applicator system in terms of field homogeneity, accuracy of field, strength and

frequency, safety, choice of treatment volume, thermometry and clinical quality assurance, has been largely underestimated.

The use of thermosensitive magnetoliposomes associated with local hyperthermia has been attempted in cancer therapy (Amigorena and Bonnerot, 1998; Berthier *et al.* 2000; Rodriguez-Paris *et al.* 1993).

In one study, one hundred twelve patients with glioblastoma multiformae (GM) received hyperthermia. The results demonstrated significantly improved survival rates of GM patients, with acceptable toxicity (Sneed *et al.* 1998). At the end of 2000, the first prototype of a clinical MFH therapy system was set up at the Charité Medical School, Campus Virchow-Klinikum, Clinic of Radiation Oncology in Berlin (Jordan *et al.* 2001). With the equipment used in this therapy system, brain tumors as well as prostate and other cancer entities can be treated homogeneously with the required alternating magnetic field. The system is equipped for thermal mapping, so that during alternating magnetic field application the temperature can be measured on-line in the target region and at free eligible reference points. The temperature profile and other relevant data such as power and setup parameters are displayed on a computer during therapy. System control and thermometry have been implemented with new application software. The alternating magnetic field strength is manually adjusted to the desired steady-state temperature in the tumor, i.e. the average temperature of at least three target measurement points. Ideal candidates for MFH brain tumor applications are circumscribed glioblastomas, brain metastases, and residual disease after glioblastoma resection and recurrent brain tumors.

Recently, it was reported that scientists in Germany have succeeded in using magnetic forces to guide gene therapy in animal experiments (Mckinney, 2002).

1.1.6. Application of magnetic carriers—challenges

Challenges in MCT include superparamagnetism; desired particle size; biocompatibility; specific functionality for target recognition; strong magnetization; low magnetic aggregation; chemical stability and large surface area for high capacity; regeneration and sterilizability; carrier homogeneity and process economics. Of these

characteristics, the most important properties are superparamagnetism, size and targeting (Xu *et al.* 1999).

Superparamagnetism

Paramagnetic materials remain magnetized only when an external magnetic field is applied. This property is beneficial for two reasons: 1) The magnetic material will be retained while the field is applied, and released upon the field's removal. 2) The material will not aggregate after the field is removed. In contrast, ferromagnetic and ferrimagnetic materials remain magnetized after external field removal. The remaining magnetism often induces magnetic aggregation. However, in general, paramagnetic carriers are attracted to a magnetic field much more weakly than ferromagnetic or ferrimagnetic materials. Materials with high magnetism, but paramagnetic, would be ideal candidates for MCT. Materials with this type of magnetic property are known as superparamagnetic materials. These materials have a small crystal diameter, usually around 50 nm. In single-domain spherical particles, this critical diameter represents the volume at which magnetization can be reversed by an applied field. The term "single-domain particle" refers to a magnetic particle that undergoes uniform magnetization (Halliday *et al.* 1988). This behavior is equivalent to that displayed by paramagnetic materials, with one important difference in superparamagnetic materials, that is the magnetic moment is more than 10^5 times larger than that seen in paramagnetic materials (Garcia *et al.* 1999). Also, with carriers being in the submicron and nanosize range, the residual magnetic field can be considered negligible. As a result, permanent magnetization can be avoided and magnetic flocculation minimized. Not surprisingly, the characteristics of the magnetic materials determine their potential range of applicability.

Desired size-nanosize

The magnetic carriers used in bioseparations are typically immobilized on microcapsules or particles that range in size from 25 nm to 20 μm. The latter particles are generally constructed from cross—linked polymer strands.

The desired size of the magnetic carrier depends on the specific application since both extremes of the size range can be advantageous. Previously, enzyme

immobilization required the use of submicron carriers in order to achieve a sufficiently high surface area to counteract the loss of enzyme activity. For the separation of bio-molecules, magnetic carriers of 0.5 to 2 μm diameter (e.g. Biomags®) have been reported to be optimal (Menz *et al.* 1986). For the separation of cells, magnetic carriers of 5 μm diameter (e.g. Dynabeads®), which are of similar size to the cells themselves appear to be the most convenient, however, this technique was only used *in vitro.*

Currently, these particles are of great interest for biomedical applications *in vivo* (medical imaging, drug targeting, gene therapy and hyperthermia treatment of tumors). For these applications, it is important to avoid mechanical instability (i.e. sedimentation under gravity) and magnetic flocculation, a phenomenon in which magnetic particles agglomerate due to magnetic forces.

Hyperthermia treatment of tumors needs to generate heat locally and evenly in tumors. The magnetic carriers must localize deep inside the patient's body, to minimize heating of the rest of the organism and maximize effectiveness of transformation of the RF field energy into heat. Success depends on the frequency and on the nature of the particles, including size (Chan *et al.* 1993; Jordan *et al.* 1997; Chan *et al.* 1997; Jordan *et al.* 1999). Therefore, proper selection of the particles and the field parameters is extremely important for effective treatment.

It is known that suspensions of magnetic particles often become aggregated if the particle size is too large. Rubin (1994) has followed the kinetics of particle aggregation after sonication, by measuring the increase in light transmission. His observation suggests that the more stable the suspension, the more effective it is in producing excellent negative MRI contrast.

A solution to this size dilemma is to develop neutral nanoparticles (superparamagnetic materials) with adsorbed ligands that prevent aggregation. With particles being in the nanosize range, the residual magnetic field can be considered negligible and thermal energy and surface forces prevail. As a result, mechanical instability can be avoided and magnetic flocculation is minimized.

Nanosize particles provide additional advantages. The large particle has a much higher surface area, increasing non-specific protein binding. Since many immunological responses rely on surface antigen recognition, the nanosize should result in a reduced immunological response (Everett *et al.* 2001). Iron-based magnetic carriers in the nanosize have improved magnetic properties and would be superior to the existing iron oxide-based carriers. Nanosize magnetic particles would also greatly facilitate delivery of the magnetic label to the target cells (www.stemcell.com), as show in Figure 1.1.6.

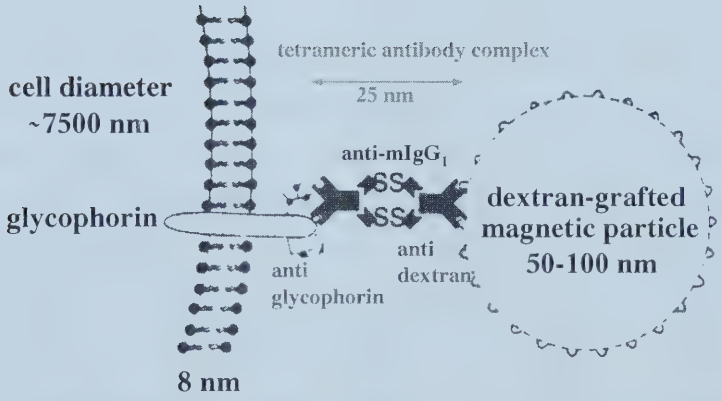

Figure 1.1.6. Relative size of magnetic particles for antibody–antigen complexes

Nanoparticles 10 nm or smaller are required before functionalization for effective transportation through the extracellular spaces (a few tens of nm) in the brain. Their size increases when coating specific bio-molecules onto the particle surface.

Indeed, particle size is an important concern when considering diffusion within a tissue or escape from a reticuloendothelial system. Large particles can also

physically irritate the surrounding tissue or even embolize small blood vessels and capillaries, effects that must be taken into account for specific applications.

Targeting

Molecular recognition between magnetic carriers and targets is critical in the application of MCT. To make a target magnetic, the target has to be recognized by and attached to a magnetic carrier. This requires the magnetic particles to be functionized, usually by derivatizing a surface or by putting a specific ligand onto the particle that could be recognized by targets. In its application, MCT refers to the tailoring of physical, chemical and surface properties of magnetic particles to enable selective attachment of molecules to the carrier for targeting.

One of the aims of targeting therapy is to target medications in order to minimize side effects which are major problems associated with most chemotherapy drugs used to treat cancer. Most chemotherapeutic drugs produce severe side effects because they act throughout the body, not just on tumor cells. Using magnetofection to improve the targeting of gene therapy may minimize some side effects. Magnets have been applied to improve the targeting of cancer drugs. This involves linking the drugs to superparamagnetic nanoparticles that are attracted to magnetic fields. Once these drugs are introduced into the blood vessels that supply a tumor, a strong magnetic field is applied to attract the nanoparticles, and the drug to which they are attached, to the tumor (McKinney, 2002).

Targeting cells by magnetic carriers is the first step in cell sorting (Olsvik *et al.* 1994), cell-based genetic therapy; targeted hyperthermia treatment of tumors (Mitsumori *et al.* 1996) and in detection with MRI (Weissleder *et al.* 1997; Yeh *et al.* 1993; Yeh *et al.* 1995; Schoepf *et al.* 1998). One of two approaches can be used in this step, either 1) attaching magnetic carriers to the cell surface (Handgretinger *et al.* 1998) or 2) internalizing biocompatible magnetic particles by fluid phase endocytosis (Yeh *et al.* 1993; Schoepf *et al.* 1998); receptor mediated endocytosis (RME) (Moore *et al*, 1998) and phagocytosis (Weissleder *et al.* 1997). The first approach is often used *in vitro* applications (Tsai *et al.* 1992). The second approach is for cells that possess high-efficiency in internalizing receptors. The fluid phase pathway and phagocytosis are relatively inefficient (Schoepf *et al.* 1998).

Magnetic targeted delivery techniques might include molecular recognition based on specific interactions between antibody-antigen, biotin-streptavidin or cell receptor-ligand. Magnetic concentration, injection through a catheter into a local artery combined with magnetic particle retention (Kuznetsov *et al.* 1997), or a combination of the above are additional targeted delivery techniques.

1.2. Surface engineering of magnetic particles used as targeted carriers

1.2.1. An overview of targeted magnetic carriers

The recognition of targets by magnetic carriers can be considered as a key-lock relation as shown in Figure 1.2.1.1. The targets (locks) vary from infected cell to ions. In biological applications, the keys could be antibody, streptavidin or specific ligands.

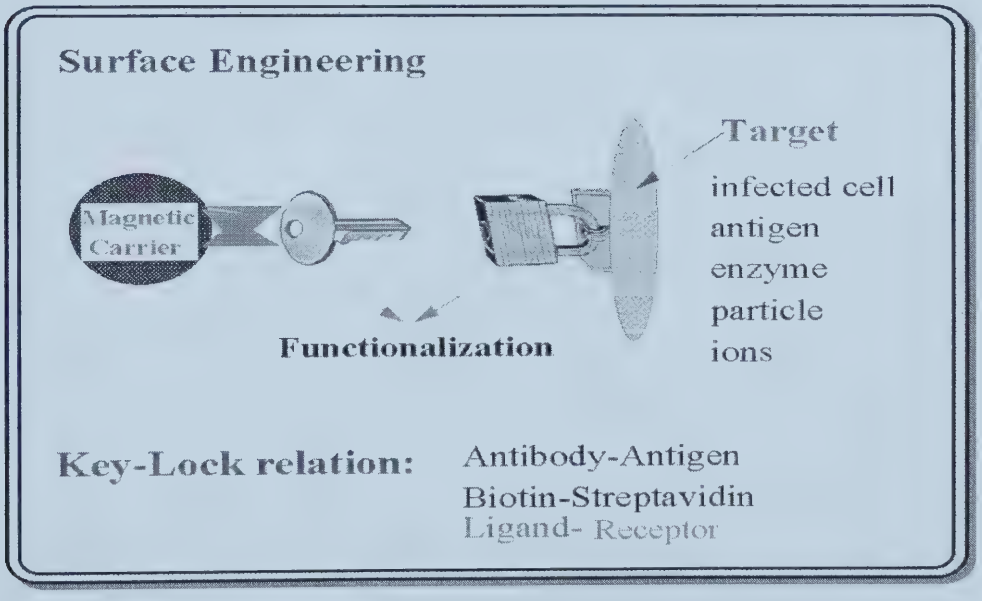

Figure 1.2.1.1. Key-Lock relationship for targeting carriers.

A variety of surface modification methods to incorporate desired functional groups onto the particle surface have been discussed (see section 1.1.3). The incorporated functional groups of the modified particles have been used for covalent binding, via different activation procedures, of an antibody, streptavidin or specific

ligands to the particle surfaces. The conjugated particles are then used for applications such as imaging, specific cell labelling and cell separation, hyperthermia treatment of tumors and drug delivery.

Suitable polymers can be used for functionalization. Hydrophilic polymers yield different functional groups that can bind enzymes and ligands covalently by means of one of their amino residues in conjunction with a derivatization agent. In some cases the derivatizing agent is a spacer.

Some of the possible derivatization schemes are shown in Figure 1.2.1.2.

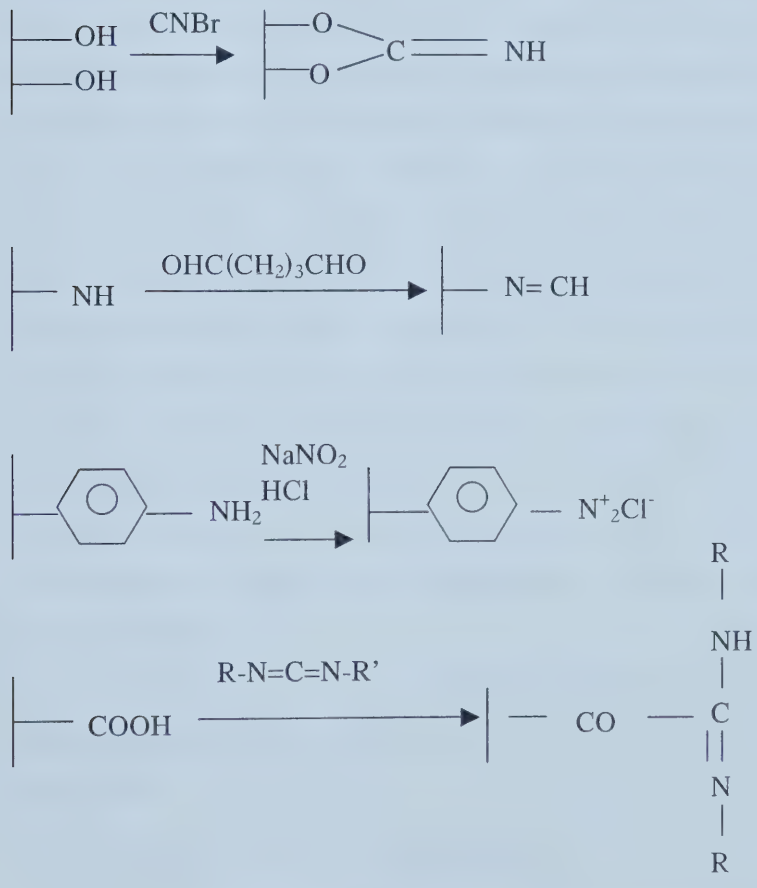

Figure 1.2.1.2. Typical derivatization methods used in the design of desired magnetic carriers

Polymers with hydroxyl groups such as polysaccharides (1) can be derivatized by the cyanogen bromide (CNBr) method (Kronick and Gilpin, 1986). Polymers with

amino group (2) are often preferred because they can be derivatized easily by glutaraldehyde, which yields highly reactive groups (Patton *et al.* 1985). Polymers with diaminobenzene groups (3) can be derivatized cheaply using the diazotization method (Chagnon *et al.* 1987). Polymers with carboxyl groups (4) carry negative charges at pH values corresponding to physiological conditions, which avoid non-specific adsorption. The carboxyl groups can be derivatized by the carbodiimide method (4) (Malaiya and Vyas, 1988).

From a molecular perspective, the binding process between "Key" and "Lock" (see Figure 1.2.1.1), for example antibody and antigen, can be viewed as moving from an electrostatic interaction to solvent displacement, then to steric selection, and finally to charge and conformational rearrangement (Alberts *et al.* 1994). As "Key" approaches "Lock" from 20 to 10 nm, coulombic attractive/repulsive forces dominate. In this region, both the lock and the key reorient themselves so as to maximize attractive interactions. If this interaction is stronger than the repulsive forces, the process continues with the goal of adjusting orientation. The second step in molecular recognition, which occurs from 10 to 1 nm, involves the displacement of solvent molecules. The third step in the molecular recognition process involves steric fit and the matching of groups, which allows for attractive interactions. Various conformational changes are involved in both the key and the lock molecules in this step. The final step in the molecular recognition process comprises charge redistribution and conformational rearrangement. These processes eventually bind the key to the lock.

"Key-Lock" interactions could also involve noncovalent interactions such as hydrogen-bonding, ionic-bonding, and hydrophobic interactions, as well as van der Waals forces.

1.2.2. Targeted magnetic carriers

Magnetic particles with antibody complexes

In vertebrates, the immune system protects the organism from invading pathogens and cancer. This defence system generates proteins known as immunoglobulins or antibodies. In general, these proteins consist of two identical

heavy chains (V_H domain) and two identical light chains (V_L domain) linked by disulfide bonds that recognize a specific region (epitope) on the foreign substance (antigen). Each of these chains contains a variable sequence in the amino-terminal, with the rest consisting of conserved sequences.

The heavy-chain constant region determines the class of antibody (IgM, IgG, IgD, IgA, or IgE) and thus its function. The variable regions of both chains contain several hypervariable domains known as complementarity-determining regions (CDRs). These CDRs form the antigen-binding site, which in turn determines the specificity of the antibody.

Another important aspect of the antibody structure relates to the hinge region in which the two heavy chains are united. This area exhibits conformational flexibility, which allows a relative motion of lateral combining site. This motion, in turn, increases CDR availability for binding.

Studies of antigen binding have revealed that more residues on the heavy chain CDRs bind with antigen than residues in the light-chain CDRs. Thus the V_H domain seems to be more intensely involved in antigen binding than the V_L domain. In addition, the formation of the antibody-antigen complex often produces conformational changes in one or both of the bio-molecules. These changes tend to facilitate a stronger interaction. The functions of the constant region in the antibody are mostly to influence conformational changes and other biological functions in an immune system.

Every cell shows specific antigenic properties, which allow this cell to be recognized by a specific antibody (Ab) and, therefore, antibodies are the most appropriate ligands for use in targeting carriers. Antibodies are extremely expensive but subsequent improvements in the technology of producing monoclonal antibodies (mAb) by hybridoma cells have reduced the production cost to a viable level. Three methods are used to label the cell surface antigens (Ag) with magnetic carriers. In the direct method, the Ab linked to the carriers is specifically adsorbed onto Ag present on the targeted cell. In the indirect method, the ligand (anti-Ab) linked to the carriers is attached to an antibody (1st Ab) specific to the antigen present on the targeted cell. The third method is shown in Plate 1.2.2.

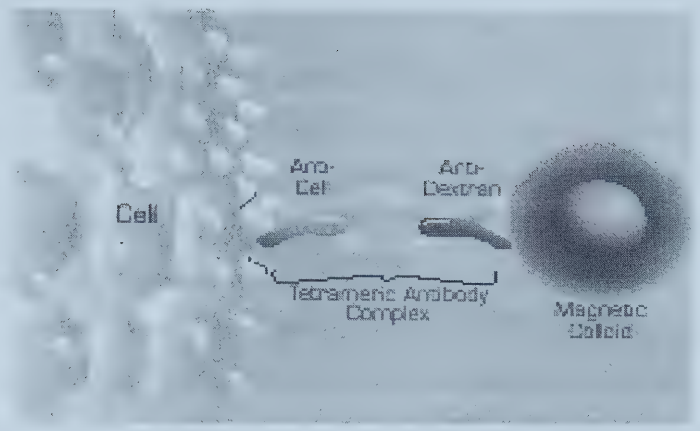

Plate 1.2.2. Magnetic particles with antibody as targeting carriers (www.stemcell.com)

Targeted cells (human) are cross-linked to magnetic carriers (for example: magnetic dextran iron particles) using tetrameric antibody complexes comprised of two murine IgG mAb held in tetrameric array by two rat anti-mouse IgG mAb molecules (www.stemcell.com). One murine Ab molecule recognizes the Ag on surface and the other recognizes the dextran on the magnetic carriers.

An example for using magnetic particles-antibody carriers was demonstrated by Tchikov *et al* (2001). Experiments were performed with human leukemia cell-line REH and albumin-based immunomagnetic carriers prepared as described by Winoto-Morbach *et al* (1994). Briefly, the carriers were prepared by high-pressure homogenization of emulsions containing albumin and magnetite. Pressures were chosen to prepare carriers of mean diameter of 0.5 to 1 μm. The magnetic particles activated with tosyl chloride were covalently coupled with anti-Bw6 monoclonal antibody to form carriers. HLA-Bw6 antigen-positive cells were cultured at 37 °C in 5 % CO_2, and washed with PBS. The carriers were added to the cell sample, incubated at 4 °C for 15 min, and without wash submitted to the magnetophoresis device for cell count.

Magnetic particles with streptavidin-biotin complexes

In recent years, biotechnologists have become intrigued by the strong interaction between the vitamin biotin and egg-white avidin ($K_D = 10^{-15}$ M). This interest results from the need to manipulate bio-molecules in biotechnology settings (Garcia *et al.* 1999). The biotin-avidin interaction is almost irreversibly, could satisfy this need, as biotin-labelled bio-molecules can be isolated using immobilized avidin. Because avidin is glycosylated and highly alkaline, it can also bind other molecules, such as the sugar-binding lectins (Garcia *et al.* 1999). To minimize these nonspecific interactions, researchers have attempted to remove the carbohydrate residues. As yet, these approaches have not borne fruit. This is because avidin is not susceptible to glycosidases. Another strategy for minimizing nonspecific interactions relies on an analogous molecule known as streptavidin. This molecule, which is obtained from the bacterium *Streptomyces avidinii*, is a tetramer with two-fold symmetry. It consists of four identical 14 kD subunits, each with a high affinity for biotin. The subunits are arranged as two pairs located on opposing faces of the molecule. This bacterial protein displays remarkable similarity with avidin in terms of its biotin-binding properties. On the other hand, it is not glycosylated and is not as basic as avidin. Nevertheless, streptavidin provides not only a high affinity-binding site, but also a high capacity for binding biotin or biotinylated molecules, because of its tetrameric structure (Wilchek and Bayer, 1990).

The detection of receptors for cytokines and hematopoietic factors typically of low density associated with surfaces of cells is of great scientific interest. Since cells can respond to cytokine stimulation even when the number of receptors is low, the importance of new techniques of high sensitivity for low-density receptor detection is evident. Adhesion is the basis behind many techniques with detecting immunospecific molecules on surfaces of cells, and adhesive interactions can be investigated by using immunospecific particles as research tools (Florin *et al.* 1994; Pierres *et al.* 1996). As a result, as few as 200 tumor necrosis factor (TNF) receptor molecules per cell could be detected with streptavidin-coated magnetic particles coupled to biotinylated TNF carriers (Tchikov *et al.* 2001). The adhesion of magnetic particles to the surfaces of target cells was evaluated by counting the number of

magnetically labelled cells using magnetophoresis that involves measuring the velocity of the cell (Tchikov *et al.* 1999). Cells treated with magnetic particles as described above were detected and counted differentially as magnetically labelled and unlabeled cells. The calibration of the magnetic force and the sensitivity of detection due to the high gradient of the magnetic field were evaluated by measuring magnetophoresis of erythrocytes containing methemoglobin as described previously (Winoto-Morbach *et al.* 1994). Briefly, cells labelled with a single carrier per cell were detectable by magnetophoresis. Despite the recent progress in developing the instrument for velocimetry (Chalmers *et al.* 1999), it still suffers from the poor rate of measurement compared to the fluorescence-activated cell sorter (FACS), which is capable of measuring multiparameter signals from many thousands of cells per minute (Tchikov *et al.* 2001). This is important for measuring cell subpopulations for a clinical laboratory analysis (Müller-Ruchholtz *et al.* 1998). Such measurements can be performed without velocimetry by counting the number of cells in a similar manner as done with a hemocytometer, and this approach was employed successfully for detecting cell surface Ag in Tchikov's previous study (Tchikov *et al.* 1999).

Biotin–streptavidin binding was practically irreversible under the experimental conditions. The sensitivity of the method was defined by the minimum number of bio-TNF molecules detectable on cell surfaces (Tchikov *et al.* 2001). It is evident that magnetic particle-streptavidin carriers are sensitive probes for detecting the biotinylated cytokines bound to their respective cytokine receptors. Regarding their practical value, the findings can be of interest in applications of biotinylated TNF to investigation of the TNF receptor expression regulation, or for increasing the therapeutic index of TNF, and such therapy has been recently employed (Moro *et al.* 1997). In the prospective development of method, with further improvement of sensitivity of the labelling system along with increased magnetic field gradients, it may be possible to detect cell-bound ligands by the magnetophoresis method with sensitivity comparable to the biological sensitivity of cells responding to cytokine signal. Thus, immunomagnetic carriers can serve as sensitive probes for evaluating the expression of low-density receptors on cells (Tchikov *et al.* 2001).

Magnetic particles with ligand complexes targeting receptors

Cells communicate either through direct contact or via the secretion of chemical substances that are recognized by a receptor in the target cell. In the latter case, cell receptors can appear on the surface of the cell or inside the cell. If the receptor is located on the surface of the cell, then the receptor-ligand complex forms at the cell surface. If the receptor is inside the cell, however, the ligand must diffuse through the cell membrane or be transported by vesicles. Cell receptors act as signal transducers, converting the binding event into signal inside the cell that modulates its behavior.

From the above studies, magnetic carriers can target one kind of specific cell or organ by a special receptor on its cell surface. If this receptor is unique, the magnetic carriers can target only this cell and organ. This is very useful in MRI, cell sorting, cancer therapy and drug delivery. Moore *et al* (1988) measured transferrin receptor gene expression by NMR imaging, but until now very little work has been done in this area. This has been our specific area of interest.

1.3. Asialoglycoprotein receptor- ligand for targeting to hepatocyte cells

1.3.1. Asialoglycoprotein receptor (ASGPR)

A receptor responsible for the specific binding of asialoglycoproteins was originally identified as a constituent of rat liver plasma membranes (Pricer and Ashwell, 1971). This receptor was then isolated from whole rabbit liver (Hudgin *et al.* 1974) and characterized as a homogeneous glycoprotein of known molecular weight (MW) (Kawaski and Ashwell, 1976b) and carbohydrate sequence (Kawaski and Ashwell, 1976a) from chicken liver. Later it was further isolated from a variety of hepatic subcellular organelles, including the Golgi complex, the smooth endoplasmic reticulum (microsomes), and lysosomes (Pricer and Ashwell, 1976). On the basis of molecular techniques, it has been deduced that the murine ASGP receptor is comprised of two subunits, murine hepatic lectin-1 (MHL-1) and MHL-2 (Hong *et al.* 1988; Takezawa *et al.* 1993). In rats, three distinct bands were visualized by Cooomassie Blue staining with apparent MW of 43, 54, and 64 kDa, which were

designated RHL–1, RHL–2, and RHL–3, based on rat hepatic lectin (RHL). While the human lectin (HL) was initially believed to consist of a single polypeptide H1 of 41 or 46 kDa, the presence of a second subunit H2 was later established (Bischoff and Lodish, 1987; Spiess and Lodish, 1985; Spiess *et al.* 1985).

The isolated binding protein has been characterized as a water-soluble glycoprotein in which sialic acid, galactose, mannose and glucosamine comprising 8 % of the total molecule (Kawasaki and Ashwell, 1977).

The potential involvement of the carbohydrate moiety of the ASGPR in the binding reaction was suggested by the observation that the binding capacity of this receptor, a sialylated glycoprotein, was shown to be highly dependent upon the integrity of its normal complement of sialic acid residues (Pricer and Ashwell, 1971; Hudgin and Pricer, 1974).

The binding reaction between asialoglycoprotein and ASGPR is a saturable process. The process is proportional to receptor concentration as well as the structure of carbohydrate and NH2-terminal amino acid recognition motifs of H1 and H2 subunits of ASGPR association with HA-2 adaptor complex and clathrin in hepatocyte cell membrane coated pit.

This receptor, well described in intact (Ashwell *et al.* 1974) and perfused liver (Dunn *et al*, 1980) and in isolated hepatocytes (Steer and Ashwell, 1980; Schwartz *et al.* 1980; Weigel, 1980; Baenziger and Fiete, 1980) is an abundant protein. Around 500,000 surface ligand-binding sites were found per cell (Schwartz *et al.* 1980; Schwartz *et al.* 1981b). The purification and characterization of the receptor have been facilitated by its relative abundance (Hudgin *et al.* 1974).

1.3.2. Hepatocytes expressing ASGPRs

The main cells of the liver are known variously as hepatocytes, liver parenchymal cells, liver cells and polygonal cells. The name polygonal cell arose from the appearance in histological slides of fixed tissue. Usually blood vessels (the sinusoids) are located at two or three aspects of the cell. These two or three aspects possess microvilli that are protected from erythrocytes by the sinusoidal lining. The rest of the cell is usually in close contact with other hepatocytes. However, near the

sinusoids the cells diverge slightly from each other, forming small spaces in which extracellular fluid can collect. The functions of the liver depend not only upon the great metabolic capacity of hepatocytes, but also upon the properties of the cells that physically separate hepatocytes from blood. The two main other cell types are endothelial and Kupffer. The endothelial cells are similar in many aspects to those of other organs, but contain pores which vary in size up to 10 nm in diameter. In most mammals, there is no base membrane, however there is one in the calf and mouse liver epithelium. Endothelial and Kupffer cells are now considered to be of different origins. The Kupffer cells form a very important part of the liver, but are not peculiar to the liver (Andrews, 1979).

Hepatocytes are highly differentiated and are of characteristic appearance. They are polygonal in shape and have six or more surfaces. They have a well-defined membrane that is probably only a condensation of the peripheral protoplasm of the cells. Most hepatocytes have one large round nucleus, although bi-nuclei liver cells are not at all uncommon. Hepatocytes are easy to aggregate.

The liver of many different species contains a unique ASGPR responsible for the rapid serum clearance and lysosomal catabolism of desialylated glycoprotein bearing terminal non-reducing galactose residues. The ASGPR is localized on the hepatocytes (Pricer and Ashwell, 1971), and consequently, the liver has been recognized as a target for receptor-mediated delivery via the ASGPR (Wu *et al.* 1983). Thus, genes targeted to this receptor can be delivered specifically to the liver (Findeis *et al.* 1994). At least in the human, little information is available regarding its tissue distribution outside of the liver. In a study by Park *et al* (1998), antibodies were raised against the H1 major subunit of the human ASGPR using synthetic peptide antigens, and their binding specificity was confirmed by enzyme linked immunosorbent assay. Cell surface analysis by fluorescence-activated flow cytometry on various human tissue cell lines confirmed hepatocyte cells as the major expression site of ASGPR. Nonetheless, ASGPR was also detectable on the Jurkat T-cell line (Park *et al.* 1998). The determination of extrahepatic expression of ASGPR will have consequences in analyzing the biological role of this receptor complex as

well as having implications in designing ASGPR-mediated drug or gene delivery strategies.

ASGPR studies have been limited to the examination of ligand binding in perfused liver or to isolated hepatocytes in short-time culture until Schwartz *et al* (1981a) were able to identify a continuous hepatocyte cells line which expresses ASGPR. Their study described the characterization and quantity of the ASGPR in the human hepatoma cell line Hep G2. However, freshly isolated rat hepatocytes attained maximal ability to express ASGPRs (Steer and Ashwell, 1980).

The Hep G2 hepatoma cell line provided a convenient model to investigate receptor biosynthesis (Stockert, 1995). The Hep G2 ASGPR displays characteristics nearly identical with those of the rat or rabbit hepatocyte receptor. It is specific for asialoglycoprotein, requires Ca^{2+}, and is sensitive to neuraminidase.

1.3.3. Ligand specificity to ASGPRs on hepatocytes

Asialorosomucoid (ASOR)-galactose-terminal protein from human α_1-acid glycoprotein and galactose-derivatized complexes can be targeted specifically to hepatocytes by cell surface ASGPRs (Park *et al.* 1998; Wu *et al.* 1989).

Studies of the membrane components of human lymphocytes, granulocytes, and monocytes have identified a glycoprotein of MW = 52,000, which shows a striking similarity with human α_1-acid glycoprotein (Yoshima *et al.* 1981). α_1-Acid glycoprotein is also unique to the liver.

Early experiments focused on the delivery of agents to ASGPR on Hep G2 using galactose-terminal complexes. These agents were covalently bound to galactose-terminal carriers such as asialofetuin (Wu *et al.* 1983, 1985; Keegan-Rogers and Wu, 1990), ASOR (Wu *et al.* 1988), galactose-terminated neoglycoproteins (Ponzetto *et al.* 1991; Fiume *et al.* 1981) and asialoglycoprotein-polylysine (ASOR-PL) (Findeis *et al.* 1994).

Asialorosomucoid (ASOR)

Glycoproteins are proteins that bear carbohydrate chains. α_1-Acid glycoprotein (orosomucoid) is one of the glycoproteins isolated from the plasma of

various mammals. It is distinguished from other plasma glycoproteins because it contains far more carbohydrate, including a large amount of sialic acid, than other plasma proteins. For this reason, it is highly soluble in water (Gahmberg and Anderson, 1978). Once the terminal sialic acids are removed, these circulating serum glycoproteins are rapidly and specifically cleared from the circulation by an ASGPR–mediated process (Ashwell and Morell, 1974). This desialylated α_1-acid glycoprotein has terminal, nonreducing galactose residues, and is sialic acid free orosomucoid (ASOR) (Yoshima *et al*, 1981).

Kawasake and Ashwekk (1977) showed that the removal of the terminal sialic acid from plasma proteins results in the formation of ASOR bearing galactosyl residues as the newly formed, terminal sugar. In mammalian species, the latter are recognized by an ASGPR whereby the entire protein is removed from the circulation, transported into the hepatocyte, and catabolized in the lysosomes.

Acidic asparagine-linked sugar chains of α_1-acid glycoprotein (orosomucoid) display species differences (Yoshima *et al.* 1981). Human α_1-acid glycoprotein contains 5 to 6 acidic asparagine-linked sugar chains per protein molecule. α_1-Acid glycoprotein (orosomucoid) of pooled normal human plasma has been shown to be heterogeneous on starch-gel electrophoresis. Near its isoelectric point (pH 2.7), this protein resolves into several polymorphic forms. After removal of the sialic acid residues, two main bands were noted near pH 5. The protein present in these two bands appears to represent genetically determined variants. Orosomucoid of human origin is analyzed by sodium dodecyl sulfate-polyacrylmide gel electrophoresis (SDS-PAGE) and shows a single band at an apparent MW of 44,000 (Findeis *et al.* 1994). The MW of human ASOR was found to be around 40,000 (Steer and Shwell, 1980).

Galactose derivatized complexes

Early experiments focused on the delivery of agents covalently bound to carriers such as asialofetuin and galactose-terminated neoglycoproteins. The ASGPR-mediated endocytosis of the asialoglycoproteins carried the bound agent into cells (Fundeis *et al.* 1994). Simple galactosyl residues coupled to polyethylenimine

(PEI) gave an efficient vector that selectively transfected hepatocytes via ASGPR-mediated endocytosis (Zanta *et al.* 1997). When 5 % of the PEI nitrogen was grafted with a galactose structure, small and stable particles were formed upon complexation with plasmid DNA. These carriers were essentially toroids having a size of 50-80 nm and a zeta-potential close to zero (Bettinger *et al.* 1999).

A foreign gene can be targeted to hepatocytes, and the resultant gene expression made to persist by using ASOR-poly- (L-lysine)-DNA complex. This soluble DNA carrier system consists of two covalently linked components. One is poly-(L-lysine) that can bind DNA in a strong but non-damaging interaction and the other is ASOR that can bind ASGPRs. This galactose-derivatized complex can be targeted specifically to hepatocytes via the cell surface ASGPR, which is unique to this type of cells (Wu *et al.* 1988).

1.3.4. Asialoglycoprotein receptor-mediated endocytosis

The ASGPR provides an unusually well characterized model to study the uptake of specific ligands by hepatocytes related via a receptor-mediated endocytosis (RME).

RME is a universal mechanism for the uptake of macromolecules by cells. The inhibition of RME of galactose-terminating glycoproteins by receptor-specific antibodies confirmed that their uptake was initiated by binding to ASOR or galactose derivatized complexes on the surface of hepatocytes (Baeniziger and Fiete, 1986).

As shown that in Figure 1.3.4, the ASGPR binding site is ASOR recognition motifs. It is a lattice at the vertices of a triangle with sides of 15, 22, and 25 Å (ASGPR trimer). Galactose (Gal–1) and Gal–2 of the triantennary oligosaccharide of ASOR are bound to RHL-1, and Gal-3 is bound to RHL-2/3 of ASGPRs (Stockert, 1995). To initiate internalization at a coated pit, soluble coating components (HA-2 and clathrin triskelions) in membrane associate with ASGPR trimer invaginate to form coated vesicles (Pearse, 1981).

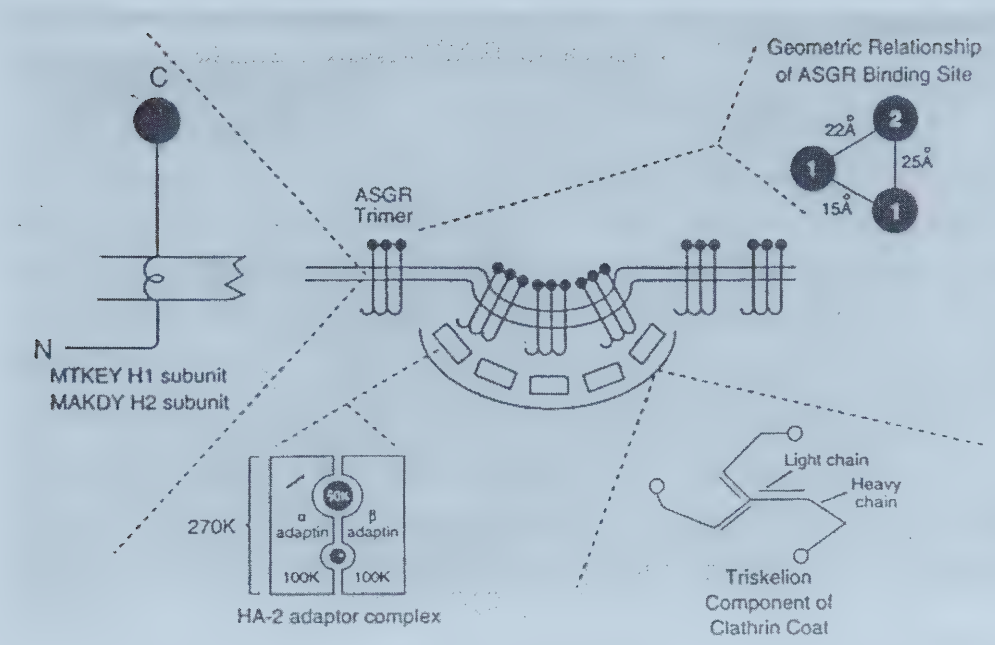

Figure 1.3.4. Receptor association with HA-2 adaptor complex and clathrin in plasma membrane coated pit (Stockert, 1995)

Once a receptor-ligand complex migrates into a coated pit, it is internalized in the clathrin-coated vesicle. The formation of the coated vesicle is short lived. The newly formed smooth vesicles will fuse with a lysosome, and a digestive vacuole (secondary lysosome) will be formed in which lysosomal hydrolases are put in contact with the endocytosis material. This results in the dissociation of the receptor-ligand complex. It is assumed that after dissociation, the receptor is recycled back to the cell surface to be reutilized and the ligand was catabolized within the body of this organelle (Tanabe *et al.* 1979; Tuikens *et al.* 1977; Tolleshaug *et al.* 1979; Steer and Ashwell, 1980).

1.3.5. Targeting genes to hepatocytes by ASGPRs

Gene transfer techniques include the uses of retrovirus (Mulligan, 1991), adenoviruses (Rosenfield *et al.* 1992), REM (Wu and Wu, 1988), direct injection and liposomes. Receptor-mediated targeted delivery of DNA has been successfully applied using protein ligands directed to the hepatic ASGPRs (Wu and Wu, 1988; 1991). A major advantage to the use of ASGPR is that it is a cell surface receptor

that is highly selective for hepatocytes. Thus, genes targeted to this receptor can be delivered specifically to the liver.

Wu and Wu (1988) have developed a system for targeting foreign DNA to hepatocytes *in vitro* using a soluble DNA carrier that takes advantage of RME to achieve internalization. ASOR was chemically coupled to poly- (L-lysine) to form a conjugate (Li *et al.* 1973). Various proportions of conjugate DNA were tested to determine conditions that maximized DNA content in a soluble complex and limited solubility of complexes. To test the targetable gene delivery system, ASOR-poly- (L-lysine) conjugate was complexed with the plasmid pSV2CAT containing the gene for chloramphenicol acetyltransferase (CAT) driven by an SV-40 promoter (Gorman *et al*, 1982). They used a model system consisting of human hepatoma cell line Hep G2. The results showed that Hep G2 cells incubated with the complex were transformed as indicated by the appearance of CAT activity.

The ASGPR-mediated endocytosis of the glycoproteins carried the bound agent into cells. These hepatocyte-directed vectors have been developed that includes one key feature thought to favor *in vivo* gene delivery to the liver: electrostatically neutral carriers that avoid nonspecific binding to other cells. This system is based on a 5 % galactose-bearing polyethylenimine (PEI-gal) polymer that is condensed with plasmid DNA to neutrality. Hep G2 cell lines were transfected 10^4 to10^5-fold more efficiently than murine fibroblasts, when transfection was assessed by histochemical staining (beta-galactosidase). Approximately 50 % of the hepatocytes were selectively transfected in the presence of 10 % serum. Transfection was suppressed by removal of the targeting galactose residues, by their replacement with glucose. The results from comparative and competitive experiments clearly indicate that the ASGPR is involved in transfection of hepatocytes with neutral PEI-gal/DNA complexes.

Wu *et al* (1989) presented evidence that a foreign gene driven by natural mammalian regulatory elements can be targeted to hepatocytes by ASGPR-mediated endocytosis and the resultant gene expression made to persist.

All of the above studies suggest that the liver can be targeted by galactose-teriminated complexes through ASGPRs on the cell surface hepatocytes of the liver.

2. HYPOTHESIS AND OBJECTIVES

HYPOTHESIS

The liver has been recognized as a useful target for receptor-mediated delivery via the asialoglycoprotein receptor (ASGPR), a cell surface receptor that is highly selective for hepatocytes. Galactose-terminal glycoprotein (ASOR) can target specifically to hepatocytes by binding to the ASGPR. Receptor-mediated delivery is more efficient than fluid phase endocytosis pathways. The hydrophilic properties of carriers reduce or prevent tendencies of carriers to aggregate and to bind nonspecifically to cells.

It is therefore postulated that galactose-derivatized superparamagnetic nanoparticles (Gal-beads) may be used as potential hepatocyte-targeted carriers by exploiting ASGPR-mediated endocytosis.

OBJECTIVES

There are four main objectives to this project:

- To prepare and characterize galactose-derivatized superparamagnetic nano-particles.
- To develop an assay to quantify ASGPR on the surface of Hep G2 cells (a human continuous hepatocytes cell line), based on ^{125}I-ASOR binding.
- To evaluate the toxicity of Gal-beads (Hep G2 cell line).
- To characterize the uptake of Gal-beads by Hep G2 cells *in vitro*.

The long-term pharmaceutical goals of this approach include the magnetic separation of hepatocyte cells, diagnostic magnetic resonance imaging (MRI) of the liver and hyperthermia treatment of liver tumors. Such carriers are also expected to be of particular importance as delivery devices for cell-based genetic therapies (i.e. bring DNA into hepatocytes). It is envisaged that it may be possible to augment the localization of a biologically active substance delivered by targeted magnetic nano-carrier technology through selective localization strategies such as the application of external magnets.

3. EXPERIMENTAL

3.1. Materials

Lactose monohydrate, calcium chloride, sulfuric acid, potassium carbonate anhydrous, sodium chloride, sodium iodide, dibasic sodium phosphate, monobasic sodium phosphate, dimethyl sulfoxide and ammonium persulfate were purchased from BDH Inc., Canada. Acetic anhydride, methanol, sodium hydroxide, chloroform and HPLC water were purchased from Caledon Laboratories LTD, CANADA. Sodium cyanoborohydride, phenol, resorcinol, copper sulfate, isoamyl alcohol, sodium metabisulfite, galactose, mannose and chloramine-T hydrate were purchased from Aldrich Chemical Company Inc., USA. Cellulose dialysis tubing (T_2 membrane 6000 to 8000 Da MWCO) and Surestain^{TM} Wright-giemsa were purchased from Fisher CANADA. Sialic acid was obtained from ChemAlta, Edmonton. Hydrochloric acid was purchased from EM Science, an Associate of Merck Germany. ^{125}I in sodium hydroxide solution was purchased from Amersham CANADA. Orosomucoid (α_1 –acid glycoprotein, bovine and human), iodogen (1,3,4,6-tetrachloro-3α,6α-diphenyl glycouril, BSA (bovine serum albumin), glutaraldehyde, SDS, EDTA, glycine, Tris base (Tris [hydroxymethyl] aminomethane), MTT (3-[4,5-dimethylthiazol-2yl]-2,5-diphenyl- tetrazolium bromide), cytochrome C and 5-bromo-2'-deoxyuridine were obtained from Sigma-Aldrich. Acrylamide/bisacrylamide solution (40 %), SDS-PAGE molecular weight marker and TEMED (*N,N,N',N'*-tetramethylethylenediamine) were obtained from BIO-RAD USA. Developer and fixer were obtained from Kodak CANADA. The Hep G2 cell line (liver tumor) was obtained from the American Type Culture Collection (ATCC) USA. Fetal Bovine Serum (FBS; 10 %) was purchased from Cansera, CANADA. The 143B human osteosarcoma cell line was supplied by Aihua Zhou, Faculty of Pharmacy and Pharmaceutical Sciences, University of Alberta. HEPE buffer solution (1 M), which contained HEPES (N-2-hydroxyethylpiperazine-N'-2-ethane sulfonic acid 238 g/L) in water, was purchased from Sigma-Aldrich CANADA. Trypsin-EDTA was purchased from Gibco BRL.

3.2. Superparamagnetic nanoparticles

3.2.1. Characteristics

Magnetic nanoparticles and amino-activated magnetic nanoparticles, in the form of nanoparticle colloidal suspensions, were provided by Dr Xu's laboratory (Department of Chemical and Materials Engineering, University of Alberta). Dr Xu's group also supplied the transmission electron microscope (TEM) micrograph and the diagram of the superparamagnetic characteristics of these nanoparticles.

Size distribution

The size distribution was measured with a dynamic light scattering scanning (BI-90, Brookhaven Instruments Corporation, New York, U.S.A) particle sizer. To reduce the dust contamination, distilled water, with the same buffer as the nanoparticle colloidal solution, was filtered through a 0.45 μm membrane filter, and after mixing the nanoparticle colloidal suspension, one drop of the suspension was added to a cuvette. The cuvette was placed in the instrument sample compartment, which was at ambient temperature (20-25 °C) during the measurement. During the laser-illuminating step, the movement of the particles was measured and the size and size distribution was calculated.

Zeta potential

The zeta potential measurement was carried out using a Zetaphoremeter III (SEPHY/CAD INSTRUMENTATION FRANCE) fitted with a rectangular cell, a pair of hydrogenated palladium electrodes, a laser-illumination system and video (CCD camera)-viewing system. About 50 mL of colloidal solution was used to fill the electrophoresis cell. Through the laser-illuminating and video-viewing system, the movement of particles at the stationary layer in the cell was tracked 5 times for each direction by alternative change of positive/negative electrode potential. Then the software analyzed the captured images and provided the value for the zeta potential along with other information such as mobility, conductivity and concentration of solution. The environmental temperature was kept at 22±0.1 °C during measurement. Each test was repeated, and the value was reported as an average of three runs.

Usually the error was less than 5 %, except at high electrolyte concentration (10^{-2} M), when a 10 % variation was obtained.

3.2.2. Stability studies

One year after preparation, the size and zeta-potential of magnetic nanoparticles (nanoparticle colloid solutions) were re-determined using the same methods described above.

3.3. Galactose-derivatized superparamagnetic nanoparticles (Gal-beads)

3.3.1. Preparation and characterization

Preparation of Gal-beads

As shown in Figure 3.3.1, Gal-beads were synthesized from the amino-terminated magnetic nanoparticles and lactose in the presence of a reducing agent such as sodium cyanoborohydride.

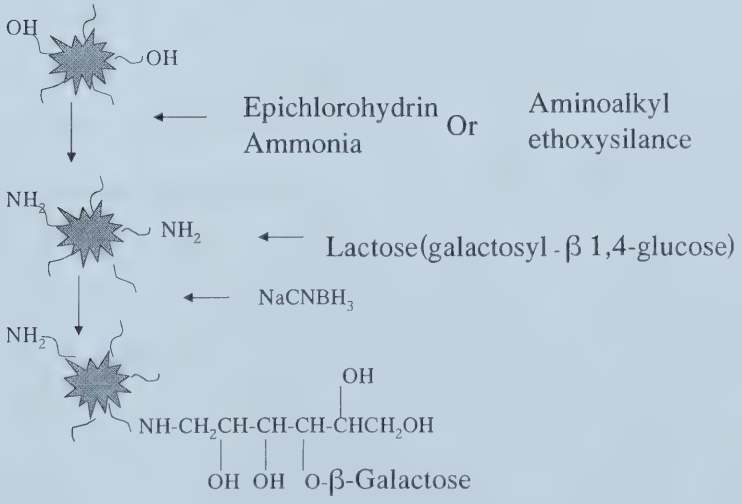

Figure 3.3.1. Principle of preparation of Gal-beads

Procedure: Amino-terminated magnetic nanoparticles (250 mg) in colloidal suspension were placed in a reaction bottle. Lactose (1 mM; 3 mL) was added to this suspension. After mixing well, sodium cyanoborohydride (5 mM in 3 mL water) was then added and the resulting suspension was gently shaken 3-4 times a day for 7 days. On the final day, the particles were settled by placing a magnet on the bottom of the reaction bottle. The aqueous layer was removed with a pipette and the reaction bottle was filled with fresh water (5 mL). The mixture was briefly shaken, the particles again settled with the aid of a magnet and the water removed. This washing procedure was repeated five times with water and then with water/ methanol 1/1 (3x) and finally methanol (2x). Then methanol (4.5 mL) containing acetic anhydride (0.5 mL) was added to the particles and the mixture shaken for 3 h (once per h), to cap any free amines. Finally the particles were washed in the reverse order of the previous cycle and diluted with 5 mL water.

Neutral particles (Control particles):

Amino-terminated magnetic nanoparticles (250 mg) in colloidal suspension were placed in a reaction bottle, with methanol (4.5 mL) containing acetic anhydride (0.5 mL). The mixture was shaken over 3 h (once per h). The particles were washed with methanol 5 mL (2x), water/methanol (1/1), 5 mL (3x) and with water 5 mL (5x), as before. The particles were stored in 5 mL water.

Determination of galactose content on Gal-beads

Procedure: Eight screw cap Pyrex® culture tubes (13x100 mm) were labelled and charged with the following: 0, 40, 60, 80, 100 and 120 μL of galactose standard solution (1 mg/mL), suspended Gal-beads (2 mL), or neutral particles (2 mL), respectively. The standard solution volume of each tube was brought to 2 mL with distilled water and 5 % phenol reagent (1 mL) was added to each tube. Concentrated sulfuric acid (4 mL) was carefully added to each tube and the tubes were sealed and mixed for 1 min. The samples were then allowed to stay still at room temperature for 15 min. The spectrophotometer was set to a wavelength of 490 nm and the instrument was zeroed with water as the blank. The absorbance of each of the standards and samples was measured and the absorbance versus μg of galactose for

the standards was plotted (see Figure 4.2.1). The galactose content of the Gal-beads was estimated from the standard curve.

3.3.2. Stability of Gal-beads

The size and quantity of galactose were re-determined on Gal-beads one month later after coupling the galactose onto the magnetic nanoparticles using the previous procedure.

3.4. ASGPR assay of Hep G2 cell line with ^{125}I-ASOR

Receptor (ASGPR)-mediated endocytosis of Gal-beads by hepatocytes (Hep G2) *in vitro* was studied. An estimate of the number of receptors on Hep G2 cells was estimated using ^{125}I-ASOR.

3.4.1. Preparation and analysis of ASOR

Preparation of ASOR

Orosomucoid (bovine serum) and orosomucoid (human serum) (10 mg) were separately dissolved in 1 mL of water. An equal volume of 0.1 N sulfuric acid was added to the solution, and the resulting mixture was heated at 80 °C for 1 h in a water bath to hydrolyze terminal sialic acids from the glycoprotein. The acidolysis mixture was removed from water bath, neutralized with aqueous 0.1 N NaOH, dialyzed against water for 2 days using cellulose dialysis tubing and then lyophilized for 24 h. The ASOR obtained by this method was collected, weighed and stored in a container at 4 °C.

Sialic acid content of ASOR

Preparation of reagents:

To prepare amyl alcohol, isoamyl alcohol (200 mL) was mixed with concentrated hydrochloric acid (1 L), and the solution was left for a week. The alcohol was washed with water (200 mL; 10x), dried over anhydrous potassium carbonate, and then distilled. The fraction with a b.p. of 130-133 °C was used.

To prepare resorcinol reagent, resorcinol (2 g) was dissolved in distilled water (100 mL). Ten mL of this solution was added to hydrochloric acid (80 mL) containing copper sulfate (0.25 mL of 0.1 M). The volume of the reagent was made

up to 100 mL with distilled water. The reagent was prepared at least 4 h prior to its use. The solution was stable for a week when stored in the refrigerator.

To prepare standard solution, sialic acid (1.1 mg) was dissolved in distilled water to 10 mL. Standard solutions (150 μL, 300 μL, 450 μL and 600 μL) contain 16.5 μg, 33.0 μg, 49.5 μg and 66.0 μg of sialic acid, respectively.

To prepare sample solutions, ASOR (2.1 mg) was dissolved in distilled water to 12 mL. Orosomucoid (2.5 mg) was dissolved in distilled water to 12 mL. These solutions (2 mL) contain 350~400 μg of ASOR and orosomucoid, respectively.

Procedure:

The samples (2 mL) were pipetted into three tubes. Resorcinol reagent (2 mL) was added to two of the tubes (test samples) and 2 mL of blank reagent was added to the third tube (sample blank). The standard solutions were prepared in the same manner. The tubes were heated for 15 min at 110 °C in an oil bath. After heating, the tubes were cooled under tap water (~14 °C). Amyl alcohol (5 mL) was then added and the tubes were shaken vigorously. The tubes were placed in ice water for 15 min, then the contents were transferred to centrifuge tubes, and spun at 800 r.p.m for one min. The tubes were placed in ice water again and left there until amyl alcohol phase was transferred to a cuvette and read at 580 nm. From the sialic acid standard curve (see Figure 4.3.1) and the absorbance of ASOR and orosomucoid (see Table 4.3.1.4), the residual sialic acid content of ASOR (a) and orosomucoid (b) were calculated and reported as a percent of original orosomucoid sialic acid content.

3.4.2. Labelling of ASOR with ^{125}I

The chloramine-T method

ASOR (100 μg) was mixed with approximately 1 mCi of $Na^{125}I$. Fresh chloramine-T (CT; 10 μL of 2.5 mg/mL) was added to the reaction vial and the mixture was gently shaken for 30 sec. Then fresh sodium metabisulfite (Na-Met; 10 μL of 5 mg/mL) was added to the mixture and shaken gently for 15 sec. Finally, fresh sodium iodide (NaI; 20 μL of 1 M) was added, and the whole mixture was gently shaken for 5 sec. The mixture was loaded onto a prepacked Sephadex PD-10-desalting column (containing Sephadex G-25M pre-washed 3 times with PBS). The

vial was rinsed with PBS and the washing aliquot was transferred to the column. The column was then eluted with PBS and each eluent fraction (300 μL) was collected separately in numbered tubes. The radioactivity of each tube was measured with a Packard Minaxi γ AUTO-GAMMA® 5000 Series. The fractions containing the ASOR were pooled in tubes, labelled, placed in containers and stored at 4 °C.

Iodogen labelling technique

Procedure: A glass test tube (12x100 mm) was plated with 200 μL of iodogen solution (2.5 mg iodogen/50 mL chloroform) and labelled. The solvent was evaporated with a steady stream of N_2 gas. ASOR (50 μL; 2 mg/mL) was added to this tube. To another glass test tube was added phosphate buffer (20 μL, 0.5 M, pH 7.1) and $Na^{125}I$ (1 mCi). The solution was mixed well, and then the phosphate buffer and $Na^{125}I$ mixture was transferred to the iodogen-containing tube. The mixture was incubated for 45 min at room temperature with occasional gentle agitation. The mixture was removed from the tube and placed in a clean glass test tube. The reaction was stopped by adding aqueous NaI (70 μL; 1 N) to the reaction mixture. This reaction mixture was allowed to stand for 20 min at room temperature. Separation of ^{125}I-ASOR was carried out by gel-filtration with a prepacked Sephadex PD-10-desalting column containing Sephadex G-25M. Before the Sephadex G-25M was used, ASOR (20 mg in 1 mL of PBS) was percolated through it, followed by a 25 mL PBS wash. The reaction mixture was loaded onto the column, and the reaction tube was rinsed with PBS and likewise transferred to the column. The column was eluted to separate the materials on it and each eluent (300 μL) was collected separately in numbered tubes. The radioactivity of each eluent was monitored with a Packard Minaxi γ AUTO-GAMMA® 5000 Series. The fractions containing the ASOR were pooled, labelled, placed in containers and stored at 4 °C. Total recovered ^{125}I-ASOR was determined photometrically at 280 nm. Totally three labelling were conducted.

Stability study: The labelled product (^{125}I-ASOR) was stored in a refrigerator at 4 °C. Stability was checked after two weeks and four weeks, using this gel-filtration procedure.

Electrophoresis (SDS-PAGE)

Preparation of reagents:

To prepare 4x Tris 6.8 solution, Tris base (6.05 g) and SDS (0.4 g) were dissolved in distilled water to 40 mL. The pH was adjusted to 6.8 with 1 N HCl, and this solution was added to distilled water to make 100 mL. The final solution was filtered through a 0.45 μm filter and stored at 4 °C.

To prepare 4x Tris 8.8 solution, Tris base (91 g) and SDS (2 g) were dissolved in distilled water to 300 mL. The pH was adjusted to 8.8 with 1 N HCl, and the solution was added to distilled water to 500 mL. The final solution was filtered through a 0.45 μm filter and stored at 4 °C.

To prepare concentrated running buffer (5x stock solution), Tris base (15.0 g), glycine (72.0 g) and SDS (5.0 g) were dissolved in distilled water to 1 L. The solution was stored at 4 °C. For each run, 60 mL of this concentration stock solution was diluted with 240 mL of distilled water.

To prepare sample buffer, distilled water (3.8 mL), Tris-HCl (0.5 M; 1.0 mL), glycerol (0.8 mL), 10 % (w/v) SDS (1.6 mL), β -mercaptoethanol (0.4 mL), and 0.5 % (w/v) bromophenol blue (0.4 mL) were mixed and the buffer was stored at 4 °C.

To prepare 10 % ammonium persulfate (APS), APS (10 g) was dissolved in distilled water to 100 mL. This solution is freshly prepared prior to use.

Procedure:

A 10 % polyacrylamide separating gel solution was prepared according to the protocol in Table 3.4.2.1. The separating gel solution was added into the assembled gel chamber and water-saturated isobutyl alcohol was overlaid on the top of separating gel solution until the gel was polymerized (~1 h). The water-saturated isobutyl alcohol was removed. The stacking gel solution was prepared as indicated in Table 3.4.2.2. The stacking gel solution was poured on the top of the separating gel, and the comb was inserted directly into the stacking gel until it polymerized (~45

min). After polymerization was complete, the gels were placed into the running chamber. The running buffer was added into the running chamber. The samples were prepared as indicated in Table 3.4.2.3 and heated at 95 °C for 5 min. The samples, including the molecular weight marker, were loaded carefully in the sample pockets and the gel was run at 100 V until that the blue dye reached the end of gel.

Table 3.4.2.1. Separating gel solutions.

Components	5 %	7 %	10 %	15 %
40 % AA/Bis	1875 µL	2625 µL	3750 µL	5625 µL
4xTris 8.8	3750 µL	3750 µL	3750 µL	3750 µL
Distilled Water	9375 µL	8375 µL	7500 µL	5625 µL
10 % APS	50 µL	50 µL	50 µL	50 µL
TEMED	10 µL	10 µL	10 µL	10 µL

Table 3.4.2.2. Stacking gel solution.

Components	**Amount**
40 % AA/Bis acrylamide (Bis)	500 µL
4xTris 6.8	1250 µL
Distilled Water	3750 µL
10 % APS	25 µL
TEMED	5 µL

Table 3.4.2.3. Preparing samples.

Components	**Amount**	**PBS**	**Sample Buffer**
Marker	7 µL (7 µg)	0 µL	
Orosomucoid	5 µL (5 µg)	10 µL	15 µL
ASOR	2.5 µL (5 µg)	12.5 µL	15 µL
Labelled-ASOR	15 µL	0 µL	15 µL

Autoradiography

Procedure: Aliquots (15 µL) of ^{125}I-ASOR (2-3 x 10^6 cpm) were run on a 10 % acrylamide gel as described in the procedure for electrophoresis. The gel was air-dried. In a darkroom, the sample (dried gel) was placed in the film cassette, and the sample was covered with plastic wrap to prevent it from sticking to the film. A sheet of X-ray film was placed on top of the sample, then closed and secured the film cassette. The film was exposed for the desired length of time (24 h) and at the

appropriate temperature (-20 °C). After the exposure, the removed film was developed as follows. The film was immersed in the developing solution for 5 min at 18 to 20 °C, and then washed (1 min) in running water at room temperature. The film was then immersed in fixing solution for 5 min at 18 to 20 °C, then washed (15 min) in running water and allowed to dry.

3.4.3. ASGPR assay of Hep G2 and 143B cell lines

Cell line culture

Trypsin solution was prepared by diluting from 10x trypsin-EDTA with PBS buffer. 10x trypsin-EDTA contains 0.5 % trypsin and 5.3 mM EDTA-4Na [prepared with 5.0 g of trypsin (1:250), 2.0 g of EDTA-4Na and 8.5 g of NaCl/L]. The trypsin solution was stored at –5 to –20 °C.

EMEM (Eagle's minimum essential medium) for Hep G2 was purchased from ATCC, and stored at 2 to 8 °C when not in use. The liquid medium was used directly when it was pre-warmed to 37 °C.

EMEM (Eagle's minimum essential medium) for 143B was purchased from Gibco BRL. The powder was stored at 2 to 8 °C in the dark and kept dry. Preparation of liquid medium from powder involved dissolving the powder in 970 mL of distilled water. The powdered medium was added to water with gentle stirring, and the inside of package was rinsed to remove all traces of powder. Then, $NaHCO_3$ (3.7 g) was added to the solution. The solution was diluted to the desired volume (1 L) with water, and stirred until the entire solid had dissolved. The pH of medium was adjusted to 0.2-0.3 pH units below desired final working pH because pH will usually raise 0.1-0.3 units after filtration. The pH was adjusted by adding 1 N NaOH or 1 N HCl, then the container was kept closed until the medium was filtered. The medium was sterilized immediately by membrane filtration, and this medium was stored at 4 °C until use.

Hep G2 cells from ATCC were thawed by gentle agitation in a water bath at 37 °C. Thawing should be rapid (approximately 2 min). All of the operations were carried out under strict aseptic conditions. The thawed cells were transferred to a 75 cm^2 tissue culture flask and diluted with the recommended complete culture medium.

It is important to avoid excessive alkalinity of the medium during recovery of the cells. Prior to the addition of the Hep G2 cells, the culture flask containing the growth medium was placed into the incubator for at least 15 min to allow the medium to reach its normal pH (7.0 to 7.6). The cell culture was then incubated at 37 °C in a suitable incubator (5 % CO_2 in air atmosphere).

Hep G2 cells were maintained in Eagle's minimum essential medium with Earle's BSS and 2 mM L-glutamine (EMEM) that is modified by ATCC to contain 1.0 mM sodium pyruvate, 0.1 mM nonessential amino acids and 1.5 g/L sodium bicarbonate supplemented with 10 % fetal bovine serum. Incubation of the cultures was carried out at 37 °C with a 5 % CO_2 in air atmosphere and propagated every 4-5 days by trypsin.

Osteosarcoma, 143B TK^- human cells were maintained in 90 % Eagle's minimum essential medium in Earle's BSS with 0.015 mg/mL 5-bromo-2'-deoxyuridine, 10 % fetal bovine serum. This cell line is thymidine kinase deficient (TK^-) and is resistant to 5-bromo-2'-deoxyuridine. Cultures were incubated at 37 °C with a 5 % CO_2 in air atmosphere and propagated every 3-4 days by trypsinization.

Propagation of Hep G2 and 143B: Hep G2 grows slower and is sticker than 143B, so the time of trypsinizing cells for subculture or cell counting is critical. First, the medium was removed from the tissue culture flask, and enough PBS was added to cover the cell monolayer for washing (2x). The flask was swirled to distribute the solution evenly, and then the buffer was removed. After the final wash, 1 mL of trypsin solution was added to cover the cell monolayer. The flasks were placed in an incubator at 37 °C until the cells just began to detach (8-10 min for Hep G2 and 3-4 min for 143B). The adherent cells were loosened, and the cells were viewed under microscope (CK 40-F100, Olympus Optical Co, Ltd Japan) to check whether all cells had detached from the growth surface. When all cells had detached, medium-containing serum (9 mL) was added to the cells to inactivate the trypsin. The cells were gently pipetted to make sure cell clumps were broken up. The cells were then centrifuged at 1,000 x *g* for 10 min (DYNAC Centrifuge, CAT, No. 0101, Becton, Dickinson and Company, U.S.A) and the supernatant was discarded. The pellet was suspended in 10 mL of medium-containing serum until cell clumps were broken up.

The cells were then counted using a hemocytometer and distributed to fresh flasks for subculture.

Wright-stain of Hep G2: Hep G2 cells were seeded in six-well plates 3 days prior to staining. At the time of staining, each well was washed with 1 mL PBS (2x). 500 μL aliquots of 75 % alcohol was added to the well as fix solution and kept the well at room temperature for 10 min. After the cells were dried, one drop of Surestain™ Wright-giemsa was added to each well and staining was allowed to proceed at different intervals (20 sec, 30 sec, 40 sec and 1 min). Each well was washed with distilled water and dried. The cells viewed under phase contrast microscope (ECLIPSE, TS 100, Nikon, Japan), and pictures were recorded at 100x magnification.

Quantification of ASGPR on cell membranes

Procedure:

Hep G2 cells were seeded in tissue culture dishes 5 days prior to assay (0.3-0.5x10^6 cells/dish). At the time of assay, the cells were near confluence (1-1.5x10^6 cells/dish). 143B cells were seeded 2 days prior to assay (0.3-0.5x10^6 cells/dish). At the time of assay, the cells were near confluence (1-1.5x10^6 cells/dish). Dishes were incubated for 5 min at room temperature in EMEM (no FBS). Cells were then incubated for 5 min at 4 °C in PBS containing 1.7 mM Ca^{2+}. The PBS was removed. PBS (1 mL) containing 1.7 mM Ca^{2+}, 0.2 mg of cytochrome C and 2 μg of ^{125}I - ASOR (117-138 x10^6 Bq/μg) was added to each dish. The dishes were incubated for 2 h at 4 °C. At that time, the dishes were rinsed with 1 mL of PBS (3x). Diluted trypsin (1 mL) was added to each dish and allowed to stand 30 min. The radioactivity was counted in the Packard Minaxi γ AUTO-GAMMA® 5000 Series.

One set of dishes was allowed to bind ^{125}I-ASOR in this procedure and thereafter was rinsed and incubated for 15 min at 4 °C with PBS containing 5 mM EDTA.

Estimation of the number of cell surface ASGP receptors:

Cell surface ASGP receptors were estimated using the following formula:

$[(A \times 10^{-9} \times 6.023 \times 10^{23})/ 10^6 \times B]$ (Schwartz *et al*, 1980).

A is the quantity of cell membrane bound ^{125}I –ASOR in nanograms. It was derived from the following equation.

A=[(radioactivity of cell membrane bound ^{125}I –ASOR)/ radioactivity of total added ^{125}I -ASOR)] x (protein quantity of total added ^{125}I -ASOR). B is the molecular weight of ASOR.

ASGPR competition binding study

Hep G2 cells (1-1.5x10^6 cells/dish) were incubated with 1 mL PBS containing 1.7 mM Ca^{2+}, 2 μg of ^{125}I–ASOR (117-138 x10^6 Bq/μg) and 0.2 mg of cytochrome C at 4 °C for 60 min. The cells were washed to remove unbound ^{125}I–ASOR. Mannose (100 μL, 650 mM) was added to each of the first six dishes, to reach the final concentration of 65 mM per dish. Similarly, galactose (100 μL, 650 mM) was added to each of the second six dishes to reach a final concentration of 65 mM per dish, orosomucoid (200 μg) was added to each of the third six dishes, and PBS (1 mL) containing 5 mM EDTA was added to a fourth six dishes. Each had replicate reaction. Cells were again incubated at 4 °C and the residual cell-bound radioactivity was determined on samples removed at timed intervals (0, 15, 30, 60, 90 and 120 min). Radioactivity was counted using a Packard Minaxi γ AUTO-GAMMA® 5000 Series.

3.4.4. Toxicity of Gal-beads on Hep G2 cells

The toxicity of galactose-derivatized superparamagnetic nanoparticles (Gal-beads) to hepatocytes (Hep G2) *in vitro* was determined using the following procedure. The cells were suspended in EMEM medium supplemented with 10 % fetal bovine serum (FBS) and diluted to 8x10^3 cells/mL, and then plated in 100 μL volumes into 96-well micro plates. The cells were incubated at 37 °C, 5 % CO_2 for 24 h. The test Gal-beads were diluted to final concentrations of 3 mg/mL, 300 μg/mL, 30 μg/mL, 3 μg/mL, 0.3 μg/mL and 0.03 μg/mL. Aliquots (100 μL) of these bead suspensions were added to 10 wells of a 96-well plate. As a control, EMEM (100 μL) was added to cells in 10 of the wells, instead of beads. As a background, EMEM (100 μL) was plated in wells without cells. The plates were incubated for 5

days at 37 °C in a humidified atmosphere containing 95 % air and 5 % CO_2. At the end of incubation, MTT (50 μL of a 1 mg/mL solution) was added to each well. The plates were incubated at 37 °C for 4 h. The medium was aspirated from the plates, leaving about 20 μL of medium in each well. Since living cells metabolize the MTT in their mitochondria and formed blue crystals, 150 μL of DMSO (dimethyl sulfoxide) was then added to each well and the plates were shaken (15 min) to dissolve the formed crystals. The plates were then read immediately at 540 nm on an ELISA plate reader (Vmax kinetic microplate reader, Molecular Devices Corp., Sunnyvale, Ca), and the percent viability of cells was calculated. The average of the experimental 10 wells was subtracted from the average of 10 wells containing no cells (background) and divided by the average of the control Hep G2 (no beads). For each MTT assay, the control Hep G2 (no Gal-beads) cell viability was by definition 100 %.

3.5. Cell-uptake study

3.5.1. Uptake of Gal-beads

Preparation of cell culture media:

C-EMEM was EMEM (Eagle's minimum essential medium) liquid medium containing 10 % (v/v) FBS (sterile fetal bovine serum) and was used for Hep G2 cell culture. H-EMEM (HEPE-EMEM) was EMEM liquid medium containing 20 mM HEPES buffer solution. The solution had a pH 7.2 to 7.5 and a pKa 7.3 at 37 °C. Media were stored at 2 to 8 °C.

Procedure:

Hep G2 cells were seeded onto tissue culture dishes (35 mm plastic) 2, 3, 5 days prior to assay ($0.3\text{-}0.5 \times 10^6$ cells/dish). At the time of assay, pre-warmed PBS (1 mL) was used to wash each dish (2x). Gal-beads (200 μL per dish) and pre-warmed H-EMEM (1 mL) were dispersed evenly over each dish. The dishes were incubated at 37 °C for 2 h. At that time, the dish was washed with PBS (1x), and the C-EMEM (1 mL) was added to each dish. The dishes were further incubated at 37 °C for 24 h. Then, each dish was washed with 1 mL PBS (3x). Aliquots (500 μL) of 70 % alcohol were added to each dish as fix solution, and then the dishes were kept at room

temperature for 10 min. Each dish was washed with PBS (1 mL; 3x), and then kept in PBS. The cells viewed under a phase contrast microscope (ECLIPSE, TS 100, Nikon, Japan), and pictures were recorded at 40x, 100x, 200x and 400x magnifications.

3.5.2. Galactose-challenge binding study

The experimental conditions were the same as described for the uptake of Gal-beads (above) except for the following changes: Galactose was added to three dishes, to a concentration of 65 mM, followed by incubation for 30 min, 1 h and 2 h with Gal-beads. Pictures were taken with phase contrast microscope (ECLIPSE, TS 100, Nikon, Japan) at 100x magnifications.

4. RESULTS AND DISCUSSION

4.1. Superparamagnetic nanoparticles

4.1.1. Physical properties

Size and size distribution:

Dr Xu's laboratory in Department of Chemical and Material Engineering at University of Alberta prepared two types of particles in the form of nanoparticle colloid suspensions. These two types of particles are designated particles (1) and particles (2).

The sizes of particles (1) and (2), as well as the size of particles (1) and (2) after one year of storage at room temperature (RT) were determined with a dynamic light scattering scanning (BI-90, Brookhaven Instruments Corporation, New York, U.S.A) particle sizer. The results are shown in Table 4.1.1. The original data are shown in Appendix.

Table 4.1.1. Volume average sizes of two batches of particles after preparation and one year of storage at RT.

Particles Batch	After Preparation (nm)	One Year Storage at RT (nm)
1	61	86
2	127	141

Size distribution by weight is plotted on a semilog scale resulting in a symmetrical curve. Assuming particles of different sizes are of equal density, the weight distribution is equal to the volume distribution. Thus, the volume fraction in a given size class is equal to the weight fraction in that size class. The volume average size is frequently the desired result, in order to ascertain where the largest fraction of the total particle mass is located (Provder, 1996). Volume average size of particles

(1) was found to be 61 nm. Size distribution was 10 % below 37 nm; 25 % below 46 nm; 50 % below 58 nm; 75 % below 72 nm and 90 % below 89 nm (see Figure 4.1.1.1).

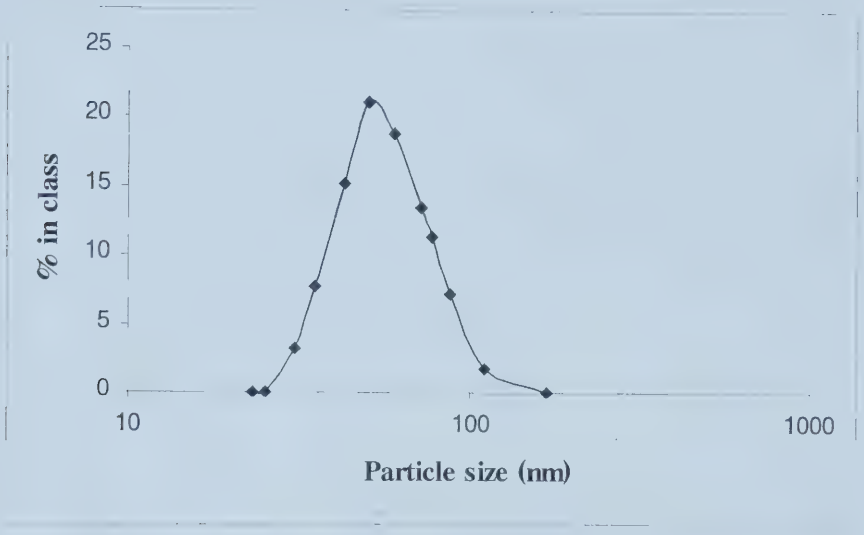

Figure 4.1.1.1. Size distribution of particles (1) (Dynamic light scattering scanning particle sizer).

The volume average size of particles (2) was 127 nm (see Table 4.1.1), and the size distribution was found to be 10 % below 63 nm; 25 % below 83 nm; 50 % below 114 nm; 75 % below 156 nm and 90 % below 207 nm.

The particle size was determined again after one year of storage at RT and the results are as follows. Volume average of particles (1) was 86 nm (see Table 4.1.1) after one year of storage at RT as compared to the original size of 61 nm. Size distribution was 10 % below 48 nm; 25 % below 61 nm; 50 % below 80 nm; 75 % below 104 nm and 90 % below 131 nm. The volume average size of particles (2) was 141 nm (see Table 4.1.1) after one year of storage at RT (the original size was 127 nm). Size distribution was 10 % below 70 nm; 25 % below 93 nm; 50 % below 127 nm; 75 % below 173 nm and 90 % below 229 nm.

Size and size distribution of the particles (1) were also determined by Beckman coulter particle analyzer. The instrument was provided courtesy of Beckman Company. The results are shown in Figure 4.1.1.2. The original data are shown in Appendix.

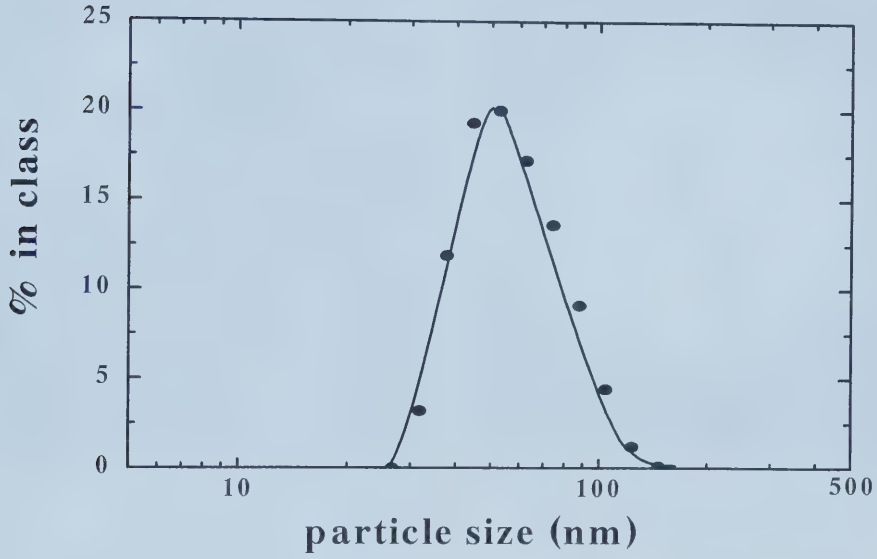

Figure 4.1.1.2. Size distribution of particles (1) (Beckman coulter particle analyzer)

The volume average size of particles (1) was found to be 69.6 nm. About 82 % of particles were below 88 nm (see Figure 4.1.1.2). Comparing this particle size distribution with data in Figure 4.1.1.1, shows that the two kinds of equipment yielded essentially identical results. The same principle of particle size measurement is used in these two kinds of equipment. Particles are in constant random thermal, or Brownian, motion. This motion causes the intensity of light scattered from the particles to form a moving speckle pattern. This movement can be detected as a change in intensity with time with suitable optics and a photomultiplier. Large particles move more slowly than small particles, so that the rate of fluctuation of the light scattered from them is also slower. Photon correlation spectroscopy uses the

rate of change of these light fluctuations to determine the size distribution of the particles scattering the incident light (Bohren and Huffman, 1983).

Shape of particles

To determine rough sizes, shape of the particles, a JEOL-2010 transmission electron microscope (TEM) (Nikon, Japan) was used to obtain TEM micrographs.

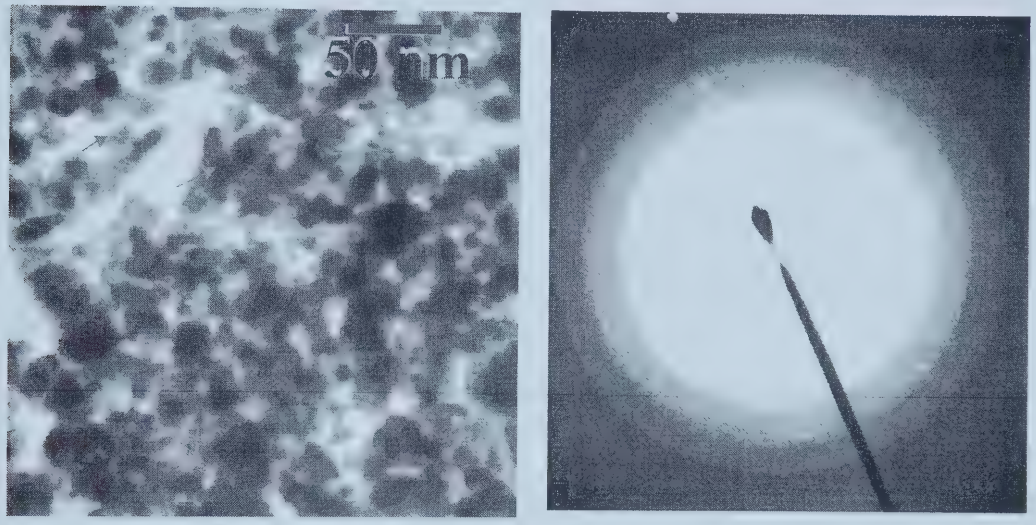

Plate 4.1.1. Transmission electron microscope (TEM) micrography of particles (1). Arrows (left panel) point to particles.

The left TEM picture in Plate 4.1.1 shows that the diameters of particles (1) are roughly around 50 nm. The shapes of the particles ranged from oval to spherical. The right image (Plate 4.1.1) is an electron diffraction pattern of particles. The evident bright rings indicate that the particle was highly crystalline. The pictures are courtesy of Dr. Xu, Department of Chemical and Material Engineering, University of Alberta.

4.1.2. Zeta potential

The electrostatic charge (zeta potential) of particles (1) and (2) was calculated from the electrophoretic mobility, which was determined with a Zetaphoremeter III (SEPHY/CAD INSTRUMENTATION FRANCE). The average zeta potential of particles (1) and particles (2) (after one year stored at room temperature) was –43.9 ± 1.7 mV (see Figure 4.1.2) and -38.5 ± 5.2 mV, respectively. Both particle types do not easily aggregate.

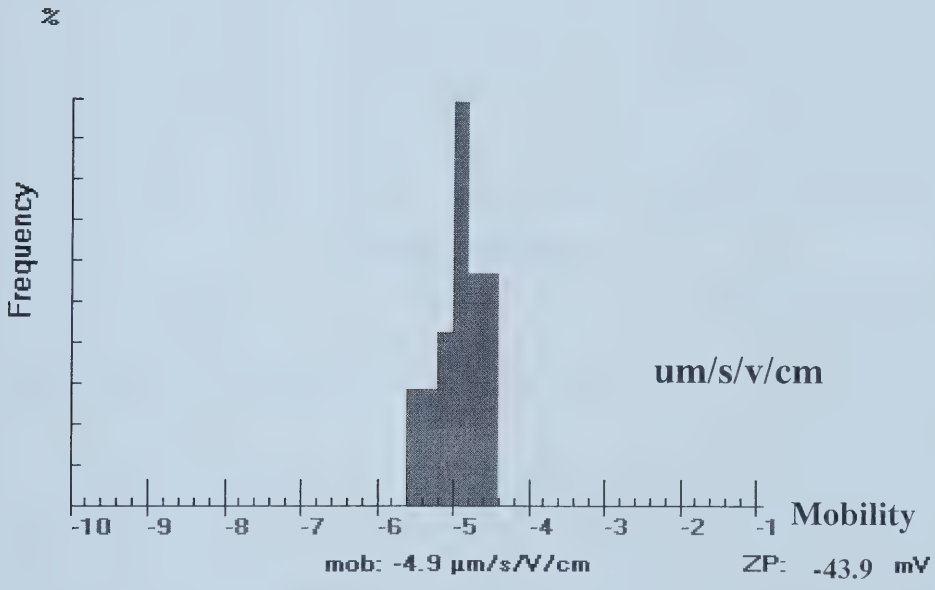

Figure 4.1.2. Mobility diagram of particles (1) using Zetaphoremeter III.

The purpose of determining the zeta potential is to further confirm the stability of the particles. Usually when the value of zeta-potential is ±30 mV or more, the suspension is considered to be stable. If the charge on the particle is high, the particles repel one another and the colloid is stable. If the charge is near zero, the random motion (Brownian movement) of the particles causes them to agglomerate. The zeta potential is zero at the isoelectric point (iep). For pharmaceutical applications, particles are studied under physiological conditions. If the pH of the suspension of particles is far away from its isoelectric point (iep), the particles are stable (Hunter, 1981).

4.1.3. Superparamagnetic characteristics

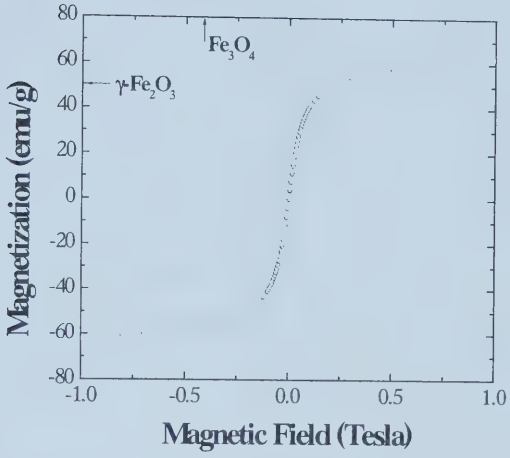

Figure 4.1.3. Superparamagnetic properties of particles (1).

The superparamagnetic characteristics of particles (1) were measured with a vibrating sample magnetometer (VSM) (Quantum design 9T-PPMS DC Magnetometer/AC Susceptometer San Diego. Ca. USA). Figure 4.1.3 is courtesy of Dr. Xu, University of Alberta. The magnetization curve shows the magnetization (*M*) versus the applied magnetic field *(H)*. This typical M-H curve shows that particles (1) can be highly magnetized in a reversible fashion, i.e. they are superparamagnetic. When the external magnetic field was zero, the particles exhibited no residual magnetization, i.e. permanent magnetization was avoided and magnetic flocculation was therefore minimized. The saturation magnetization of the superparamagnetic particles made by Dr.Xu's group was found to be between the value of magnetite (Fe_3O_4: 80 emu/g) and maghemite (r-Fe_2O_3: 52.7 emu/g) (Xu *et al.* 1999).

4.2. Galactose-derivatized superparamagnetic nanoparticles (Gal-beads)

4.2.1. Physical properties and characterization

Physical properties

Two different sizes of galactose-derivatized magnetic nanoparticles (Gal-beads) were prepared by reacting amino-terminated magnetic particles and lactose in the presence of the reducing agent sodium cyanoborohydride. Among these Gal-beads, Gal-beads (1) were prepared from superparamagnetic nanoparticles (particles 1, size: 86[70 FWHM] nm). As shown in Table 4.2.1.1, the volume average size and the full width half maximum of the Gal-beads (1) distribution curve after galactose-derivatization was found to be 278[309] nm (see Appendix). Neutral particles (1) were made from the same batch of particles (1). The volume average size was 302[280] nm.

Table 4.2.1.1. Volume average size of the particles, neutral particles and Gal-beads.

Particles Batch	After Preparation (nm)	One Year Storage at RT (nm)	Neutral Particle Size (nm)	Gal-Beads (nm)
1	61[42]	86[70]	302[280]	278[309]
2	127[125]	141[138]	326[308]	337[372]

*[] FWHM distribution

Galactose coupling to particles is a two-phase reaction. The lactose solution was added to particles to give a uniform distribution before adding $NaBH_3CN$. After the distribution appeared to be homogeneous, $NaBH_3CN$ was added and mixed again, resulting in Schiff base formation between the aldehyde group of the open glucose form of lactose and the amino group of the particles. The reason for adding $NaBH_3CN$ was to form a strong covalent linkage to the particles. Currently, the optimum condition for coupling lactose to the particles has not yet been established.

Experimental conditions of 1 mM lactose per g of particles and one week were chosen for the coupling reaction in order to maximize conjugation. Finally, the particles had to be washed many times to remove residual $NaBH_3CN$, before adding acetic anhydride. This washing is necessary as the solution could bubble out of the vial when the strong base $NaBH_3CN$ reacts with acetic anhydride. To avoid charge association between the control (neutral particles which have no galactose attached) and the negatively charged cell membrane, the positive charges of particles were neutralized using acetic anhydride.

Characterization of the Gal-beads

Table 4.2.1.2 and Figure 4.2.1 show the linearity of a representative standard curve for galactose quantification over a concentration range from 0 to 60 μg/mL. Correlation coefficient (r^2) values for all standard curves are higher than 0.98.

Table 4.2.1.3 shows the UV absorption of Gal-beads and the concentration of galactose in Gal-beads. The instrument was zeroed with neutral particle suspension as the blank. The concentrations of galactose in two types of Gal-beads were 42.7 $\pm$ 2.6 μg/mL and 38.3 $\pm$ 3.8 μg/mL (n=3), respectively.

Table 4.2.1.2. UV absorption of standard galactose using the phenol/sulfuric acid reaction and spectrophotometric determination at wavelength of 490 nm.

	1	2	3	4	5	6
X (μg/mL)	0	20	30	40	50	60
Y (Absorption)	0	0.218	0.327	0.438	0.556	0.681

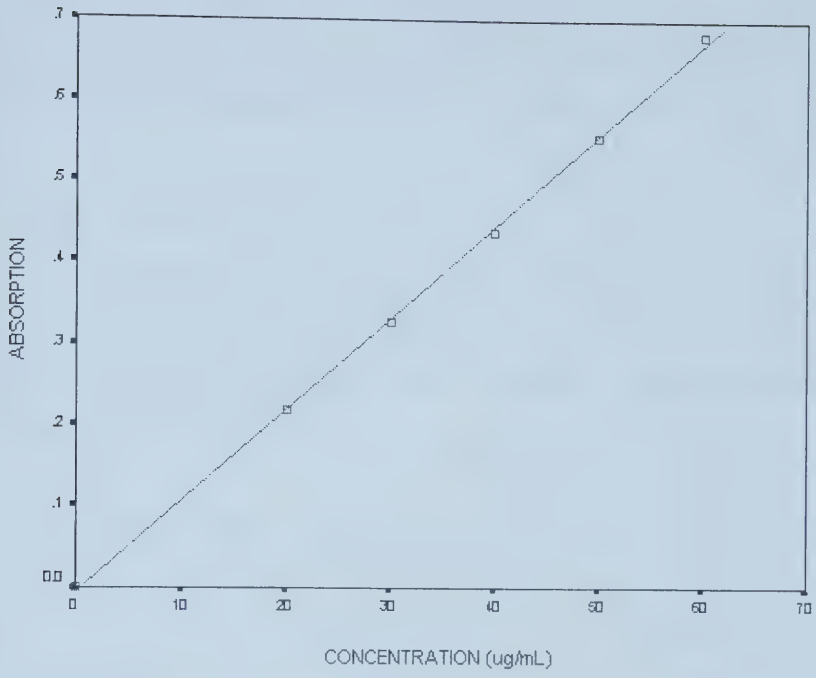

Figure 4.2.1. Standard curve for galactose using the phenol/sulfuric acid reaction and spectrophotometric determination at wavelength of 490 nm.

Table 4.2.1.3. UV absorption of galactose in Gal-beads using the phenol/sulfuric acid reaction and spectrophotometric determination at wavelength of 490 nm and concentration of galactose in Gal-beads (μg/mL).

Gal-Beads Batch	Concentration (μg/mL)
1	42.7 ± 2.6
2	38.3 ± 3.8

The principle of determination of galactose concentration using the phenol/sulfuric acid reaction was described by Dubois *et al.* (1956). Simple sugars give an orange yellow color when treated with phenol and concentrated sulfuric acid. The reaction is sensitive and the color is stable. By use of this phenol-sulfuric acid reaction, a method has been developed to determine ppm levels of sugars and related substances. The data shows that the coupling yields were consistent from batch to

batch. Therefore, the experimental conditions described in Section 3.3.1 (1 mM lactose per 250 mg of particles and one week coupling) can be used in future experiments, however, conjugation yield have not been optimized.

4.2.2. Stability

One month after lactose coating or capping the size of Gal-beads and neutral particles, respectively both increased in size, as shown in Table 4.2.2.1. Aggregation occurred three months later (data not shown). The reason for this aggregation needs to be further studied.

Table 4.2.2.1 Volume average sizes of Gal-beads and neutral particles after one month of lactose coating.

Batch	Neutral Particles (nm)	Gal-Beads (nm)
1	314	290
2	376	365

Table 4.2.2.2 shows that minimum loss of galactose from Gal-beads has occurred within a month of coupling ($p>0.05$), indicating those surface area effects are not factors in stability.

Table 4.2.2.2. Concentration of galactose in Gal-beads (μg/mL).

Gal-Beads Batch	After Lactose Coating	One Month After Lactose Coating
1	42.7 ± 2.6	40.0 ± 4.8
2	38.3 ± 3.8	39.2 ± 3.7

4.3. Estimate of ASGPRs on Hep G2 and 143B cell surfaces

4.3.1. Quantity and purity of ASOR

ASOR was prepared from both bovine and human orosomucoid. Four preparations of ASOR were made by mild acid hydrolysis to remove sialic acid residues. The results shown in Table 4.3.1.1 indicate that the average yield ASOR was 84 % when made from orosomucoid by this method.

Table 4.3.1.1. Quantity of ASOR made from orosomucoid.

Orosomucoid Source	Orosomucoid Treated (mg)	ASOR Recovered (mg)
1 (bovine)	10.6	9.2
2 (bovine)	10.7	8.8
3 (human)	10.4	9.0
4 (human)	10.2	8.2

Desialylation of ASOR:

Table 4.3.1.2 and Figure 4.3.1 depict a representative standard curve for galactose over a concentration range from 0 to 33 μg/mL. Correlation coefficient (r^2) values for all standard curves are higher than 0.99.

Table 4.3.1.3 and Table 4.3.1.4 showed the UV absorption and quantity of sialic acid in products of ASOR and original orosomucoid. Average 90.6 % of sialic acid was removed from orosomucoid.

Table 4.3.1.2. Concentration and UV absorption of standard sialic acid using the resorcinol/sialic acid reaction and spectrophotometric determination at wavelength of 580 nm.

	1	2	3	4	5
X (μg/mL)	0	8.2	16.5	24.8	33.0
Y (Absorption)	0	0.025	0.062	0.121	0.152

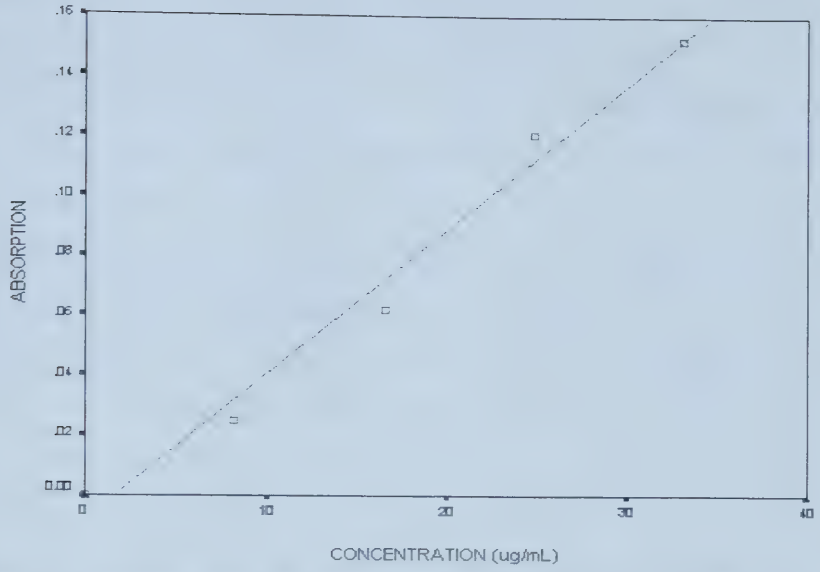

Figure 4.3.1. Standard curve for sialic acid using the resorcinol/sialic acid reaction and spectrophotometric determination at wavelength of 580 nm.

Table 4.3.1.3. UV absorption of sialic acid in ASOR and orosomucoid using the resorcinol/sialic acid reaction and spectrophotometric determination at wavelength of 580 nm.

	Product 1	**Product 2**	**Product 3**	**Product 4**
ASOR	0.003	0.004	0.002	0.001
Orosomucoid	0.134	0.111	0.095	0.082

Table 4.3.1.4. Sialic acid content in four batches of ASOR and orosomucoid.

	Product 1	**Product 2**	**Product 3**	**Product 4**
ASOR(μg)	4.54	4.95	4.125	3.713
Orosomucoid(μg)	58.58	49.09	42.49	37.29
Sialic acid (%)	7.75	10.08	9.71	9.95
Desialylation (%)	92.25	89.92	90.29	90.05

From the data shown in Table 4.3.1.4, 90.6 % of the sialic acid was removed from orosomucoid during the preparation of ASOR by cleavage of terminal sialic acid residues from the branched carbohydrates on the surface of bovine and human

orosomucoid using mild acid hydrolysis. The quantitative estimation of sialic acid content was estimated using the method of Svennerholm (1957).

Evidence reported by Yoshima *et al.* (1981) indicated that the sugar chains of α1-acid glycoprotein (orosomucoid) showed species differences. However, the oligosaccharide pattern of the glycoprotein of the same species seemed to be quite constant. Tomlinson *et al.* (1992) reported that sialidase treatment removed >90 % of membrane sialic acid from sheep and human erythrocytes.

Sialic acid cleavage can be performed either by mild acid hydrolysis (pH 1.6 at 80 °C for 1 h) (Findeis *et al*, 1994) or sialidase treatment (Tomlinson *et al,* 1992). However, sialidase is not easily removed after enzymatic treatment. Some of the properties of ASOR prepared by mild acid hydrolysis (pH 1.6 at 80 °C for 1 h.) were compared with those of neuraminidase-treated α_1-acid glycoprotein. The electrophoretic resolution of the glycoprotein prepared by mild acid hydrolysis seems to be extended to more acidic pH values both by starch-gel and free moving boundary electrophoresis. A further expression of this change is probably the difference in the pH range to exhibit two bands in electrophoresis. These variants are not sub-units of native α_1-acid glycoprotein, but represent modifications of naturally occurring proteins. Further, it was shown that the difference in the electrophoretic mobility between the two variants was not due to any difference in amide content. Immunochemically, the two variants share the same determinants (Schmid *et al*, 1967).

Electrophoresis (SDS-PAGE)

Electrophoresis was performed to study ASOR prepared from bovine and human orosomucoid after desialylation. Plate 4.3.1.1 shows that ASOR prepared from bovine orosomucoid is not identical to that prepared from human orosomucoid. Human ASOR showed a single band, but the bovine ASOR had two bands. Molecular weight markers of 368,00 to 52,000 bracketed both bovine and human ASOR preparations, indicating a somewhat higher than reported in the literature. Findeis *et al* (1994) reported that human orosomucoid analyzed by SDS-PAGE shows a single band (apparent MW 44,000) after staining with Coomassie blue, whereas

human ASOR is reported to have a MW of 40,000 (Steer and Shwell, 1980). Electrophoresis was also performed to study the cold iodine labelled ASOR (iodogen labelling technique). The bands of ASOR and I-ASOR (Plate 4.3.1.2) do not show any great differences in electrophoretic mobility between iodinated and non-iodinated ASOR.

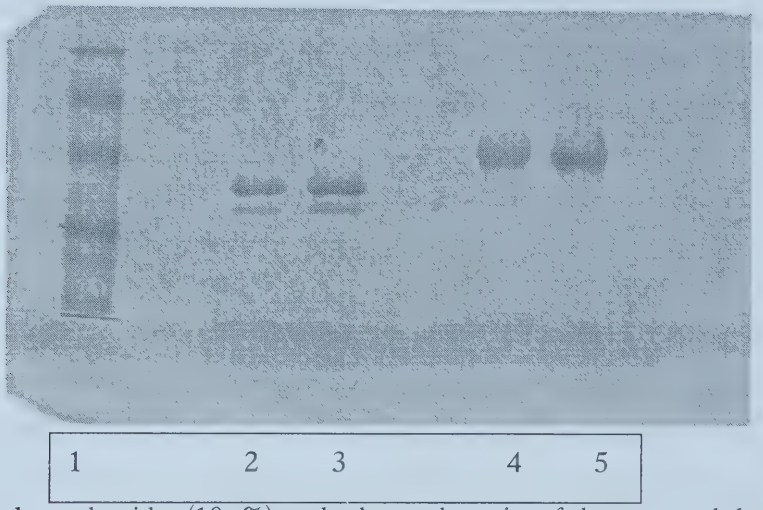

Plate 4.3.1.1. Polyacrylamide (10 %) gel electrophoresis of human and bovine ASOR products. Lane 1 is the MW marker (MW 19000, 27200, 36800, 52000, 70000 and 107000). Lanes 2 and 3 are bovine ASOR, and lanes 4 and 5 are human ASOR.

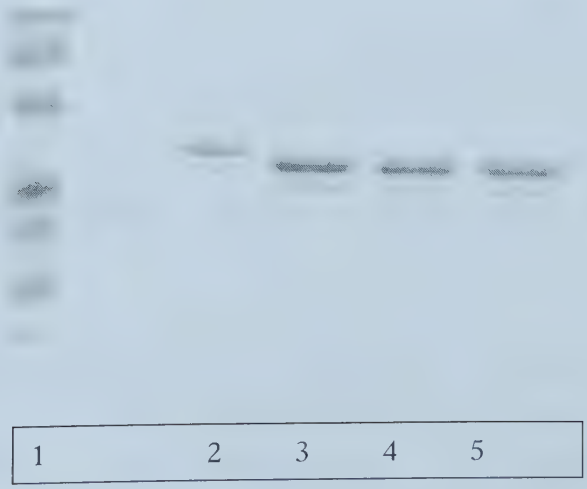

Plate 4.3.1.2. Polyacrylamide (10 %) gel electrophoresis of cold iodine labelled bovine ASOR made by iodogen technique. Lane 1 is the MW marker, lane 2 is orosomucoid, lane 3 is ASOR and lanes 4 and 5 are I-ASOR.

Plate 4.3.1.2. Polyacrylamide (10 %) gel electrophoresis of cold iodine labelled bovine ASOR made by iodogen technique. Lane 1 is the MW marker, lane 2 is orosomucoid, lane 3 is ASOR and lanes 4 and 5 are I-ASOR.

The electrophoretic data imply that iodination via the iodogen technique did not change the ASOR mobility during labelling indicating that the protein was not destroyed during labelling during labelling. The MWs of ASOR and labelled ASOR range from 368,00 to 520,00. ^{125}I-labelled ASOR was similarly prepared with the iodogen labelling technique (Morin *et al*, 1997; Kawasaki and Ashwell, 1977). Radioiodination involved incubating ASOR with buffered Na^{125}I.

Autoradiography

Autoradiography was performed to study the quality of ^{125}I-ASOR by both the chloramine-T method (Greenwood and Hunter, 1963) and the iodogen method, using the method of Voytas and Ke (1999). Plate 4.3.1.3 shows the 10 % polyacrylamide gel electrophoresis used to obtain the autoradiogram shown in Plate 4.3.1.4.

Plate 4.3.1.4 shows that the bands of ^{125}I -ASOR labelled by the chloramine-T method are thicker, longer and darker than the bands of ^{125}I -ASOR labelled by the iodogen labelling technique. It suggested the protein of ^{125}I-ASOR (bovine) made using this chloramine-T method had been changed even that this method had a high labelling efficiency (see Table 4.3.1.5). ^{125}I-ASOR (human) prepared using the iodogen labelling technique (lane 5) wasn't visible due to the low concentration of ^{125}I-ASOR in this gel (Plate 4.3.1.3). However lane 5 is visible in autoradiography (Plate 4.3.1.4) because of the radioactivity of ^{125}I-ASOR. The one band of ^{125}I-ASOR by the iodogen labelling technique indicating that protein wasn't change during labelling.

Table 4.3.1.5. Radiolabelling yields and radioiodination condition using the chloramine-T and iodogen methods.

Labelling Method	Radiolabelling Yield	Labelling Time
Iodogen	48 %	2.5 h
Chloramine-T	70 %	1 h

Plate 4.3.1.3. Polyacrylamide (10%) gel electrophoresis of the human and bovine ^{125}I-ASOR. Lane 1 is MW marker. Lane 2 is bovine ASOR, lane 3 is ^{125}I-ASOR (bovine) made by the chloramine-T method, lane 4 is human ASOR and lane 5 is ^{125}I-ASOR (human) made by iodogen labelling.

Plate 4.3.1.4. Autoradiogram of the gel in Plate 4.3.1.3. The time of exposure to film was 24 h.

4.3.2. Characterization of ^{125}I–ASOR

^{125}I-ASOR products were prepared from human ASOR using the iodogen labelling technique.

Radiolabelling yield

The reaction mixture was applied to a column of Sephadex G-25M, whereby two peaks were revealed. The first peak contained ^{125}I-labelled ASOR. Collection of this fraction provided a recovered radiolabelling yield of 48 % (n=3) (Figure 4.3.2.1).

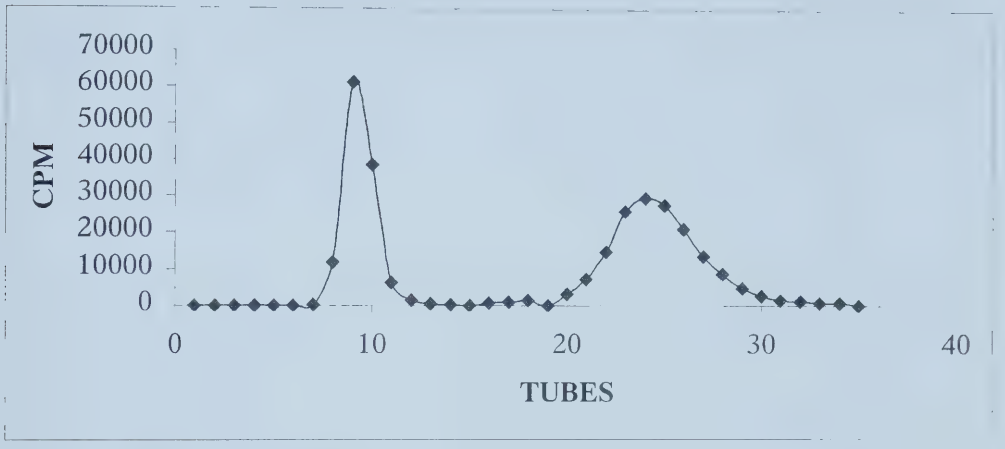

Figure 4.3.2.1. Purification of the radiolabelling reaction mixture on Sephadex G-25M. Tubes 8, 9, 10, 11 contained the ^{125}I-labelled ASOR. Tubes 21 to 28 contained free iodide.

Specific activity

The specific activity of ^{125}I-ASOR was calculated by dividing the total recovered radioactivity by the quantity of recovered ASOR.

Table 4.3.2.1 and Figure 4.3.2.2 show the linearity of a representative standard curve for standard ASOR with concentrations ranging from 0.937 to 25 μg/100 μL. Correlation coefficient (r^2) values for all standard curves are higher than 0.99.

The UV absorption and radioactivity of ^{125}I-labelling ASOR (Figure 4.3.2.3) were used to determine the quantity of ASOR protein recovered from the column. The recovery of ASOR was 68 % (Table 4.3.2.2). The specific activity of the first labelling product (^{125}I-ASOR) was 117 x 10^6 Bq/μg. Other two labellings were 161 x 10^6 Bq/μg and 138 x 10^6 Bq/μg, respectively.

Table 4.3.2.1. Concentration and UV absorption of standard ASOR using spectrophotometric determination at wavelength of 280 nm.

	1	2	3	4	5	6
Y (μg/100 μL)	0.937	1.875	3.75	6.25	12.5	25
X (Absorption)	0.014	0.020	0.039	0.064	0.102	0.213

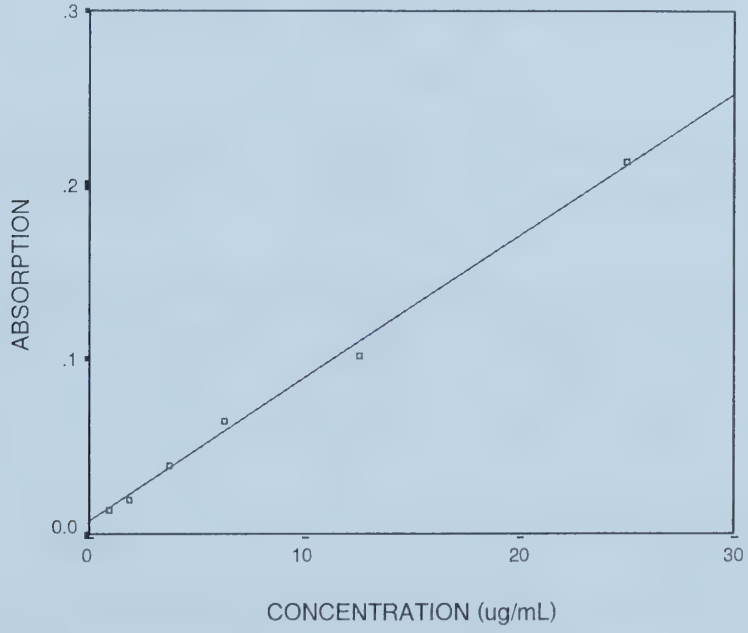

Figure 4.3.2.2. Standard curve of ASOR using spectrophotometric determination at wavelength of 280 nm.

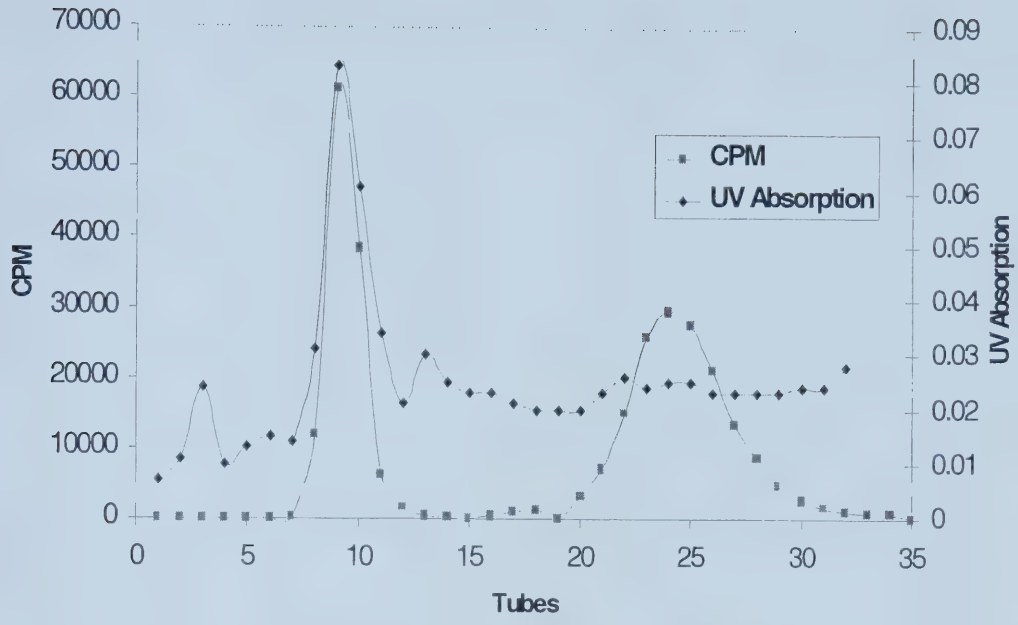

Figure 4.3.2.3. Purification of the radiolabelling reaction mixture on Sephadex G-25M and UV absorption using spectrophotometric determination at wavelength of 280 nm.

Table 4.3.2.2. Quantity of ASOR in products of ^{125}I-ASOR.

	Tube 8	**Tube 9**	**Tube 10**	**Tube 11**
X (Absorption)	0.031	0.083	0.061	0.034
Y (μg/100μL) x 3	8.9	27.0	19.9	10.0

Stability

When the labelled protein was stored at 4 °C for two weeks (Figure 4.3.2.4), only one peak (labelled product) was observed upon rechromatography of the labelled material. No free iodine was detected. However, a second peak (free iodide) was present after four weeks (Figure 4.3.2.5). These results show that ^{125}I-ASOR can be stored at 4 °C for two weeks before use.

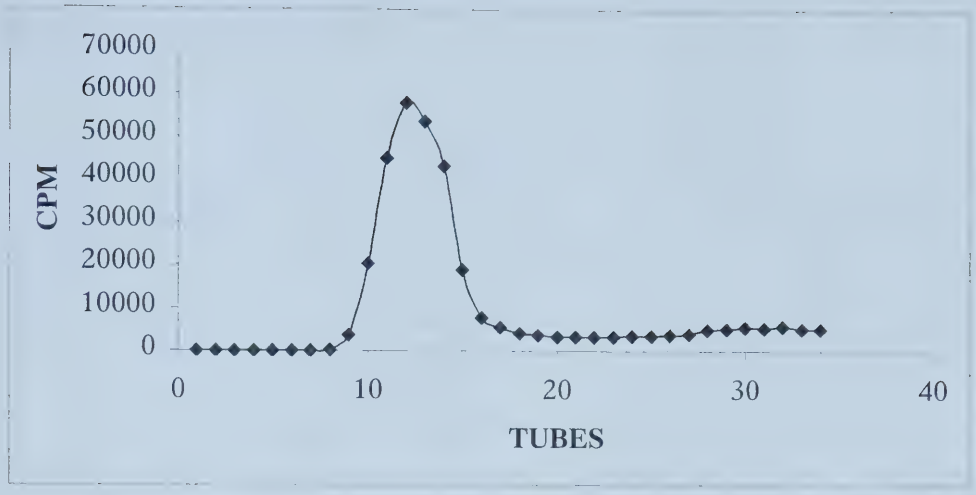

Figure 4.3.2.4. ^{125}I-Labelled ASOR, after two weeks storage at 4 °C, on Sephadex G-25M.

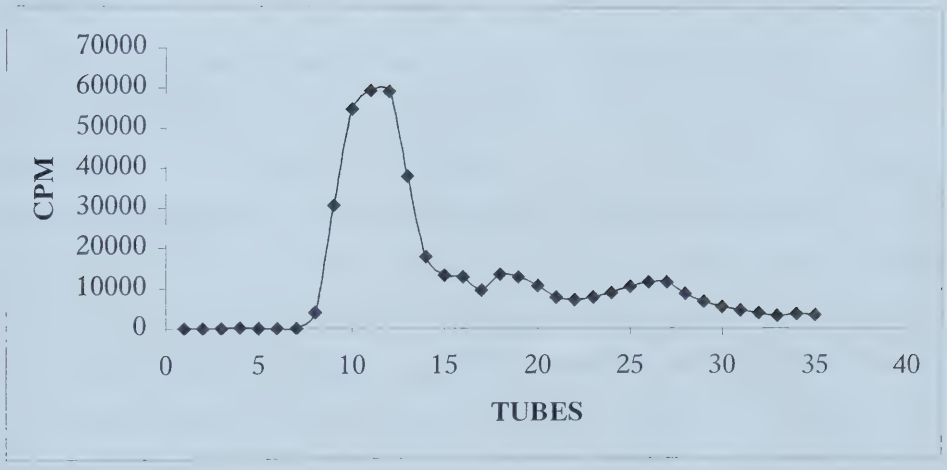

Figure 4.3.2.5. ^{125}I-Labelled ASOR, after four weeks storage at 4 °C, on Sephadex G-25M.

4.3.3. ASGP receptors on Hep G2

Hep G2 cells were incubated with ^{125}I-ASOR to estimate the number of ASOR binding sites (ASGPRs) on the cell surface, using the method of Schwartz *et al.* (1980) (Table 4.3.3). Control studies used 143B cells, which do not express ASGPR. These binding studies indicate that the number of ASGPRs ranges from 95,000 to 140,000 per cell. The bound radioactivity on 143B cells (control cell line)

was 1/10 of Hep G2 cell binding. These values are somewhat lower than reported for freshly isolated rat hepatocytes.

Table 4.3.3. ASGP receptors on Hep G2 cells.

Radioactivity of ^{125}I-ASOR (CPM)	ASOR (ng)	Estimated Number of Receptors Per Cell
13898	9.4	140,000
10137	7.4	112,000
9104	6.3	95,000

It has been reported that theoretically there are 500,000 surface binding sites per cell on freshly isolated rat hepatocytes (Schwartz *et al,* 1980). In practice, quantification of ASGPRs on isolated rat hepatocytes has provided a wide range of values from 50,000 to 200,000 receptors per cell (Steer and Ashwell, 1980; Baenziger *et al*, 1980).

There are several reasons why the values reported here for Hep G2 cells are lower than literature values for freshly isolated hepatocytes. In general, it is acknowledged that hepatocytes not freshly isolated, and cancer cell lines, may express less receptor protein than freshly isolated hepatocytes (Schwartz *et al,* 1981). Furthermore, Hep G2 cells grow as monolayers, whose receptors on the basolateral surface may not be accessible to the ^{125}I-ASOR which is added to the cell culture for receptor quantification. Finally, the specific conditions under which binding studies are conducted may alter the apparent number of receptors identifiable on the hepatocyte cell surface.

The Hep G2 cell line was derived from cancerous hepatic tissue of a 15-year-old male Caucasian (American Type Culture Collection). The cells were epithelial in morphology. The cells produce alpha-fetoprotein, albumin, alpha2-macroglobulin, alpha1-antitrypsin, transferrin, alpha1-antichymotrypsin, haptoglobin, ceruloplasmin, plasminogen, complement (C3, C4), C3 activator, fibrinogen, alpha1-acid glycoprotein (orosomucoid), alpha 2-HS glycoprotein, beta-lipoprotein and retinol

binding protein. There is no indication that this line harbors a hepatitis B virus genome.

4.3.4. Competitive binding of ^{125}I-ASOR on Hep G2 cells

The Figure 4.3.4 shows that no significant dissociation of bound radioactive ligand (^{125}I–ASOR) from the Hep G2 cell surface was detectable upon dilution either in the presence of saturating levels of orosomucoid, or mannose. Galactose, however, competed for binding to the ASGPR receptors. Complete dissociation could be achieved by adding the calcium-chelating agent EDTA, indicating that Ca^{2+} is needed to bind to ASGPRs (Stockert, 1995). As shown in Section 1.3.4, the ASGPR binding site is a lattice at the vertices of a triangle with sides of 15, 22, and 25 Å (ASGPR trimer). Galactose units of the triantennary oligosaccharide of ASOR bind simultaneously to ASGPR (Stockert, 1995). Galactose is a small molecule that competes for each binding site, but with lower affinity than that of molecules like ASOR that can simultaneously occupy all three sites. The current data indicate that galactose does compete with ^{125}I-ASOR binding to Hep G2 cells.

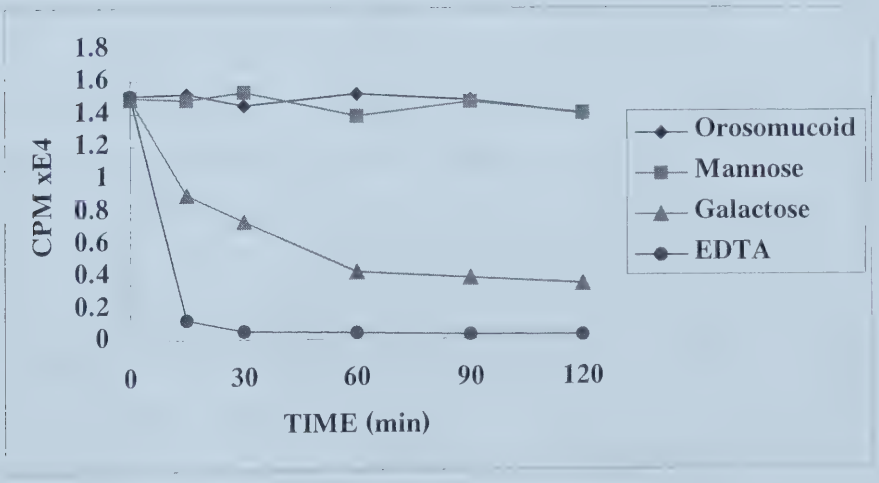

Figure 4.3.4. Dissociation of cell-bound ^{125}I-ASOR in the presence of various competition binding reagents.

4.3.5. Toxicity of Gal-beads

The MTT cell survival assay showed that the toxic concentration of the Gal-beads (1) on Hep G2 cell line was 1.5 mg/mL (Figure 4.3.5). Below this concentration, Gal-beads had no observed toxicity. Acute iron toxicity leading to death through acidosis in human occurs when more than 200-250 mg of iron per kilogram of body weight is reached (see section 1.1.4).

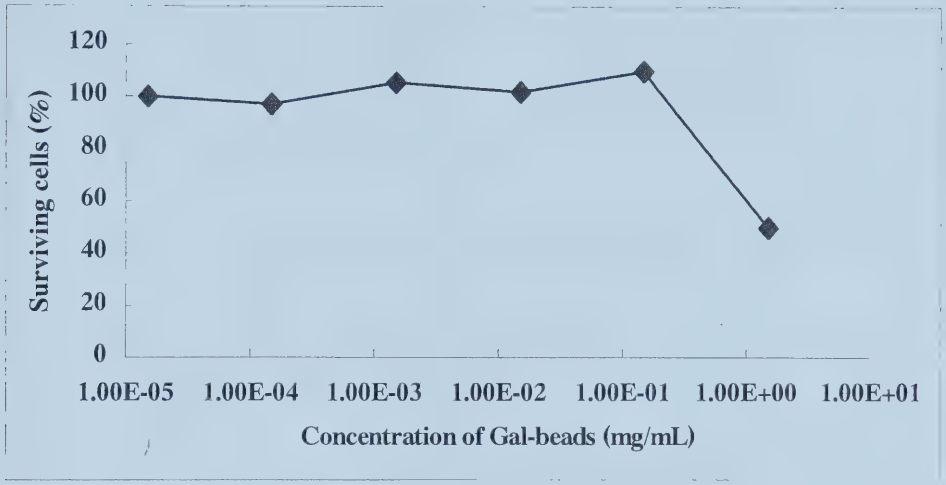

Figure 4.3.5. Toxicity of Gal-beads.

The interaction of Gal-beads (1) with cells was studied using the MTT assay. The MTT assay, which quantifies cell viability, cell survival and cell growth, can be used to rapidly evaluate the toxic properties of Gal-beads *in vitro*. The MTT assay is easy to setup and may provide clues to that. Extreme results (30 % survival or less) in more than one cell line should be taken seriously. The MTT assay however is not recommended for the current application due to high variability and non-specificity. Better assays are necessary. The toxicity of Gal-beads should thus be investigated with more specific methods *in vivo* using histopathological and morphological methods and cytogenetic analysis.

The important factors, which determine the biocompatiblity and toxicity of Gal-beads, are the magnetically responsive components such as magnetite, iron, the size of the Gal-beads, their matrix substance, their coatings and the possible desorption of biological constituents from the magnetic core.

4.4. Uptake of Gal-beads

4.4.1. Photomicrographs of Gal-bead uptake by Hep G2 cells.

Gal-beads (1) (volume average size: 278 nm) were prepared from superparamagnetic nanoparticles (particles 1, volume average size: 86 nm). The uptake of this type of Gal-beads and neutral particles by Hep G2 and 143B cells was investigated (Plate 4.4.1.1 and Plate 4.4.1.2). Phase contrast microscopy of Gal-bead uptake by Hep G2 cells over 5 days of culture (2, 3, 5), at several magnifications (40x, 100x, 200x, and 400x), also were taken (Plate 4.4.1.3 and Plate 4.4.1.4). The uptake of Gal-beads by Hep G2 cells was greater than with neutral particles. 143B cells displayed no visible uptake of Gal-beads.

4.4.2. Gal-bead uptake by Hep G2 cells in the presence of galactose: a challenge study

The characterization of Gal-bead uptake by Hep G2 cells was also determined when galactose had been added to the cell culture (Plate 4.4.2).

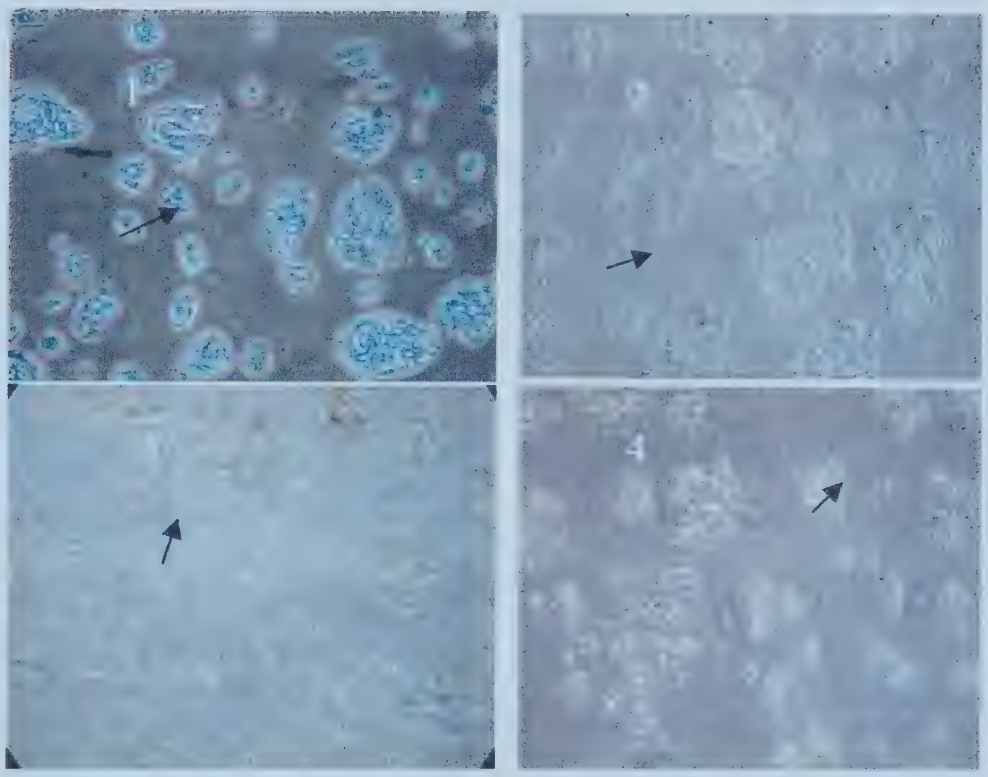

Plate 4.4.1.1. Hep G2 cell uptake of Gal-beads. All cells were cultured for three days and pictures were taken at 200x magnification. Picture 1 shows Hep G2 cells stained with Wright stain. An arrow pointed to one cell. The blue colour shows cytoplasm and purple delineates the nucleus of the cell. Picture 2 shows Hep G2 as a control. Nothing was added to these cells. Pictures 3 and 4 show the uptake of Gal-beads. An arrow points out the Gal-beads (yellow spots) taken up by the cells.

Plate 4.4.1.2. Uptake of Gal-beads and neutral particles. All cells were cultured for five days and the pictures were taken at 100x magnification. Pictures 1 and 2 show the absence of cellular uptake of neutral particles. Pictures 3 and 4 show the uptake of Gal-beads. Arrows in pictures 3 and 4 point to Gal-beads (yellow spots) which were taken up by cells.

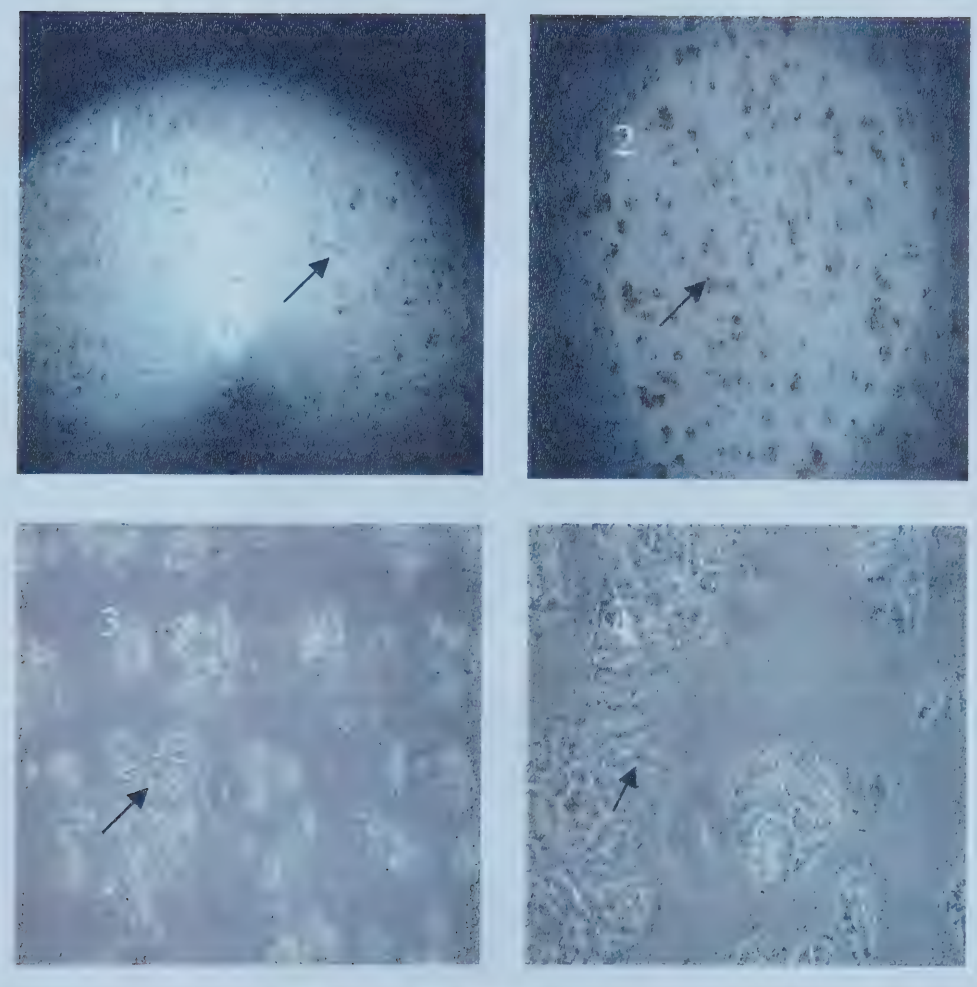

Plate 4.4.1.3. Different magnifications depicting uptake of Gal-beads by Hep G2 cells cultured for three days. Yellow spots in pictures show the particles inside the cells. Picture 1 has 40x magnification, picture 2 is at 100x, picture 3 at 200x and picture 4 at 400x magnifications. The arrows point at internalized Gal-beads (yellow spots).

Plate 4.4.1.4. Photomicrographs showing uptake of Gal-beads by Hep G2 cells after different periods of cell culture. All pictures were taken at 100x magnification. Picture 1 shows uptake of Gal-beads by cells cultured for two days prior to addition of Gal-beads, picture 2 shows uptake for a three-day-old culture and picture 3 shows uptake by a five-day-old culture. Arrows point to internalized Gal-beads (yellow spots).

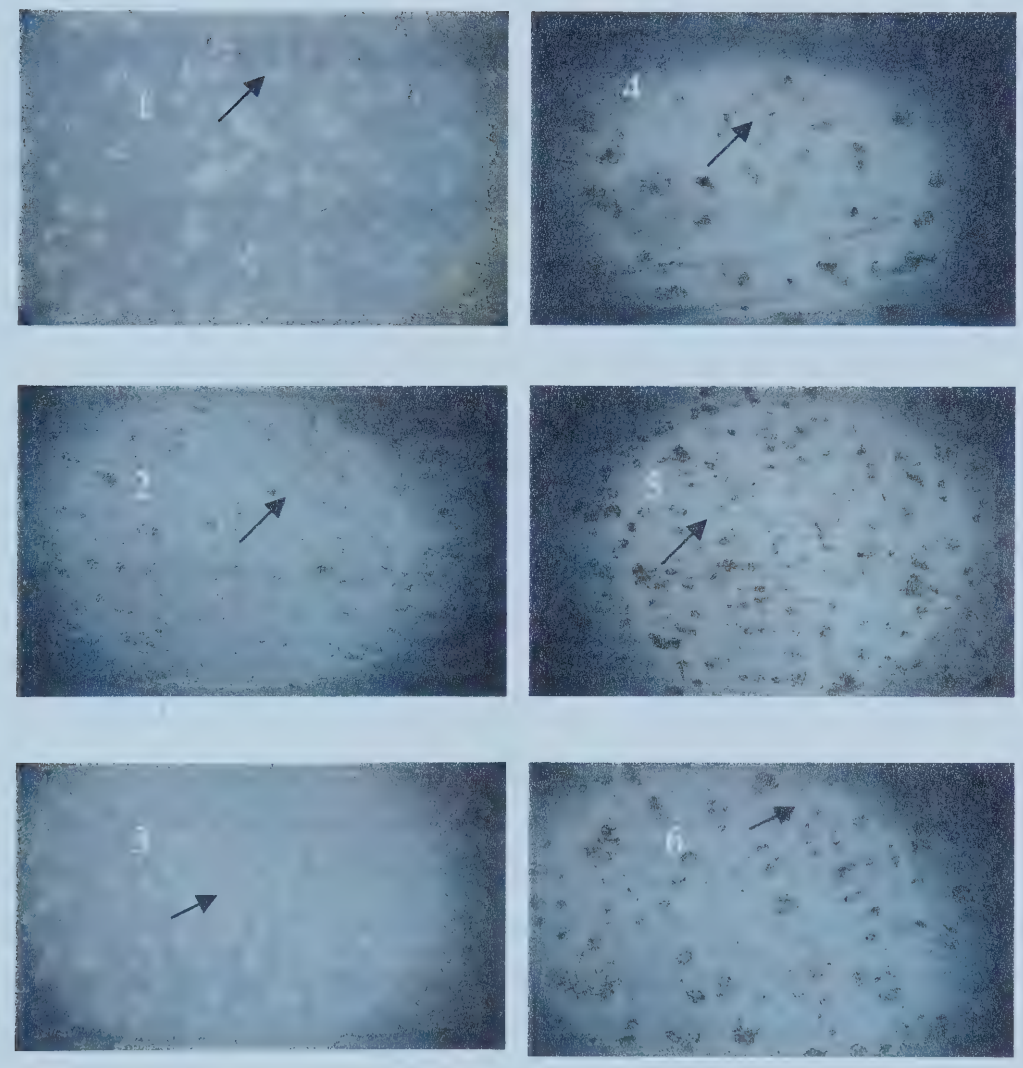

Plate 4.4.2. Uptake of Gal-beads by Hep G2 cells in the presence of galactose. Pictures 1, 2 and 3 show the uptake of Gal-beads with galactose after incubations of 30, 60 and 120 min, respectively. Pictures 4, 5 and 6 show the uptake of Gal-beads with no competing galactose, following a 2 h incubation. Arrows point at internalized Gal-beads (yellow spots).

5. SUMMARY AND CONCLUSIONS

This project addresses the development of superparamagnetic nanoparticles as targeted magnetic carriers. Specifically, galactose-derivatized superparamagnetic nanoparticles have been prepared, and their specific uptake by a human hepatocyte cell line (Hep G2) has been investigated.

This project was developed in co-operation between our group and Dr Xu's group in the Department of Chemical and Material Engineering at the University of Alberta.

Two size groups of nanoparticles, 61 nm (particles 1) and 127 nm (particles 2), were prepared by Dr Xu's group. TEM of these particles showed rough sizes, with shapes from oval to spherical. One year after preparation, the sizes of these two particle size groups changed from 61 nm to 86 nm; 127 nm to 141 nm at room temperature. The zeta potentials of these two groups of particles are -43.9 ± 1.7 mV and -38.5 ± 5.2 mV, respectively. Particles (1) have superparamagnetic characteristics.

Two different sizes of galactose-derivatized magnetic nanoparticles (Gal-beads) were prepared by reacting amino-terminated magnetic particles and lactose in the presence of the reducing agent sodium cyanoborohydride. Among these Gal-beads, Gal-beads (1) (size 278 nm) were prepared from superparamagnetic nanoparticles (particles 1, size 86 nm). One month after preparation, the surface content of galactose changed insignificantly ($p>0.05$) from 42.7 ± 2.6 (μg/mL) to 40.0 ± 4.8 (μg/mL) and sizes changed from 278 nm to 290 nm, respectively.

The molecular target of this delivery system, the asialoglycoprotein receptors (ASGPRs) are specific to hepatocytes. The binding between the ^{125}I-galactose-terminal glycoprotein (^{125}I-ASOR) and ASGPRs located on the cell surface of Hep G2 can be competitively displaced by galactose. Binding studies have shown that the number of ASGPRs per cell ranges from 95,000 to 140,000 which are lower than literature values for freshly isolated hepatocytes. ASOR was prepared by cleavage of terminal sialic acid residues from the branched carbohydrates on the surface of orosomucoid (α_1-acid glycoprotein), which was isolated by dialysis against water using Cellulose Dialysis Tubing. The quantitative estimation of sialic acid was

carried out using the resorcinol method and an average 91 % sialic acid was removed from orosomucoid. ^{125}I-label was incorporated into ASOR by the iodogen technique. ^{125}I-ASOR was purified using Sephadex G-25M size-exclusion chromatography. Electrophoresis (SDS-PAGE) and autoradiography were used to check quality of ^{125}I-ASOR.

The uptake of Gal-beads by Hep G2 cells was greater than with neutral particles. Furthermore, this uptake of Gal-beads was challenged by the addition of galactose, as seen with the aid of a phase contrast microscope. In contrast, the negative control cell line (143B human osteosarcoma) displayed no visible uptake of Gal-beads. Phase contrast microscopy of uptake of Gal-beads by Hep G2 in different stages of culture (2, 3 and 5 days) and different magnifications (40x, 100x, 200x, and 400x) also were taken. The MTT cell survival assay showed that the toxic concentration of Gal-beads was around 1.5 mg/mL. The results obtained in this study encourage further study of Gal-beads as potentially selective carriers for targeting the liver.

Further studies include: (1) to increase the stability of Gal-beads at room temperature (25 °C) and 37 °C, (2) to determine the physical properties of Gal-beads, (3) to quantity how many cells take up Gal-beads using Flow Cytometry or magnetocytometry and (4) to obtain electron microscope images of the Gal-beads in Hep G2 cell line in order to know exact position, as well as size constrains for Gal-bead uptake.

6. BIBLIOGRAPHY

Adalsteinsson, O., Lamotte, A., Baddour, R. F., Colton, C. K., Ollak, A. and Whitesides, G. M. (1979) Preparation and magnetic filtration of polyacrylamide gels containing covalently immobilized proteins and a ferrofluid. *J. Mol. Catal.* **6,** 199-225.

Alberts, B., Bray, D., Lewis, J., Raff, M., Roberts, K. and Watson, J. D. Eds. (1994) *Molecular Biology of the Cell*. New York: Garland.

Alexiou, C., Arnold, W., Hulin, P., Klein, R.G., Bergemanne, C. and Lubbe, A.S. (2001) Magnetic mitoxantrone nanoparticle detection by histology, X-ray and MRI after magnetic tumor targeting. *J. Magn. Magn. Mater.* **225,** 187-193.

Amigorena, S. and Bonnerot, C. (1998) Role of B-cell and Fc receptors in the selection of T-cell epitopes. *Curr. Opin. Immunol.* **10**, 88-92.

Andrews, W H H. Ed (1979). *Liver*. Great Britain.

Antoine, J. C., Ternynck, T., Rodrigot, M. and Avrameas, S. (1978) Lymphoid cell fractionation on magnetic polyacrylamine-agarose beads. *Immunochemistry*. **15,** 443-452.

Ashwell, G. and Morell, A. G. (1974) The Role of Surface Carbohydrates in the Hepatic Recognition and Transport of Circulating Glycoproteins. *Adv. Enzymol. Relat. Areas. Mol. Biol.* **41**, 99-128.

Assembly of Life Sciences (U.S), Subcommittee on Iron, Committee on Medical and Biological Effects of Enviromental Pollutants, Division of Medical Sciences, National Research Council. Ed. (1979) *Iron*. University Park Press, Baltimore.

Autenshlyus, A. I., Brusintsov, N. A. and Lockshin, A. (1993) Magnetic-sensitive dextran-ferrite immunosorbents for diagnostic and therapy. *J. Magn. Magn. Mater.* **122,** 360-363.

Baenziger, J. U. and Fiete, D. (1980) Galactose and N-acetylgalactosamine-specific endocytosis of glycopeptides by isolated rat hepatocytes. *Cell.* **22**, 611-620.

Baeniziger, J. U., and Fiete, D. (1986) Separation of two populations of endocytic vesicles involved in receptor-ligand sorting in rat hepatocytes. *J. Biol. Chem.* **261,** 7445-7454.

Banerjee, s. k. and Moskowitz, B.M. (1985) Ferrimagnetic properties of magnetite. In Kirschvink, J. L., Jones, D. S. and Mac Fadden, B. J. Eds Magnetite, Biomineralization and Magnetoreception inorganisms. New York, Plenum Press, Chapter 2

Baenziger, J. U., Fiete, D. and Maynard, Y. (1980) Molecular basis of oligosaccharide recognition and uptake by hepatocytes. *Fed. Proc.* **39**, 1969.

Berthier, R., Martinon-Ego, C., Laharie, A. M and Marche, P N. (2000) A two-step culture method starting with early growth factors permits enhanced production of functional dendritic cells from murine splenocytes. *J. Immunol. Methods*. **239,** 95-107.

Bettinger, T., Remy, J. S.and Erbacher, P. (1999) Size reduction of galactosylated PEI/DNA complexes improves lectin-mediated gene transfer into hepatocytes. *Bioconjug. Chem.* **4,** 558-561.

Bohren, C. F. and Huffman, D. R. (1983) Absorption and scattering of light from small particles. Wiley Interscience.

Bogdanov, A. Jr.and Weissleder, R. (1998) The development of in vivo imaging systems to study gene expression. *Ophthalmic. Genetics*. **16**, 5-10.

Bischoff, J. and Lodish, H.F. (1987) Two asialoglycoprotein receptor polypeptides in human hepatoma. *J. Biol. Chem*. **262,** 11825-11832.

Brezovich, I. A.and Meredith, R. F. (1989) Practical aspects of ferromagnetic thermoseed hyperthermia. *Radiol. Clin. North. America.* **27,** 589-602.

Brusentsov, N. A., Gogosov, V. V., Brusentsova, T. N., Sergeev, A. V., Jurchenko, N. Y., Kuznetsov, A. A, and Shumakov, L. L. (2000) Evaluation of ferrimagnetic fluit, ferii- and ferromagnetic suspensions for the site specific radiofrequency-induced hyperthermia of sarcoma cells in vitro. *3th International Conference on the Scientific and Clinical Applications of Magnetic Carriers.* May 3-6, 2000 Roatock, Germany.22.

Bulte, J W., de Jonge, M. W., Kamman, R. L., Zuiderveen, F. T. H and de Leij, L. (1993) Magnetite as a potent contrast-enhancing agent in magnetic resonance imaging to visualize blood-brain barrier disruption. *Acta. Neurochir. S* **57**, 30-34.

Bulte, J. W. M.and Brooks, R. A. (1997) Magnetic nanoparticles as a contrast agents for MR imaging. In Hafeli, U., Schutt, W, Tell, J. and Zborowski, M. Eds. *Scientific and Clinical Applications of Magnetic Carriers*, Plenum Press, New York, 527-544.

Burn, M. A. and Graves, D. J. (1987) Application of magnetically stabilized, fluidized beds to bioseparations. *React. Polym.* **6**, 45-50.

Canon, K. K. (1981) Magnetic toners. Japanese patent 58 07,646[83 07,646]. Appl. 81/106,364,8 July 1981.

Chachuat, A. and Bonnemain, B. (1995) European clinical experience with endorem. A new contrast agent for liver MRI in 100 patients. *Radiologe*. **35**, 274-276.

Chalmers, J. J., Zhao, Y., Nakamura, M., Melnik, K., Lasky, L., Moore, L. and Zborowski, M. (1999). An instrument to determine the magnetophoretic mobility of labeled, biological cells and paramagnetic particles. *J. Magn. Magn. Mater.* **194,** 231-241.

Chagnon, M. S., Groman, E. V., Lee, J. and Whitehead, R. A. (1993) Magnetic particles for use in separations. (1987) Magnetic particles for use in separations. U.S. Patent 4,695,393.

Chan, D. C. F., Kirpotin, D. B. and Bunn. P. A. (1993) Synthesis and evaluation of colloidal magnetic iron oxides for the site-specific radiofrequency-induced hyperthermia of cancer. *J. Magn. Magn. Mater.* **122,** 374-378.

Chan, D. C .F., Kirpotin, D. B.and Bunn, P. A. (1997) Physical chemistry and in vivo tissue heating properties of colloidal magnetic iron oxides with increased power absorption rates. In Hafeli, U., Schutt, W., Teller, J and Zborowski, M. Eds. *Scientific and Clinical Applications of Magnetic Carriers*. Plenum Press, New York, 607-618.

Chaplin, M. F. and Kennedy, J. F. Eds. (1994) *Carbohydrate Analysis: A Practical Approach*. United Kingdom: Oxford University Press.

Charmot, D. (1989) Preparation of monodisperse, magnetizable composite metal polymer microsphere. *Prog. Colloid. Polymer. Sci.* **79,** 94-100.

Crotty, J. J. (1971) Acute iron poisoning in children. *Clin. Toxicol.* **4,** 615-619.

Cullity, R. D. (1972) Introduction to magnetic materials, USA, Addison Wesley Co.

Danielsen, H., Funderud, S., Nustad, K., Reith, A. and Ugelstad, J. (1986) The interaction between cell-surface antigens and antibodies bound to monpdisperse polymer particles in normal and malignant cells. *Scand. J. Immunol.* **24,** 179-187.

De Cuyper, M. and Joniau, M. (1988) Magnetoliposomes: formation and structural characterisation. *Eur. Biophys. J.* **15**, 311-319.

Dekker, R. F. H. (1989) Immobilisation of a lactose onto a magnetic support by covalent attachment to polyethyleneimine-glutaraldehyde-activated magnetite. *Appl. Biochem. Biotechnol.* **22,** 289-310.

Dubois, M., Gilles, K. A., Hamilton, J .K., Rebers, P. A. and Smith, F. (1956) Colorimetric method for determination of sugars and related substances. *Anal. Chem.* **28,** 350-356.

Dunn, W. A., Hubbard, A. L. and Aronson, N. N. (1980) Low temperature selectively inhibits fusion between pinocytic vesicles and lysosomes during heterophagy of ^{125}I-asialofetuin by the perfused rat liver. *J. Biol. Chem.* **255,** 5971-5978.

Dunnill, P. and Lilly, M. D. (1974) Purification of enzymes using magnetic bio-affinity materials. *Biotechnol. Bioeng.* **16,** 987-990.

Eley, C. G. S., Schmidt, P. G. and Fujii, G. (1986) Delivery vehicles with amphiphile-associated active ingredients for drugs and diagnostic agents. Eur. Patent Appl. EP 272,091 22, June 1988, US Patent Appl. 942,093, 15 Dec. 1986.

Everett, E. C. (2001) Iron nanoparticles as potential magnetic carriers. *J. Magn. Magn. Mater.* **225**, 17-20.

Findeis, M. A., Wu, C. H. and Wu, G. Y. (1994) Ligand-based carrier systems for delivery of DNA to hepatocytes. *Methods. Enzymol.* **247,** 341-351.

Fiume, L., Busi, C., Mattioli, A., Balboni, P. G. and Barbanti-Brodano, G. (1981) Hepatocyte targeting of adenine-9-β-D-arabinofuranoside 5'-monophosphate(ara-AMP) coupled to lactosaminated albumin. *FEBS. Lett.* **129**, 261-264.

Florin, E. L., Moy, V. T. and Gaub, H. E. (1994) Adhesion forces between individual ligand-receptor pairs. *Science.* **264,** 415-417.

Forrest, G. C. (1977) Development and application of a fully automated continuous flow radioimmunoassay system. *Am. Clin. Biochem.* **14,** 1-11.

Gabrielsen, O. S., Horsnes, L., Ruet, A. and Oyen, T. B. (1989) Magnetic DNA affinity purification of yeast transcription factor T-a new purification for the ultrarapid isolation of near homogeneous factor. *Nucleic. Acids. Res.* **17**, 6253-6267.

Gahmberg, C. G., and Andersson, L. C. (1978) Leukocyte surface origin of human alpha1-acid glycoprotein (orosomucoid). *J. Exp. Med.* **9**, 507-521.

Garcia, A. A., Bonen, M. R., Ramirez-Vick, J., Sadaka, M., Vuppu, A. Eds. (1999) *Bioseparation Process Science.* Blackwell Science, Inc. USA.

Gaudernack, G., Leivestad, T., Ugelstad, J. and Thorsby, E. (1986) Isolation of pure functionally active $CD8^+$ T cells. *J. Immunol. Methods.* **90,** 179-187.

Gorman, C. M., Moffat, L. F., and Howard, B. H. (1982) Recombinant genomes which express chloramphenicol acetyltransferase in mammalian cells. *Mol. Cell. Biol.* **2**, 1044-1051

Greenwood, F. C. and Hunter, W. M. (1963) The preparation of ^{131}I-labelled human growth hormone of high specific radioactivity. *Biochem. J.* **89,** 114-123.

Guesdon, J. C. and Avrameas, S. (1977) Magnetic solid phase enzyme-immunoassay. *Immunochemistry.* **14,** 443-447.

Gupta, P. K.and Hung, C. T. (1994) In Willmott, N.and Daly, J. Eds. *Microspheres and Regional Cancer Therapy*. CRC Press, Boca Raton, FL, 71.

Hafeli, U. O. and Pauer, G. J. (1999) In vitro and in vivo toxicity of magnetic microspheres. *J. Magn. Magn. Mater*. **194**, 76-78.

Häfeli, U.O., Pauer, G. J., Roberts, W. K., Humm, J. L. and Roger, M. M. (1996) Magnetically targeted microspheres for intracavitary and intraspinal Y-90 radiotherapy. In Häfeli, U.O., Schütt, W. Teller, J. and Zborowski, M. Eds. *Scientific and Clinical Applications of Magnetic Carriers*, Plenum Press, New York. 501-516.

Halliday, D and Resnick, R. Eds (1988) *Fundamentals of Physics*. New York: Wiley.

Handgretinger, R., Lang, P., Schumm, M., Taylor, G., Neu, S., Koscielnak, E., Niethammer, D. and Klingebiel, T. (1998) Isolation and transplantation of autologous peripheral CD34+ progenitor cells highly purified by magnetic-activated cell sorting. *Bone. Marrow. Transpl.* **21**, 987-993.

Hodgson, J. (1991) Chromatography of complex carbohydrates. *Biotechnology.* **9**, 149-150.

Hong, W., Le, A. V. and Doyle, D (1988) Identification and characterization of a murine receptor for galactose-terminated glycoproteins. *Hepatology.* **8,** 553-558.

Horisberger, M. (1976) Immobilization of protein and polysaccharide on magnetic particles: selective binding of microorganism by Concanavilin A-magnetite. *Biotechnol. Bioeng*. **18,** 1647-1651.

Hudgin, R. L., Pricer, W. E., Jr., Ashwell, G., Stockert, R. J. and Morell, A. G. (1974) The isolation and properties of a rabbit liver binding protein specific for asialoglycoproteins. *J. Biol. Chem.* **249**, 5536-5543.

Hultman, T., Stahl, S., Hornes, E. and Uhlen, M. (1989) Direct solid phase sequencing of genomic and plasmid DNA using magnetic beads as solid support. *Nucleic. Acids. Res.* **17,** 4937-4946.

Hunter, R. J. Ed (1981) *Zetapotential in colloid science*. Academic press

Isaacs, A., Daintith, J. and Martin, E. Eds (1991) *Concise Science Dictionary.* New York, Oxford University Press.

Ishii, F., Takamura, A. and Noro, S. (1984) Magnetic microcapsules for in vitro testing as carrier for intravascular administration of anticancer drugs: preparation physicochemical properties. *Chem. Pharm. Bull.* **32**, 678-684.

Jordan, A., Scholz, R., Hauff, K. M., Johannsen, M., Wust, P., Nadobny, J., Schirra, H., Schmidt, H., Deger, S., Loening, S., Lanksch, W and Felix, R. (2001) Presentation of a new magnetic field therapy system for the treatment of human solid tumors with magnetic fluid hyperthermia. *J. Magn. Magn. Mater.* **225,** 118-126.

Jordan, A., Scholz, R., Wust, P., Schirra, H., Schiestel, T., Schmidt, H and Felix, R (1999). Endocytosis of dextran and silan-coated magnetite nanoparticles and the effect of intracellular hyperthermia on human mammal carcinoma cells in vitro. *J. Magn. Magn. Mater.* **194,** 185-196.

Jordan, A., Wust, P. Scholz, R., Faehling, H., Krause, J. and Felix, R. (1997) Magnetic Fluid Hyperthermia (MFH). In Hafeli, U., Schutt, W. S., Teller, J. and Zborowski, M. Eds. *Scientific and Clinical Applications of Magnetic Carriers*. Plenum Press, New York, 569-595.

Josephson, L., Tung, C. H., Moore, A. and Weissleder, R. (1999) High-efficiency intracellular magnetic labeling with novel superparamagnetic-Tat peptide conjugates. *Bioconjug. Chem.* **10,** 186-191.

Juckett, M., Zheng, Y and Yuan, H. (1998) Heme and the Endothelium. Effects of nitric oxide on catalytic iron and heme degradation by heme oxygenase. *J. Biol. Chem.* **273**, 23388-23397.

Kantor, A. B., Gibbons, I., Miltenyi, S.and Schmitz, J. (1998) In Recktenwald, D. and Radbruch, A. Eds. *Cell Separation Methods and Applications*. Marcel Dekker, Inc., New York, Hong Kong.

Kawasaki, T. and Ashwell, G. (1976a) Carbohydrate structure of glycopeptides isolated from a hepatic membrane-binding protein specific for asialoglycoproteins. *J. Biol. Chem.* **251,** 5292-5299.

Kawasaki, T. and Ashwell, G. (1976b) Chemical and physical properties of a hepatic membrane protein that specifically binds asialoglycoprotein. *J. Biol. Chem.* **251**, 1296-1302.

Kawasaki, T. and Ashwell, G. (1977) Isolation and characterization of an avian hepatic binding protein specific for N-acetylglucosamine-terminated glycoproteins. *J. Biol. Chem.* **252,** 6536-6543.

Keegan-Rogers, V. and Wu, G. Y. (1990) Targeted protein of hepatocytes from galactosamine toxicity in vivo. *Cancer. Chemother. Pharmacol.* **26**, 93-96.

Kemshead, J. T., Heath, L., Gibson, F. M., Katz, F., Richmond, F., Treleaven, J. and Ugelstad, J. (1986) Magnetic microspheres and monoclonal antibodies for the depletion of neuroblastoma cells from bone marrow: experiences, improvements and observations. *Br. J. Cancer*. **54**, 771-778.

Kim, D. K., Zhang. Y., Kehr, J., Klason, T., Bjelke, B.and Muhammed, M. (2001) Characterization and MRI study of surfactant-coated superparamagnetic nanoparticles administered into the rat brain. *J. Magn. Magn. Mater.* **225,** 256-261.

Kiwada, H., Sato, J., Yamada, S. and Kato, Y. (1986) Feasibility of magnetic liposomes as a targeting device for drugs. *Chem. Pharm. Bull*. **34,** 4253-4258.

Kolarik, L. O., Priestly, A. J. and Wiess, D. E. (1977) The Sirofloc process for turbidity and color removal. *Public Aspirations Realities Water Resource Management,* 7th *Federal Convention of the Australia Water and Wastewater Association*. Canberra, 143-161.

Kresse, M., Wagner, S., Pfefferer, D., Lawaczeck, R., Elste, V. and Semmler, W. (1998) Targeting of ultra small superparamagnetic iron oxide (USPIO) particles to tumor cells in vivo by using transferrin receptor pathways. *Magn. Reson. Med.* **40**, 236-242.

Kronick, P. L., Campbell, G. L. and Joseph, K. (1978) Magnetic microspheres prepared by redox polymerization used in a cell separation based on gangliosides. *Science.* **200,** 1074-1076.

Kronick, P. L.and Cilpin, R. W. (1986) Use of superparamagnetic particles for isolation of cells. *J. Biochem. Biophy. Methods.* **12**, 73-80.

Kuznetsov, A. A., Harutyunyuan, A. R., Dobrinsky, E. K., Dobrinsky, V. I., Filippov, V. I., Malenkov, A. G., Vanin, A. F and Kuznetsov, O. A. (1997). Ferro-Carbon Particles. In Hafeli, U., Schutt, W, Teller, J and Zborowski, M. Eds. *Scientific and Clinical Applications of Magnetic Carriers.* Pleum Press, New York, 379-390.

Lacava, Z. G. M., De Azevedo, R. B., Lacava, L. M., Martins, E. V., Garcia, V. A. P, Rebula, C. A., Lemos, A. P. C., Sousa, M. H., Tourinho, F. A., Morais, P. C. and Da Silva, M. F. (1999) Toxic effects of ionic magnetic fluids in mice. *J. Magn. Magn. Mater.* **194,** 90-95.

Lauffer, R. B. Ed. (1992) *Iron and Human Disease*. CRC Press, Boca Raton, FL.

Lea, T., Nustad, K., Funderud, S., Vartdal, F., Berge, A., Ellingsen, T., Schmid, R., Stenstad, P. and Ugelstad, J. (1988) Monosized, magnetic polymer particles: their use

in separation of cells and subcellular components, and in the study of lymphocyte function in vitro. *J. Mol. Recognition*, **1**, 9-18.

Lea, T., Smeland, S., Funderud, S., Vartdal, F., Davies, C., Beiske, K. and Ugelstad, J. (1986) Characterization of human mononuclear cells after positive selection with immunomagnetic particles. *Scand. J. Immuol.* **23**, 509-519.

Li, H. J., Chang, C., and Weiskopf, M. (1973) Helix-coil transition nucleoprotein-chromatin structure. *Biochemistry* **12**, 1763-1771

Liberty, P.A., Chiarappa, J .N., Hovsepian, A. C. and Rao, C. G. (1996) In Pelizzetti, E. Ed. *Fine Particles Science and Technology: from Micro to Nanoparticles.* Kluwer Academic Publishers. Amsterdam.

Longo Gonzalez, M. A. (1990) Enzyme immobilisation onto magnetic carrier support particles. *MSc Dissertation*, University of Manchester Institute of Science and Technology, Manchester.

Lübbe, A. S., Bergemann, C., Brock, J. and McClure, D. G. (1999) Physiological aspects in magnetic drug targeting. *J. Magn. Magn. Mater.* **194**, 149-155.

Lubbe, A. S., Bergemann, C., Riess, H., Schriever, F., Reichardt, P., Possinger, K., Matthias, M., Dorken, B., Herrmann, F., Gurtler, R., Hohenberger, P., Haas, N., Sohr, R., Sander, B., Lemke, A. J., Ohlendorf, D. Huhnt, W.and Huhn, D. (1996) Clinical experiences with magnetic drug targeting: a phase I study with 4'-epidoxorubicin in 14 patients with advanced solid tumors. [See comments.]. *Cancer. Research.* **56**, 4686-4693.

Malaiya, A. and Vyas, S. P. (1988) Preparation and characterization of indomethacin magnetic nanoparticles. *J. Microencapsulation.* **5**, 243-253.

Margel, S., Gura, S., Kedem, M., Melamed, O., Zuberi, M., Mandel, E., Boguslavsky, L., Sheihet, L., Partouche, E and Tennenbaum, T. (2000) Functional magnetic & non-magnetic polymeric nanoparticles of narrow size distribution: design, synthesis, surface modification & biomedical applications. *3th International Conference on the Scientific and Clinical Applications of Magnetic Carriers.* May 3-6, 2000 Roatock, Germany.

Margel, S., Zisblatt, S. and Rembaum, A. (1979) Polyglutaraldehyde: a new reagent for coupling proteins to microspheres and for labelling cell surface receptors (II). *J. Immunol. Methods.* **28,** 341-353.

Margolis, L. B. M., Namiot, V. A. and Kljukin, L. M. (1983) Magnetoliposomes: another principle of cell sorting. *Biochem. Biophys. Acta*, **735**, 193-195.

Matsunaga, T. and Kamiya, S. (1987) Use of magnetic particles isolated from magnetotactic bateria for enzyme immobilization. *Appl. Microbiol. Biotechnol.* **26**, 328-332.

McDermott, M. W., Sneed, P. K. and Gutin, P. H. (1998) Interstitial brachytherapy for malignant brain tumors. *Semin. Surg. Oncol.* **14**, 79-87.

McKinney, M. (2002) Magnets may enhance gene therapy. *Gene Therapy*. **9**, 102-109.

Menz, E. T., Havelick, J., Groman, E. V. and Josephson, L. (1986) Magnetic affinity chromatography: an emerging technology. *Am. Biotechnol. Lab*. Spt./Oct., 46-51.

Mihama, T., Yoshimoto, T., Ohwada, K., Takahashi, K., Akimoto, S., Saito, Y. and Inada, Y. (1988) Magnetic lipase adsorbed to a magnetic field. *J. Biotechnol*. **7,** 141-146.

Mitsumori, M., Hiraoka, M., Shibata, T., Okuno, Y., Nagata, Y., Nishimura, Y., Abe, M., Hasegawa, M., Nagae, H. and Ebisawa.Y. (1996) Targeted hyperthermia using dextran magnetite complex: a new treatment modality for liver tumors. *Hepato-Gastroentero.* **43,** 1431-1437.

Moro, M., Pelagi, M., Fulci, G., Paganelli, G., Dellabona, P., Casorati, G., Siccardi, A. G.and Corti, A. (1997) Tumor cell targeting with antibody-avidin complexes and biotinylated tumor necrosis factor alpha. *Cancer. Res.* **57,** 1922-1928

Molday, R. S., Yen, S. P. S. and Rembaum, A. (1977) Application of magnetic microspheres in labelling and separation of cells. *Nature*. **268,** 437-438.

Molday, R. S. and Mackenzie, D. (1982) Immunospecific ferromagnetic iron-dextran reagents for the labeling and magnetic separation of cells. *J. Immunol. Methods*. **52,** 353-367.

Molday, R. S. and Molday, L. L. (1984) Separation of cells labelled with immunospecific iron dextran microspheres using high gradient magnetic chromatography. *FEBS. Lett*. **170** , 232-238

Moore, A., Basilion, J. P., Chiocca, E. A., and Weissleder, R. (1998) Measuring transferrin receptor gene expression by NMR imaging. *Biochim. Biophys. Acta*. **1402**, 239-349.

Morin, K. W., Atrazheva, E. D., Knaus, E. E. and Wiebe, L. I. (1997) Synthesis and cellular uptake of 2'-substituted analogues of (E)-5-(2-[^{125}I] iodovinyl)-2'-deoxyuridine in tumor cells transduction with the herpes simplex type-1 thymidine kinase gene-evaluation as probes for monitoring gene therapy. *J. Med. Chem.* **40,** 2184-2190.

Mulligan, R. C. (1991) *Etiology of Human Disease at the DNA Level.* In Lindsten, J and Pettersson, U. Eds. Raven, New York.

Mykhaylyk, O., Cherchenko, A., Ilkin, A., Dudchenko, N., Rudista, V., Novoseletz, M and Zozulya, Y (2001). Glial brain tumor targeting of magnetite nanoparticles in rats. *J. Magn. Magn. Mater.* **225,** 241-247.

Mykhaylyk, O. M., Razumov, O. N., Dudchenko A. K., Pankratov, Y. V., Dobrinsky, E. K., Sosnitsky, V. N and Bakai, E. A (1997) Use of esr, mossbauer spectroscopy, and squid-magnetometry for the characterization of magnetic nanoparticles on the base of metal iron and its implications in vivo. In Hafeli, U., Schutt, W., Teller, J and Zborowski, M. Eds. *Scientific and Clinical Applications of Magnetic Carriers*. Plenum Press, New York, 1997, 177-204.

Nikolai, A., Brusentsov, V. V., Gogosov, T. N., Brusentsova, A. V., Sergeev, N. Y., Jurchenko, A. A., Kuznetsov, O., Kuznetsov, A and Shumakov, L. I. (2001) Evaluation of ferromagnetic fluids and suspensions for the site-specific radiofrequency-induced hyperthermia of MX11 sarcoma cells in vitro. *J. Magn. Magn. Mater.* **225,** 113-117.

Nilsson, H., Johansson, C. and Scheynius, A. (1987) Removal of langerhans cells from human epidermal cells suspensions by immunomagnetic particles. *J. Immunol. Methods*, **105**, 165-169.

Nye, L., Forrest, G. C., Greenwood, H., Gardner, J. S., Jay, R., Roberts, J. R. and Landon, J. (1976) Solid-phase, magnetic particle radioimmunoassay. *Clinica. Chim. Acta*. **69,** 387-396.

Olsvik, O., Popovic, T., Skjerve, E., Cudjoe, K. S., Hornes, E., Ugelstad, J. and Uhlen, M. (1994) Magnetic separation techniques in diagnostic microbiology. *Clin. Microbiol. Rev.* **7**, 43-54.

Pahl, A. L., Chandra, G. R. and Leon, W. M. M. T. (2001) Optimization of ferrofluids and protocols for the enrichment of breast tumor cells in blood. *J. Magn. Magn. Mater.* **225**, 301-307.

Park, J. H., Cho, E. W., Shin, S. Y., Lee, Y. J. and Kim, K. L. (1998) Detection of the asialoglycoprotein receptor on cell lines of extrahepatic origin. *Biochem. Biophy. Res. Commun.* **244,** 304-311.

Patton, W. F., Kim, J. and Jacobson, B. S. (1985) Rapid, high-yield purification of cell surface membrane using colloidal magnetite coated with polyvinyl: sedimentation versus magnetic isolation. *Biochem. Biophys.* Acta. **816**, 83-92

Pearse, B. M. (1981) Membrane recycling by coated vesicles. *Annu. Rev. Biochem.* **50**, 85-101.

Petit, L., Mingotaud, C., Ravaine, S. and Duguet, E. (2000) Dissymmetrisation as a first step for new difunctional particles. *3th International Conference on the Scientific and Clinical Applications of Magnetic Carriers* May 3-6, 2000 Roatock, Germany.

Pierres, A., Benoliel, A. M. and Bongrand, P. (1996) Measuring bonds between surface-associated molecules. *J. Immunol. Methods*. **196**, 105-120.

Pieters. B. R. (1989) Magnetic separation in biotechnology. *MSc Dissertation,* University of Manchester Institute of Science and Technology. Manchester.

Ponzetto, A., Fiume, L., Forzani, B., Song, S.Y., Busi, C., Mattioli, A., Spinelli, C., Marinelli, M., Smedile, A., Chiaberge, E., Bonino, F., Gervasi, G. B., Rapicetta, M. and Verme, G. (1991) Adenine arabinoside monophosphate and acyclovir monophosphate coupled to lactosaminated albumin reduce woodchuck hepatitis virus viremia at doses lower than do the unconjugate drugs. *Hepatology (Baltimore)*. **14**, 16-24.

Pourfarzaneh, M., Kamel, R. S., Landon, J. and Dawes, C. C. (1982) The use of magnetizable particles in solid phase immunoassay. *Methods. Biochem. Analysis*. **28**, 267-295.

Pricer, W. E. Jr. and Ashwell, G. (1971) The binding of desialylated glycoproteins by plasma membranes of rat liver. *J. Biol. Chem*. **246**, 4825-4833.

Pricer, W. E. Jr. and Ashwell, G. (1976) Subcellular distribution of a mammalian hepatic binding protein specific for asialoglycoproteins. *J. Biol. Chem*. **251**, 7539-7544.

Provder, T. Ed (1996) *Particle size distribution III assessment and characterization*. ICI Paints, Florida.

Pulfer, S. K., Ciccotto, S. L. and Gallo, J. M. (1999) Distribution of small magnetic particles in brain tumor-bearing rats. *J. Neuro-Oncol.* **41,** 99-105.

Pulfer, S. K and Gallo, J. M. (1997) Targeting magnetic microspheres to brain tumors In Hafeli, U., Schutt, W., Teller, J and Zborowski, M. Eds. *Scientific and Clinical Applications of Magnetic Carriers*, Plenum Press, New York. 445-456.

Rainov, N. G., Zimmer, C., Chase, M., Kramm, C. M., Chiocca, E. A., Weissleder, R.and Breakefield, X. O. (1995) Selective uptake of viral and monocrystalline particles delivered intra-arterially to experimental brain neoplasms. *Hum. Gene. Ther.* **6**, 1543-1552.

Reading, C. L., Thomas, W., Hickey, C. M., Chandran, M., Tindle, S., Ball, E. D., Poynton, C. H. and Dicke, K. A. (1987) Magnetic affinity colloid (MAC) cell separation of leukemia cells from autologous bone marrow aspirates. *J. Leukemia Research.* **11,** 1067-1077.

Recht, L., Torres, C. O., Smith, T. W., Raso, V. and Griffin, T. W. (1990) Transferrin receptor in normal and neoplastic brain tissue: implications for brain-tumor immunotherapy. [See comments.]. *J. Neurosurg.* **72,** 941-945.

Remsen, L. G., McCormick, C. I., Roman-Goldstein, S., Nilaver, G., Weissleder, R., Bogdanov, A., Hellstrom, I., Kroll, R, A. and Neuwelt, E. A. (1996) MR of carcinoma-specific monoclonal antibody conjugated to monocrystalline iron oxide nanoparticles: the potential for noninvasive diagnosis. *AJNR.* **17,** 411-418.

Robinson, P. J., Dunnill, P. and Lilly, M. D. (1973) The properties of magnetic supports in relation to immobilized enzyme reactors. *Biotechnol. Bioeng.* **15,** 603-606.

Rocha, F. M., Pinho, S. C. D., Zollner, R. L., Santana, M. H. A. (2001) Preparation and characterization of affinity magnetoliposomes useful for the detection of antiphospholipid antibodies. *J. Magn. Magn. Mater.* **225,** 101-108.

Rodriguez-Paris, J. M., Nolta, K. V. and Steck, T. N. (1993) Characterization of lysosomes isolated from diatyostelium discoideum by magnetic fractionation. *J. Biol. Chem.* **268,** 9110-9116.

Rosenfeld, M. A., Yoshimura, K., Trapnell, B. C., Yoneyama, K., Rosenthal, E. R., Dalemans, W., Fukayama, M., Bargon, J., Stier, L. E., StratFord-Perricaudet, L., Perricaudet, M., Guggino, W. B., Pavirani, A., Lecocq, J. P. and Crystal, R. G. (1992) In vivo transfer of the human cystic fibrosis transmembrane conductance regulator gene to the airway epithelium. *Cell.* **68,** 143-155.

Rubin, D. L., Muller, H. H., Young, S. W., Hunke, W. A. and Gorman, W. G. (1994) Optimization of an oral magnetic particle formulation as a gastrointestinal contrast agent for magnetic resonance imaging. *Invest. Radiol.* **29,** 81-86.

Sato, S. B., Sako, Y., Yamashina, S. and Ohnishi, S. (1986) A novel method for isolating specific endocytic vesicles using very fine ferrite particles coated with biological ligands and high gradient magnetic separation technique. *J. Biochem.* **100,** 1481-1492.

Saslawski, O., Weingarten, C., Benoit, J. R. and Couveur, P. (1981) Magnetically responsive microspheres for the pulsed delivery of insulin. *Life. Sci.* **42,** 1521-1528.

Schaffer, B. K., Linker, C., Papisov, M., Tsai, E., Nossiff, N., Shibata, T., Bogdanov, A. Jr., Brady, T. J. and Weissleder, R. (1993) MION-ASF: biokinetics of an MR receptor agent. *Magn. Reson. Imaging*. **11**, 411-417.

Schmid, K., Polis, A., Hunziker, K., Fricke, R. and Yayoshi, M. P. (1967) Charaterization of the salic acid-free form of α1-acid glycoproteins from human plasma. *BioChem J.* **104**, 361-365.

Schoepf, U., Marecos, E., Melder, R., Jain, R., and Weissleder, R. (1998) Intracellular magnetic labelling of lymphocytes for in vivo trafficking studies. *BioTechniques.* **24**, 642-651.

Schwartz, A. L., Fridovich, S. E., Knowles, B. B. and Lodish, H. F. (1981) Characterization of asialoglycoprotein receptor in a continuous hepatoma line. *J. Biol. Chem*. **256**, 8878-8881.

Schwartz, A. L., Marshak-Rothstein, A., Rup, D. and Lodish, H. F. (1981) Identification and quantification of the rat hepatocyte asialoglycoprotein receptor. *Proc. Natl. Acad. Sci*. U. S.A. **78,** 3348-3352.

Schwartz, A. L., Rup, D. and Lodish, H. F. (1980) Difficulties in the quantification of asialoglycoprotein receptors on the rat hepatocytes. *J. Biol. Chem.* **255,** 9033-9036.

Spiess, M. and Lodish, H. F. (1985) Sequence of a second human asialoglycoprotein receptor: conservation of two receptor genes during evolution. *Proc. Nall. Acad. Sci.* USA **82,** 6465-6469.

Spiess, M., Schwartz, A. L. and Lodish, H. F. (1985) Sequence of human asialoglycoprotein receptor cDNA. *J. Biol. Chem*. **260,** 1979-1982.

Sneed, P. K., Stauffer, P R., McDermott, M W., Diederich, C. J., Lamborn, K R., Prados, M. D., Chang, S., Weaver, K. A., Spry, L., Malec, M. K., Lamb, S. A., Voss, B., Davis, R. L., Wara, W. M., Larson, D. A., Phillips, T. L. and Gutin, P. H. (1998) Survival benefit of hyperthermia in a prospective randomized trial of brachytherapy boost +/- hyperthermia for glioblastoma multiformae. *Int J. Radiat. Oncol. Biol. Phys.* **40**, 287-295.

Sneed, P. K. and Stea, B. (1996) In Seegenschmiedt, M.H. Fessenden, P. and Vernon, C.C. Eds. *Thermoradiotherapy and Thermochemotherapy.* Vol. 2, Springer, Berlin.

Steer, C. J. and Ashwell. G. (1980) Studies on a mammalian hepatic binding protein specific for asialoglycoproteins. *J. Biol. Chem.* **255**, 3008-3013.

Stockert, R. J. (1995) The asialoglycoprotein receptor: relationships between structure, function, and expression. *Physiological Review.* **75,** 591-604.

Svennerholm, L. (1957) Quantitative estimation of sialic acids. *Biochim. Biophys Acta.* **24,** 604-611.

Takeda, K., Fujita, H. and Shibahara, S. (1995) Differential control of the metal-mediated activation of the human heme oxygenase-1 and metallothionein IIA genes. *Biochem. Biophys Res. Commun.* **207,** 160-167.

Takezawa, R., Shinzawa, K., Watanabe, Y and Akalke, T. (1993) Determination of mouse major asialoglycoprotein receptors cDNA sequence. *Biochim. Biophys. Acta.* **1172,** 220-222.

Tamaura, Y., Takahashi, K., Kodera, Y., Saito, Y. and Inada, Y. (1986) Chemical modification of lipase with ferromagnetic modifier-a ferromaganetic-modified lipase. *Biotechnol. Lett.* **8,** 877-880.

Tanabe, T., Pricer, W. E. and Ashwell, G. (1979) Subcellular membrane topology and turnover of a rat hepatic binding protein specific for asialoglycoproteins. *J. Biol. Chem.* **254**, 1038-1043.

Tchikov, V., Morbach, S. W., Kabelitz, D., Krönke, M and Schütze, S. (2001). Adhesion of immunomagnetic particles targeted to antigens and cytokine receptors on tumor cells determined by magnetophoresis. *J. Magn. Magn. Mater.* **225**, 285-293.

Tchikov, V., Schütze, S. and Krönke. M. (1999) Comparison between immunofluorescence and immunomagnetic techniques of cytometry. *J. Magn. Magn. Mater.* **194**, 242-247.

Terranova, B. E. and Burns, M. A. (1989) Continuous cell debris filtration using a magnetically stabilized fluidized bed. *Biotechnol. Prog.* **5**, 98-104.

Tolleshaug, H., Berg, T., Frolich, W. and Norum, K. R. (1979) Intracellular localisation and degradation of asialofetuin in isolated rat hepatocytes. *Biochim. Biophys. Acta.* **585**, 71-84.

Tolleshaug, H., Berg, T., Nilsson, M. and Norum, K. R. (1977) Uptake and degradation of ^{125}I-labelled asialo-fetuin by isolated rat hepatocytes. *Biochim, Biophys. Acta.* **499**, 73-84.

Tomlinson, S., Carvalho, L. P., Vandekerckhove, F. and Nussenzweig, V. (1992) Resialylation of sialidase-treated sheep and human erythrocytes by trypanosoma cruzitrans-sialidase: restoration of complement resistance of desialylated sheep erythrocytes.*Glycobiology.* **2**, 549-551.

Tsai, E., Bogdanov, A., Papisov, M., Brady, T. J. and Weissleder, R. (1992) Lymphocytes as drug carriers for MR contrast agents. *Society of Magnetic Resonance in Medicine, 11th Annual Meeting*, August 8-14, Berlin.

Tsunoda, H. (1985) Microencapsulation of magnetic ultrafines. Japanese Patent, JP 62 83,034[87 83,034] 16 April 1987, Appl. 85/223,133,7 Oct. 1985

Tuikens, P., Schneider, Y-J. and Trouvet, A. (1977) The fate of the plasma membrane during endocytosis. *Biochem. Soc. Trans.* **5,** 1809-1815

Ugelstad, j., Berge, A.and Ellingsen, T. (1988) Monosized magnetic particles and their use in selective cell separations. *Macromol. Chem. Macromol. Symp.* **17,** 177-211.

Ugelstad, j., Ellingsen, T., Berge, A. and Helgee, B. (1982) Magnetic polymer particles. PCT Patent Appl. WO 83 03,920,10 Nov.1983, NO Appl.82/1,327 23 April 1982.

Ugelstad, J., Ellingsen, T., Berge, A.and Helgee, O. B. (1987) Magnetic polymer particles and process for the preparation thereof. March 31. U.S. Patent 4, 654, 267.

Urbain, O. M. and Stemen, W. R. (1941) Magnetic flocculation for removing suspended matter from whey, distillery and yeast plant wastes, strawboard-mill wastes, etc.US Patent 2,232,294,18 Feb.1941.

Voytas, D and Ke, N. (1999). *Current Protocols in Molecular Biology.* A.3A.1-A. 3A. 10. John Wiley & Sons, Inc

Weigel, P. H. (1980) Characterization of the asialoglycoprotein receptor on isolated rat hepatocytes. *J. Biol. Chem.* **255**, 6111-6120.

Weissleder, R, Cheng, H. C., Bogdanova, A. and Bogdanov, A. (1997) Magnetically labelled cells can be detected by MR imaging. *J. Magn. Reson. Imaging.* **7**, 258-263.

Weissleder, R. (1994) Liver MR imaging with iron oxides: toward consensus and clinical practice. [letter; comment.]. *Radiology.* **193,** 593-595.

Weissleder, R. Hahn, P. F., Stark, D. D., Rummeny, E., Saini, S., Wittenberg, J., Ferrucci, J. T. (1987) MR imaging of spleen metastases: ferrite-enhanced detection in rats. *AJR.* **149**, 723-726.

Widder, K. J., Senyei, A. E. and Scarpelli, D. G. (1978) Magnetic microspheres: a model system for site-specific drug delivery in vivo. *Proc. Soc. Exp. Biol . Med.* **58**, 141-146.

Wilchek, M. and Baayer, E. A. Eds. (1990) *Methods In Enzymology Series: Avidin-Biotin Technology.* Vol 184. New York: Academic Press.

Williams, R. A. Ed (1992) Colloid and surface engineering: Applications in the process industries. Butterworth-Heinemann Ltd

Winoto-Morbach, S., Tchikov, V. and Muller-Ruchholtz, W. (1994) Magnetophoresis: detection of magnetically labelled cells. *J. Clin. Lab. Anal.* **8,** 400-406.

Wu, C. H., Wilson, J. M. and Wu, J. Y. (1989) Targeting genes: delivery and persistent expression of a foreign gene driven by mammalian regulatory elements in vivo. *J. Biol. Chem.* **264**, 16985-16987.

Wu, G. Y. and Wu, C. H. (1988) Evidence for targeted gene delivery to Hep G2 hepatoma's cells in vitro. *Biochemistry.* **27**, 887-892.

Wu, G. Y and Wu, C. H. Eds. (1991) Liver diseases, targeted diagnosis and therapy using specific receptors and ligands. Dekker, New York.

Wu, G. Y., Wu, C. H. and Stockert, R. J. (1983) Model for specific rescue of normal hepatocytes during methotrexate treatment of hepatic malignancy. *Proc. Natl. Acad. Sci.* U.S.A. **80**, 3078-3080.

Wu, G. Y., Wu, C. H and Rubin, M. I. (1985) Acetaminophen hepatotoxicity and targeted rescue: a model for specific chemotherapy of hepatocellular carcinoma. *Hepatology (Baltimore).* **5**, 709-713.

Wust, P., Seebass, M., Nadobny, J and Felix, R. (1996) In Seegenschmiedt, M. H., Fessenden, P. and Vernon, C. C. Eds. *Thermoradiotherapy and Thermochemotherapy, Vol. 1, Biology, Physiology, and Physics*. Springer, Berlin.

Xu, Z., Liu, Q. and Finch, J. A. (1997) Silanation and stability of 3-aminopropyl triethoxy silane on nanosized superparamagnetic particles: direct silanation. *Appl. Surf. Sci*, **120,** 269-278.

Xu, Z. H, Liu, Q. X. and Finch, J. (1999) An engineering of nanosize superparamagnetic particles for use in magnetic carrier technology. In Schwarz, J. A and Contescu, C. I. Eds. *Surfaces of Nanoparticles and Porous Materials.* Syracuse University, Syracuse, New York.

Yeh, T. C., Zhang, W., Idstad, S. T., and Ho, C. (1993) Intracellular labelling of T-cells with superparamagnetic contrast agents. *Mag. Reson. Med.* **30,** 617-625.

Yeh, T. C., Zhang, W., Idstad, S. T., and Ho, C. (1995) In vivo dynamic MRI tracking of rat T-cells labelled with superparamagnetic iron-oxide particles. *Mag. Reson. Med.* **33**, 200-208.

Yen, S. P. S., Rembaum, A. and Landel, R. F. (1980) Functional magnetic microspheres. US Patent. 4, 285,819,25. Aug., 1981, Appl. 116,093, 28. Jan. 1980.

Yoshima, H., Matsumoto, A. and Mizuochi, T. (1981) Comparative study of the carbohydrate moieties of rat and human plasma α1-acid glycoprotein. *J. Biol. Chem.* **256,** 8475-8484.

Zanta, M. A., Boussif, O., Adib, A. and Behr, J. P. (1997) In vitro gene delivery to hepatocytes with galactosylated polyethylenimine. *Bioconjug. Chem.* **8,** 843-844.

Zimmer, C., Weissleder, R., Poss, K., Bogdanova, A., Wright, S. C. Jr. and Enochs, W S. (1995) MR imaging of phagocytosis in experimental gliomas. *Radiology.* **197,** 533-538.

7. APPENDIX

```
                    B I - 9 0    P A R T I C L E    S I Z E R  V7.2
                    02/17/01                                07:31:12

                                --- RESULT SUMMARY ---

Sample ID: unknown     Job No.:  7493
Cycles  =   2500     Count Rate =   121.8 +/-   1.3 kcps     Dust Factor = 0.01
Runs    =   1

Measurement Parameters:
          Temp.        = 23.5 deg. C        Viscosity   =  0.922 cp
          Parameter K = 0.76E-04            Ref. Index  = 1.335
          RI Real      =  1.420             RI Imag.    =  0.000
          Dust Cutoff = 26                  Parameter a = -0.53
          Duration     =   2500 cycles
          Cumulative %:   10 %      25 %      50 %      75 %      90 %

Diffusion Coefficient:
          Effective Dia. =    61 +/-   0 nm
          Polydispersity = 0.120 +/- 0.000
          Diff. Coeff.   =  7.73E-08 cm^2/s
          Mol. Weight    =  4.4E+05 g/mole

Size Results (Volume Average):
          Volume Average Size =    61 nm  Width of Dist.  =    42 nm

LogNormal Parameters:
          Volume Median Dia. =    58 nm  GSD =  1.4

Cumulative UnderSize Results:
           10%   below    37 nm
           25%   below    46 nm
           50%   below    58 nm
           75%   below    72 nm
           90%   below    89 nm
```

BI-90 PARTICLE SIZER V7.2

~~02/17/01~~ 07:17:17

03/01/01

--- RESULT SUMMARY ---

Sample ID: unknown Job No.: 7491

Cycles = 2500 Count Rate = 55.3 +/- 1.5 kcps Dust Factor = 0.07

Runs = 1

Measurement Parameters:

Temp.	= 23.5 deg. C	Viscosity	= 0.922 cp
Parameter K	= 0.76E-04	Ref. Index	= 1.335
RI Real	= 1.420	RI Imag.	= 0.000
Dust Cutoff	= 26	Parameter a	= -0.53
Duration	= 2500 cycles		

Cumulative %:	10 %	25 %	50 %	75 %	90 %

Diffusion Coefficient:

Effective Dia. = 127 +/- 0 nm

Polydispersity = 0.241 +/- 0.000

Diff. Coeff. = 3.71E-08 cm^2/s

Mol. Weight = 1.8E+06 g/mole

Size Results (Volume Average):

Volume Average Size = 127 nm Width of Dist. = 125 nm

LogNormal Parameters:

Volume Median Dia. = 114 nm GSD = 1.6

Cumulative UnderSize Results:

10%	below	63 nm
25%	below	83 nm
50%	below	114 nm
75%	below	156 nm
90%	below	207 nm

BI-90 PARTICLE SIZER V7.2
00/00/00 00:35:39

--- RESULT SUMMARY ---

Sample ID: unknown Job No.: 8377
Cycles = 2500 Count Rate = 38.5 +/- 0.6 kcps Dust Factor = 0.05
Runs = 1

Measurement Parameters:

Temp.	= 23.5 deg. C	Viscosity	= 0.922 cp
Parameter K	= 0.76E-04	Ref. Index	= 1.335
RI Real	= 1.420	RI Imag.	= 0.000
Dust Cutoff	= 26.	Parameter a	= -0.53
Duration	= 2500 cycles		

Cumulative %: 10 % 25 % 50 % 75 % 90 %

Diffusion Coefficient:

Effective Dia.	= 86 +/- 0 nm
Polydispersity	= 0.164 +/- 0.000
Diff. Coeff.	= 5.48E-08 cm^2/s
Mol. Weight	= 8.4E+05 g/mole

Size Results (Volume Average):
Volume Average Size = 86 nm Width of Dist. = 70 nm

LogNormal Parameters:
Volume Median Dia. = 80 nm GSD = 1.5

Cumulative UnderSize Results:

10%	below	48 nm
25%	below	61 nm
50%	below	80 nm
75%	below	104 nm
90%	below	131 nm

BI-90 PARTICLE SIZER V7.2
00/00/00 00:30:53

--- RESULT SUMMARY ---

Sample ID: unknown Job No.: 8376
Cycles = 2500 Count Rate = 108.1 +/- 3.6 kcps Dust Factor = 0.01
Runs = 1

Measurement Parameters:

Temp.	= 23.5 deg. C	Viscosity	= 0.922 cp
Parameter K	= 0.76E-04	Ref. Index	= 1.335
RI Real	= 1.420	RI Imag.	= 0.000
Dust Cutoff	= 26	Parameter a	= -0.53
Duration	= 2500 cycles		

Cumulative %: 10 % 25 % 50 % 75 % 90 %

Diffusion Coefficient:

Effective Dia.	= 141 +/- 0 nm
Polydispersity	= 0.239 +/- 0.000
Diff. Coeff.	= 3.34E-08 cm^2/s
Mol. Weight	= 2.1E+06 g/mole

Size Results (Volume Average):

Volume Average Size = 141 nm Width of Dist. = 138 nm

LogNormal Parameters:

Volume Median Dia. = 127 nm GSD = 1.6

Cumulative UnderSize Results:

10%	below	70 nm
25%	below	93 nm
50%	below	127 nm
75%	below	173 nm
90%	below	229 nm

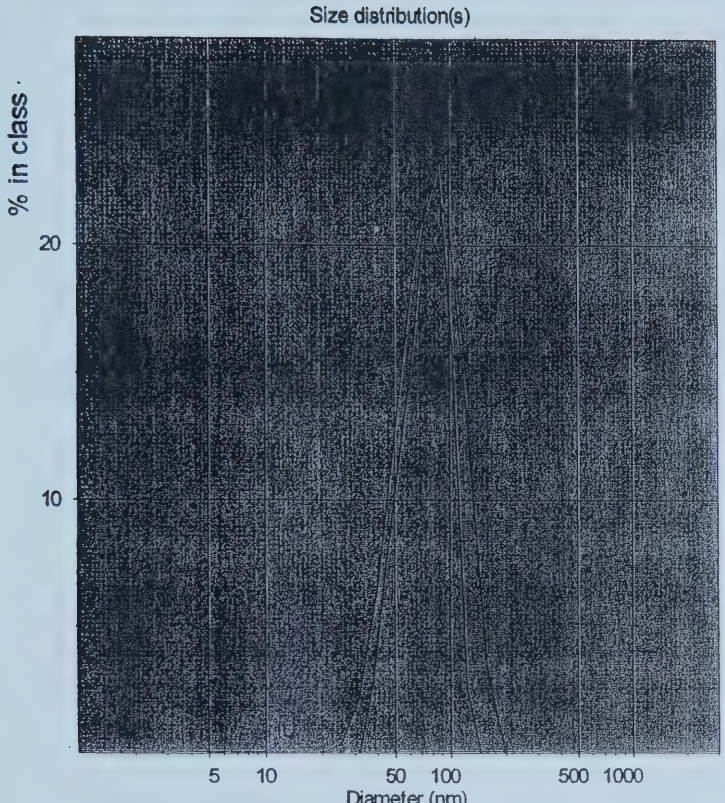

Size(nm)	Intensity	Volume
4.9	0.0	0.0
5.8	0.0	0.0
6.9	0.0	0.0
8.1	0.0	0.0
9.6	0.0	0.0
11.4	0.0	0.0
13.5	0.0	0.0
16.0	0.0	0.0
19.0	0.0	0.0
22.5	0.0	0.0
26.7	0.0	0.0
31.7	0.0	3.2
37.6	2.7	11.9
44.5	7.4	19.3
52.8	11.6	20.0
62.6	15.9	17.2
74.2	21.2	13.6
87.9	23.1	9.1
104.2	15.6	4.4
123.6	2.5	1.2
146.5	0.0	0.1
173.6	0.0	0.0
205.8	0.0	0.0
244.0	0.0	0.0

Run	Angle	KCps.	ZAve	Poly	Fit	Time
1	90	59.8	70.3	0.161	0.000643	9:56:12
2	90	59.9	69	0.181	0.000364	10:06:53
Average		59.9	69.6	0.171		

```
                BI-90  PARTICLE  SIZER V7.2
                00/00/00                    00:36:08

                        --- RESULT SUMMARY ---

Sample ID: unknown    Job No.:  8487
Cycles  =   2500    Count Rate =    46.7 +/-   1.3 kcps    Dust Factor = 0.04
Runs    =   1

Measurement Parameters:
        Temp.       = 23.5 deg. C       Viscosity   =  0.922 cp
        Parameter K = 0.76E-04          Ref. Index  = 1.335
        RI Real     =  1.420            RI Imag.    =  0.000
        Dust Cutoff = 26                Parameter a = -0.53
        Duration    =   2500 cycles
        Cumulative %:   10 %      25 %      50 %      75 %      90 %

Diffusion Coefficient:
        Effective Dia. =   278 +/-   0 nm
        Polydispersity = 0.308 +/- 0.000
        Diff. Coeff.   =  1.70E-08 cm^2/s
        Mol. Weight    =  7.7E+06 g/mole

Size Results (Volume Average):
        Volume Average Size =   278 nm  Width of Dist.  =   309 nm

LogNormal Parameters:
        Volume Median  Dia. =   243 nm  GSD =  1.7

Cumulative UnderSize Results:
          10%   below   125 nm
          25%   below   171 nm
          50%   below   243 nm
          75%   below   345 nm
          90%   below   472 nm
```

BI-90 PARTICLE SIZER V7.2
00/00/00 00:41:02

--- RESULT SUMMARY ---

Sample ID: Unknown Job No.: 8488
Cycles = 2500 Count Rate = 36.7 +/- 1.0 kcps Dust Factor = 0.03
Runs = 1

Measurement Parameters:

Temp.	= 23.5 deg. C	Viscosity	= 0.922 cp
Parameter K	= 0.76E-04	Ref. Index	= 1.335
RI Real	= 1.420	RI Imag.	= 0.000
Dust Cutoff	= 26	Parameter a	= -0.53
Duration	= 2500 cycles		

Cumulative %: 10 % 25 % 50 % 75 % 90 %

Diffusion Coefficient:

Effective Dia.	= 337 +/- 0 nm
Polydispersity	= 0.305 +/- 0.000
Diff. Coeff.	= 1.40E-08 cm^2/s
Mol. Weight	= 1.1E+07 g/mole

Size Results (Volume Average):
Volume Average Size = 337 nm Width of Dist. = 372 nm

LogNormal Parameters:
Volume Median Dia. = 295 nm GSD = 1.7

Cumulative UnderSize Results:

10%	below	152 nm
25%	below	208 nm
50%	below	295 nm
75%	below	418 nm
90%	below	572 nm